Inaugural-Dissertation
zur Erlangung der Doktorwürde der Tierärztlichen Fakultät der
Ludwig-Maximilians-Universität
München

The influence of the genetic background on the development of diabetes mellitus and associated renal lesions in GIPR^{dn}-transgenic mice

von Carola Marion Seibold
aus Augsburg

München 2015

Aus dem Zentrum für Klinische Tiermedizin der Tierärztlichen
Fakultät der Ludwig-Maximilians-Universität München
Lehrstuhl für Tierpathologie

Arbeit angefertigt unter der Leitung von Prof. Dr. Rüdiger Wanke
Mitbetreuung durch PD Dr. Nadja Herbach und Dr. Andreas Blutke

Gedruckt mit Genehmigung der Tierärztlichen Fakultät der
Ludwig-Maximilians-Universität München

Dekan: Univ.-Prof. Dr. Joachim Braun
Berichterstatter: Univ.-Prof. Dr. Rüdiger Wanke
Korreferent: Priv.-Doz. Dr. Valerie Zakhartchenko

Tag der Promotion: 18. Juli 2015

Meiner Familie

Contents

List of figures VIII

List of tables IX

List of abbreviations X

1 Introduction 1

2 Scientific background 3

2.1 Diabetes mellitus 3

2.1.1 Classification of types of diabetes mellitus 3

2.1.2 Clinical manifestation and diagnosis of diabetes mellitus . . 5

2.1.3 Diabetes mellitus-associated diseases 6

2.2 Diabetic nephropathy (DN) 9

2.2.1 Clinical stages of diabetic nephropathy 9

2.2.2 Composition and function of the glomerular filtration barrier as relating to the pathogenesis of diabetic nephropathy . . . 10

2.2.3 Morphology and pathogenesis of glomerular and tubular lesions in diabetic nephropathy 11

2.3 Murine models of diabetes mellitus 16

2.3.1 Streptozotocin-induced diabetes 16

2.3.2 Obese mouse (ob/ob) 17

2.3.3 Diabetes mouse (db/db) 17

2.3.4 Kuo Kondo mouse (KK/Ta) 18

2.3.5 Nagoya-Shibata-Yasuda mouse (NSY) 18

2.3.6 New Zealand obese mouse (NZO) 18

2.3.7 High fat diet (HFD) induced diabetes mellitus type 2 18

2.4 Murine models of diabetic nephropathy 19
2.4.1 Bradykinin receptor deficient Ins2$^{Akita/+}$ mouse 19
2.4.2 Renin-overexpressing mouse with STZ-induced diabetes . . 20
2.4.3 OVE26-transgenic FVB/N (FVB-OVE26) mouse 21
2.4.4 eNOS$^{-/-}$ mouse 21
2.4.5 Kuo Kondo - Agouti (KK-A^{y}/Ta) mouse 22
2.4.6 NONcNZO10/LtJ mouse 23
2.4.7 Decorin deficient (Dcn$^{-/-}$) mouse with STZ-induced diabetes 23
2.4.8 Mice expressing a dominant negative glucose-dependent insulinotropic polypeptide receptor (GIPR^{dn}-tg mice) 24
2.5 Influence of the genetic background on the susceptibility to diabetes mellitus and diabetic nephropathy 27
2.5.1 Inbred and congenic mouse strains and outbred stock 27
2.5.2 C57BL/6J strain 29
2.5.3 FVB/N strain 29
2.5.4 Influence of the FVB/N and C57BL/6J genetic background on diabetes mellitus and diabetic nephropathy 30

3 Materials and methods 32
3.1 Animals 32
3.1.1 Breeding 32
3.1.2 Animal husbandry 34
3.1.3 Genotyping by polymerase chain reaction (PCR) 34
3.1.4 Blood pressure measurement 37
3.1.5 Quantitative and semiquantitative determination of glucose concentrations in urine and blood 37
3.1.6 Serum parameter measurements: Creatinine, urea, triglyceride, protein and ion concentrations 38
3.1.7 Cystatin C serum concentration 38
3.1.8 Urine parameter measurements 39
3.1.9 Food and water consumption and 24h urine collection . . . 42
3.2 Perfusion fixation and processing of kidneys 42
3.2.1 Vascular perfusion fixation of the kidneys 42
3.2.2 Kidney processing for histology, immunohistochemistry and quantitative stereology 45

3.2.3 Paraffin embedding and detection of glomerular matrix proteins and TGFβ1 by immunohistochemistry 45
3.2.4 Glycolmethylacrylate and methylmethacrylate (GMA/MMA) embedding and staining of GMA/MMA sections 50
3.2.5 Glycid ether (Epon) embedding, staining of glycid ether sections and sample processing for disector analyses and electron microscopy 53
3.3 Glomerulosclerosis Index 56
3.4 Quantitative stereological analyses 57
3.4.1 Determination of the total kidney volume 57
3.4.2 Estimation of the total nephron number in both kidneys . . 57
3.4.3 Estimation of the total glomerular volume in both kidneys . 59
3.4.4 Estimation of the mean glomerular volume 60
3.4.5 Estimation of the podocyte number per glomerulus 60
3.4.6 Estimation of the mean podocyte volume 62
3.4.7 Estimation of the mean mesangial and capillary volume per glomerulus 64
3.4.8 Estimation of the capillary length density in the glomeruli . 64
3.4.9 Estimation of the mean capillary length per glomerulus . . . 65
3.4.10 Determination of the filtration slit frequency (FSF) 66
3.4.11 Estimation of the true harmonic mean thickness of the glomerular basement membrane (GBM) 66
3.4.12 Shrinkage in GMA/MMA and glycid ether embedded kidney tissue and determination of thickness of GMA/MMA sections 67
3.5 Statistical analyses 69

4 Results **71**
4.1 Clinical parameters 71
4.1.1 Body weight 71
4.1.2 Food consumption per day 72
4.1.3 Food consumption per day and body weight 73
4.1.4 Water consumption per day 74
4.1.5 Water consumption per day and body weight 75
4.1.6 Daily urine volume 76

4.1.7 Blood pressure . . . 76
4.1.8 Blood glucose concentration . . . 79
4.1.9 Serum parameters . . . 80
4.1.10 Urine analyses . . . 88
4.2 Qualitative histological findings . . . 97
4.2.1 Glomerular tuft profiles of GIPR^{dn}-tg mice . . . 97
4.2.2 Immunohistochemical detection of glomerular extracellular matrix proteins and TGF-β1 . . . 99
4.3 Glomerulosclerosis index . . . 103
4.4 Quantitative stereological parameters . . . 104
4.4.1 Total volume of both kidneys . . . 104
4.4.2 Total number of nephrons in both kidneys . . . 106
4.4.3 Volume fraction of glomeruli in the kidneys . . . 107
4.4.4 Total glomerular volume in both kidneys . . . 108
4.4.5 Total glomerular volume to body weight ratio . . . 109
4.4.6 Mean glomerular volume . . . 110
4.4.7 Mean glomerular volume to body weight ratio . . . 111
4.4.8 Numerical volume density of podocytes in the glomerulus . . . 112
4.4.9 Podocyte number per glomerulus . . . 113
4.4.10 Volume fraction of podocytes in the glomerulus . . . 114
4.4.11 Mean podocyte volume . . . 115
4.4.12 Volume fraction of mesangium in the glomerulus . . . 116
4.4.13 Mean mesangial volume per glomerulus . . . 117
4.4.14 Volume fraction of capillaries in the glomerulus . . . 118
4.4.15 Mean capillary volume per glomerulus . . . 119
4.4.16 Capillary length density in the glomerulus . . . 120
4.4.17 Mean capillary length per glomerulus . . . 121
4.4.18 Filtration slit frequency . . . 122
4.4.19 True harmonic mean thickness of the glomerular basement membrane (GBM) . . . 123

5 Discussion **124**
5.1 General aspects . . . 124
5.2 Diabetes mellitus in GIPR^{dn}-tg FVB/N and C57BL/6J mice . . . 125

5.3 Influence of the genetic background on the development of diabetic nephropathy in GIPR^{dn}-tg FVB/N and C57BL/6J mice 128
5.3.1 Kidney function of diabetic GIPR^{dn}-tg FVB/N and C57BL/6J mice 128
5.3.2 Semiquantitative analysis and quantitative stereological analyses of kidneys 131
5.4 Conclusions 140

6 Summary **142**

7 Zusammenfassung **144**

Appendix **146**

Bibliography **150**

Acknowledgement **179**

List of Figures

2.1 Schematic drawing of the glomerulus 12
2.2 Schematic drawing of the glomerular filtration barrier 13

3.1 Breeding scheme of GIPR^{dn}-tg FVB/N and C57BL/6J mice by back-crossing 33
3.2 Cardial perfusion setup 43
3.3 Perfusion of a mouse 44
3.4 Lamination of kidneys 46
3.5 Sampling for epon embedding 47
3.6 Stereological estimation of number of podocytes per glomerulus (physical disector method) 62
3.7 Estimation of the true harmonic mean thickness of the glomerular basement membrane with a logarithmic ruler 68

4.1 Body weight 71
4.2 Food consumption per day 72
4.3 Food consumption per day and body weight 73
4.4 Water consumption per day 74
4.5 Water consumption per day and body weight 75
4.6 24h-urine volume 77
4.7 Blood pressure 78
4.8 Blood glucose concentrations 79
4.9 Serum creatinine concentration 80
4.10 Serum urea concentration 81
4.11 Serum triglyceride concentration 82
4.12 Serum total protein concentration 83
4.13 Serum albumin concentration 84
4.14 Serum cystatin C concentration 85

4.15 Serum sodium concentration 86
4.16 Serum chloride concentration 87
4.17 Urine creatinine concentration 88
4.18 Estimated glomerular filtration rate (eGFR) 89
4.19 Urine urea concentration 90
4.20 Urine sodium concentration 91
4.21 Urine chloride concentration 92
4.22 Urine albumin concentration 93
4.23 Albumin excretion 95
4.24 Urine albumin creatinine ratio 96
4.25 Glomerular histology of GIPR^{dn}-tg FVB/N and C57BL/6J mice in HE stained GMA/MMA-embedded kidney tissue 97
4.26 Kidney histology of PAS-MS stained GMA/MMA-embedded tissue in GIPR^{dn}-tg FVB/N and C57BL/6J mice 98
4.27 Immunohistochemical detection of collagen IV in paraffin-embedded tissue of GIPR^{dn}-tg mice 99
4.28 Immunohistochemical detection of laminin in paraffin-embedded tissue of GIPR^{dn}-tg mice 100
4.29 Immunohistochemical detection of fibronectin in paraffin-embedded tissue of GIPR^{dn}-tg mice 101
4.30 Immunohistochemical detection of TGF-β1 in paraffin-embedded tissue of GIPR^{dn}-tg mice 102
4.31 Glomerulosclerosis index 103
4.32 Total volume of both kidneys 105
4.33 Total nephron number in both kidneys 106
4.34 Volume fraction of glomeruli in both kidneys 107
4.35 Total glomerular volume in both kidneys 108
4.36 Total glomerular volume to body weight ratio 109
4.37 Mean glomerular volume 110
4.38 Mean glomerular volume to body weight ratio 111
4.39 Numerical volume density of podocytes in the glomerulus 112
4.40 Podocyte number per glomerulus 113
4.41 Volume fraction of podocytes in the glomerulus 114
4.42 Mean podocyte volume 115
4.43 Volume fraction of mesangium in the glomerulus 116

4.44 Mean glomerular mesangial volume 117
4.45 Volume fraction of capillaries per glomerulus 118
4.46 Mean glomerular capillary volume 119
4.47 Capillary length density in the glomerulus 120
4.48 Mean capillary length per glomerulus 121
4.49 Filtration slit frequency 122
4.50 Glomerular basement membrane thickness 123

List of Tables

2.1 Pathologic classification of DN in humans by TERVAERT et al. (2010) 14
2.2 FVB/N and C57BL/6J mice in DN research 31

3.1 Outline of performed analyses 70

A.1 Summary of results of clinical analyses 147
A.2 Summary of results of clinical analyses 2 148
A.3 Summary of results of morphological analyses 149

List of abbreviations

ACR	albumin creatinine ratio
BfB	Bundesmonopolverwaltung für Branntwein
DAB	3′3-Diaminobenzidine
DN	diabetic nephropathy
eGFR	estimated glomerular filtration rate
eNOS	endothelial nitric oxide synthase
FITC	fluorescein isothiocyanate
GBM	glomerular basement membrane
GIP	glucose-dependent insulinotropic polypeptide
GIPR	glucose-dependent insulinotropic polypeptide receptor
GMA	glycolmethylacrylate
IHC	immunohistochemistry
MMA	methylmethacrylate
PAS	periodic acid Schiff
PBS	phosphate-buffered saline
PFA	paraformaldehyde
STZ	streptozotocin
TAE	Tris-acetate-EDTA
TBS	Tris-buffered saline
TE	Tris-EDTA
tg	transgenic
TGF	transforming growth factor
TNF	tumor necrosis factor
UACR	urine albumin creatinine ratio
UAE	urinary albumin excretion
VEGF	vascular endothelial growth factor
wt	wild-type control

1 Introduction

Diabetic nephropathy is one of the leading causes of end-stage renal disease and an important sequela of diabetes mellitus. Currently, an estimated 347 million people suffer from diabetes. The number of diabetic patients has doubled within a timespan of about thirty years (DANAEI et al., 2011) and the number of unreported cases is likely to be substantial. Predictions by the World Health Organization (WHO) suggest that diabetes might become the seventh leading cause of death in the year 2030 (WHO, 2011). By far the most important form of diabetes is type 2 diabetes mellitus, which accounts for 90% of cases (WHO, 1999). While insulin treatment can enable patients to live almost normal lifes, the sequelas associated with diabetes pose a serious risk to the continued health of the patients. About 20-40% of diabetics develop diabetic nephropathy (DN) as a sequela. Untreated, this condition eventually leads to renal failure, requiring renal replacement therapy in the form of dialysis or transplantation (COLLINS et al., 2012). So far, the underlying molecular mechanisms of diabetic nephropathy (DN) are only insufficiently understood. Animal models have been instrumental in the research of diabetes and its associated diseases. Mice are especially suited to the research of pathophysiological processes because of the large number of genetically modified animals available today, and their fast succession of generations. However, so far it has only been possible to recapitulate the early stages of diabetic nephropathy in mouse models. The development of mouse models that better display the later stages of diabetic nephropathy is of tantamount importance (BREYER and QI, 2010; BROSIUS et al., 2009). Several studies have demonstrated the influence of the genetic background on the susceptibility to diabetes-associated renal lesions in mice (BETZ and CONWAY, 2014; GURLEY et al., 2010, 2006). So far, many new models of diabetic nephropathy are only evaluated on one background, irrespective of its suitability for the evaluation of renal lesions. Many mouse models of diabetic nephropathy might resemble the human disease more closely, if transferred to a suitable genetic

background. One promising model of DN with a dominant inheritance pathway are mice expressing dominant negative glucose-dependent insulinotropic polypeptide receptors (GIPR) under the transcriptional control of the rat proinsulin gene promotor (HERBACH et al., 2005). Glucose-dependent insulinotropic polypeptide (GIP) plays an important role in the regulation of blood glucose levels. $GIPR^{dn}$-transgenic mice on an outbred CD1 background have already been shown to be a suitable model of diabetes mellitus and diabetic nephropathy (HERBACH et al., 2009). Clinical presentation, pancreas morphology and renal lesions closely resemble important aspects of human diabetes. A study performed on $GIPR^{dn}$ transgenic mice of CD1 and BALB/c background has already shown significant differences between the strains (POPPER, 2013). Discrepancies in mean glomerular volume, the degree of glomerular hypertrophy and podocytes numbers and volume per glomerulus correlate well with the severity of glomerulosclerotic lesions and proteinuria displayed by the two examined strains (POPPER, 2013). The FVB/N and C57BL/6J strains are popular throughout the scientific world, and are often used as genetic backgrounds for many models of diseases. The aim of this study was the determination of strain dependent differences on the development of diabetes mellitus, and how strain-dependent features influence the susceptibility to diabetes-associated kidney alterations in $GIPR^{dn}$-transgenic FVB/N and C57BL/6J mice.

2 Scientific background

2.1 Diabetes mellitus

2.1.1 Classification of types of diabetes mellitus

Diabetes mellitus (D.m.), from the greek “to pass through” (first written record by Aretaios of Cappadocia, 100 a.d.) and the latin “honey-sweet” (Thomas Willis, 1675), was among the first diseases to be described, i.e. in the Ebers papyrus, Egypt, 1500 b.c.. D.m. is comprised of a large, heterogenic group of metabolic diseases characterized by abnormal glucose metabolism. The deficient carbohydrate metabolism leads to hyperglycemia and is often accompanied by abnormalities in the metabolism of fats and proteins. Four categories of diabetes are differentiated currently (AMERICANDIABETESASSOCIATION, 2014). The first group, diabetes mellitus type 1, consist of cases in which hyperglycemia is caused by a destruction of the beta-cells, leading to an absolute insulin deficiency in humans. In humans, the destruction of the beta-cells is the result of an autoimmune reaction, with autoantibodies targeting a variety of structures and metabolism products. However, rare cases of idiopathic diabetes with a high heritability are also included in this group. Diabetes mellitus type 2 is caused by insulin resistance with relative insulin deficiency, or a primary low or impaired insulin secretion, and is responsible for approximately 90% of cases. Both genetic susceptibility and lifestyle choices play a role in the development of type 2 diabetes. A large number of genetic variations are associated with either a heightened or lowered risk of diabetes and patients often carry several genetic risk factors at once (SCHWENK et al., 2013). The risk of contracting diabetes increases further, when other risk factors like obesity, lack of physical activity or high blood pressure are also present.

Epigenetic alterations can also influence the risk of contracting diabetes mellitus, as maternal high fat diet has been shown to lead to an increased body mass index and decreased insulin sensitivity in offspring in mice (DAHLHOFF et al., 2014; SCHWENK et al., 2013). The third group includes all other specific types of diabetes. Gestational diabetes mellitus makes up the fourth group and is defined as a glucose intolerance first diagnosed during pregnancy, which does not fall under any of the other categories.

Types of diabetes mellitus (AMERICANDIABETESASSOCIATION, 2014)

1. Type 1 diabetes
   a) Immune mediated
   b) Idiopathic
2. Type 2 diabetes
3. Other specific types
   a) Genetic defects of β-cell function
      i. Chromosome 12, HNF-1α (MODY3)
      ii. Chromosome 7, glucokinase (MODY2)
      iii. Chromosome 20, HNF-4α (MODY1)
      iv. Chromosome 13, insulin promoter factor-1 (IPF-1; MODY4)
      v. Chromosome 17, HNF-1β (MODY5)
      vi. Chromosome 2, *NeuroD1* (MODY6)
      vii. MODY7-11
      viii. Transient neonatal diabetes
      ix. Permanent neonatal diabetes
      x. Mitochondrial DNA
      xi. Others
   b) Genetic defects in insulin action
      i. Type A insulin resistance
      ii. Leprechaunism
      iii. Rabson-Mendenhall syndrome
      iv. Lipoatrophic diabetes
      v. others
   c) Diseases of the exocrine pancreas
      i. Pancreatitis
      ii. Trauma/pancreatectomy
      iii. Neoplasia
      iv. Cystic fibrosis
      v. Hemochromatosis
      vi. Fibrocalculous pancreatopathy
      vii. Others
   d) Endocrinopathies
      i. Acromegaly
      ii. Cushing's syndrome
      iii. Glucagonoma
      iv. Pheochromocytoma

v. Hyperthyroidism
vi. Somatostatinoma
vii. Aldosteronoma
viii. Others

e) Drug or chemical induced
i. Vacor
ii. Pentamidine
iii. Nicotinic acid
iv. Glucocorticoids
v. Thyroid hormone
vi. Diazoxide
vii. β-adrenergic agonists
viii. Thiazides
ix. Dilantin
x. γ-Interferon
xi. Others

f) Infections
i. Congenital rubella
ii. Cytomegalovirus
iii. Others

g) Uncommon forms of immune-mediated diabetes
i. "Stiff-man" syndrome
ii. Anti-insulin receptor antibodies
iii. Others

h) Other genetic syndromes sometimes associated with diabetes
i. Down syndrome
ii. Klinefelter syndrome
iii. Turner syndrome
iv. Wolfram syndrome
v. Friedreich ataxia
vi. Huntington chorea
vii. Laurence-Moon-Biedl syndrome
viii. Myotonic dystrophy
ix. Porphyria
x. Prader-Willi syndrome
xi. Others

4. Gestational diabetes mellitus

MODY: Maturity onset diabetes of the young

2.1.2 Clinical manifestation and diagnosis of diabetes mellitus

The most prevalent form of diabetes mellitus is diabetes mellitus type 2. Unless hyperglycemia is diagnosed during routine examinations, type 2 diabetes mellitus often remains undetected over long periods of time, before clinical symptoms like polydypsia and polyuria occur. Other symptoms include poor wound healing, weight loss occasionally accompanied by polyphagia, heightened susceptibility to infections or impaired vision. While common in type 1 diabetes, hyperglycemic

ketoacidosis is rare in type 2 diabetics. The related hyperosmolar hyperglycemic state (HHS), which leads to severe dehydration, is far more common and can lead to coma or even death, if it remains untreated (CORWELL et al., 2014). According to the American Diabetes Association, the criteria, of which at least one must be fulfilled for diagnosing diabetes mellitus in a patient, are (AMERICANDIABETESASSOCIATION, 2013):

1. Symptoms of diabetes and casual plasma glucose concentration $\geq$ 200mg/dl
2. Fasting plasma glucose $\geq$ 126mg/dl after at least 8h of fasting
3. Glucose $\geq$ 200mg/dl two hours after a glucose load of 75g anhydrose glucose (oral glucose tolerance test)
4. Glycated hemoglobin (HbA_{1c}) $\geq$ 6.5% confirmed by repeated testing and standardized assays

Diagnosing diabetes by measuring HbA_{1c} remains somewhat controversial, as several other conditions besides hyperglycemia can influence the glycation of hemoglobin, i.a. anemia, iron deficiency, vitamin B(12) deficiency or folate deficiency (HARDIKAR et al., 2013).

2.1.3 Diabetes mellitus-associated diseases

Sequela of diabetes mellitus can be roughly divided into complications caused by microvascular or macrovascular damage due to persisting hyperglycemia and complications independent of blood vessel damage or dependent on both micro- and macrovascular lesions. The pathogenesis of D.m.-associated vascular damage is complex. Studies have shown loss of pericytes and development of a pro-inflammatory milieu, which in turn leads to basement membrane thickening, endothelial dysfunction and loss of barrier function (LI et al., 2012; KERN, 2007; VON TELL et al., 2006). The consequences of vascular damage include arteriosclerosis, thrombosis, tissue hypoxia due to decreased blood flow and leakage of protein into the interstitium.

Microvascular complications of diabetes: diabetic retinopathy, diabetic cardiomyopathy, diabetic neuropathy and diabetic nephropathy

Diabetic retinopathy is a very common complication of diabetes mellitus and has a non-proliferative phase, followed by a proliferative stage. During the non-proliferative phase, persistent hyperglycemia is known to cause damage to the capillaries in the retina (GERALDES et al., 2009). In some cases, exudate leaks through compromised capillaries into the macula, causing macular edema. Concomitantly, hyperglycemia also damages neuronal cells in the retina (RAJASHEKHAR et al., 2014). During the proliferative phase, neovascularisation occurs in the fundus oculi, increasing the risk of vitreous hemorrhages. Symptoms range from impaired vision to blindness.

Diabetic cardiomyopathy, first described in 1972 (RUBLER et al., 1972), is a consequence of microangiopathy with endothelial dysfunctions, abnormal metabolization (AVOGARO et al., 2004), oxidative stress, cardial autonomic neuropathy and alterations of calcium ion transients (PEREIRA et al., 2006). Patients present with cardiomegaly and diffuse myocardial fibrosis in the absence of significant coronary obstruction.

Diabetic neuropathy does not present with one clearly defined clinical picture, but rather a collection of different syndromes all caused by the same underlying processes, neuronal dysfunction and ischemia caused by insufficient blood flow through damaged capillaries (WILLIAMS et al., 1980). Both axonal degeneration and segmental demyelination of nerves can occur in diabetic neuropathy (VITAL et al., 1973). Metabolism changes have been implicated in the pathophysiology of diabetic neuropathy in animal models, but could not be substantiated in studies with human patients. Clinical presentation depends on which nerves are afflicted in each patient. Described diabetic neuropathies include amyotrophy, a wasting of sceletal muscle accompanied by muscle pain. Another form that often occurs in diabetics is the autonomic neuropathy or autonomic polyneuropathy, with a large collection of symptoms, depending on the exact location of the lesions. Common symptoms include orthostatic hypotension, gastroparesis, nausea, diarrhea, urine incontinence or retention, and pollakisuria. Correspondingly, mononeuropathy and polyneuropathy of various nerves, both sensoric and motoric, occur.

Diabetic nephropathy, more extensively described in chapter 2.2, is a progressive condition first described by Kimmelstiel and Wilson (KIMMELSTIEL and WILSON, 1936) that leads to chronic kidney insufficiency and failure. Patients with advanced diabetic nephropathy often require dialysis or an organ transplant. In 2008, 44% of US patients developing kidney failure were diabetic (CDC, 2011). Diabetic nephropathy seems to increase the risk of cardiovascular events and subclinically increased urine albumin excretion has been associated with a higher mortality rate in diabetic patients (MULLER, 1998; JARRETT et al., 1984).

Macrovascular complications of diabetes: stroke, cardiac infarction, peripheral arterial disease and diabetic myonecrosis

Atherosclerosis as a macrovascular complication in diabetic patients leads to an increased risk for strokes, myocardial infarctions and peripheral arterial disease (VAZQUEZ-BENITEZ et al., 2015). As hyperglycemia and elevated levels of fatty acids promote the formation of atherosclerotic plaques (LUSIS, 2000), diabetics have a 2-4 times higher risk for coronary artery disease and ischemic stroke. Cardiovascular disease is the leading cause of death among diabetics and accounts for 65-75% of deaths, shortening the life expectancy of diabetics by several years compared to non-diabetics of the same age group (MOSS et al., 1991). Peripheral arterial disease (PAD) is defined as atherosclerotic occlusion of lower extremities, and usually presents with intermittent claudication, rest pain, ulcers or even gangrene. As such, it is a risk factor in the development of diabetic foot, and it serves as a marker for systemic vascular diseases. While PAD also occurs in non-diabetic patients, the aetiopathology in diabetic patients seems to be different due to changes in arterial structure and function (AMERICANDIABETESASSOCIATION, 2003).

Diabetic myonecrosis is a rare, but serious condition that usually occurs in patients already suffering from diabetic retino- or nephropathy. Caused by the infarction of muscle tissue, it is most often found in the thigh and patients present with sudden unilateral pain and edema (BHASIN and GHOBRIAL, 2013).

Diabetic foot ulcer, diabetic encephalopathy and diabetic neuropathic arthropathy

Diabetic foot ulcers develop from a combination of diabetic neuropathy, which decreases sensitivity and pain reception, and peripheral vascular disease. Additionally, diabetics suffer from impaired wound healing and a compromised to abnormal immune system, which further complicates the treatment of wounds, and often makes limb amputation necessary (MOURA NETO et al., 2013).

Cognitive impairments in diabetics, referred to as diabetic encephalopathy, include memory loss, dementia, seizures and coma. Both vascular and metabolic changes, especially persisting hyperglycemia and hypoxia, are suspected to play a role in the development of brain damage (SINHA et al., 2014; MENG et al., 2013).

Diabetic neuropathic arthropathy is a progressive degeneration of the ankle joint and another rare sequela of diabetes with unclear aetiology. Denervation, caused by vascular damage and repeated trauma due to the decreased sensitivity of the limb appear to play a role in the progression of the disease (BAKER et al., 2007). Only approximately 1-2% of patients with peripheral neuropathy seem to develop Charcot arthropathy. Proinflammatory cytokines, increased osteoclast activity, neuropeptides and microvascular hyperemia are implicated in the development of diabetic arthropathy, and a genetic predisposition seems to be likely (MASCARENHAS and JUDE, 2013). Contrary to the development of diabetic foot, peripheral arterial disease seems to have a protective effect on the development of diabetic arthropathy (KAYNAK et al., 2013).

2.2 Diabetic nephropathy (DN)

2.2.1 Clinical stages of diabetic nephropathy

Diabetic nephropathy in humans is defined by a diabetic condition, albuminuria and increasingly declining glomerular filtration rate (GFR) (MOGENSEN et al., 1983). During stage 1, characterized by hyperfunction of the kidney, GFR and

albumin excretion are increased. Following stage 1 is a silent second stage, where the GFR is normal to increased, but albumin excretion returns to normal levels under good glycemic control. Stage 3, incipient diabetic nephropathy, is marked by persistent microalbuminuria (15-300 μg/min), that slowly increases and a rise in blood pressure. Stage 4, known as overt diabetic nephropathy, is characterized by macroalbuminuria, slightly increasing plasma creatinin concentrations and decreasing GFR. In stage 5, end-stage renal failure, patients additionally develop uremia and low GFR (MOGENSEN et al., 1983).

2.2.2 Composition and function of the glomerular filtration barrier as relating to the pathogenesis of diabetic nephropathy

The glomerular filtration barrier (Figure 2.1, p.12 and Figure 2.2, p.13) consists of three layers: the glomerular endothelium, the glomerular basement membrane and the slit diaphragm formed between podocyte foot processes. The fenestrated, thin endothelium lines the inside of the glomerular capillaries (KONDO and USHIKI, 1985). Approximately 30-50% of the endothelial surface are fenestrated (DEEN et al., 2001). The fenestration and flattening of the endothelial cells is induced via podocyte-derived vascular endothelial growth factor A (VEGF-A) and transforming growth factor β1 (TGF-β1) (LIU et al., 1999; KITAMOTO et al., 1997). A glycocalix, composed mainly of proteoglycans and sialoproteins (PRIES et al., 2000), covering the endothelium and extending into the fenestrae, and a layer of surface glycoproteins makes the endothelium semipermeable and allows the retention of as much as 95% of plasma proteins (HJALMARSSON et al., 2004; OHLSON et al., 2001). This glycocalix contributes little to the hydraulic resistance of the filtration barrier (DRUMOND and DEEN, 1994). The glomerular basement membrane (GBM) contains type IV collagen formed from a triple helix of α3, α4 and α5 chains that differs from the type IV collagen present in the glomerular mesangium (HARVEY et al., 1998). The type IV collagen forms a regular meshwork with round to oval pores (ISOGAI et al., 1999). The podocyte foot processes (pedicels) form a 30-40nm wide membrane-like slit diaphragm between their interdigitating processes. The podocytes attach themselves to the GBM by connecting their actin

cytosceletons with cell surface adhesion proteins, namely $\alpha 3\beta 1$ integrin and α-dystroglycan (KOJIMA and KERJASCHKI, 2002; KRETZLER, 2002), which enables the slit diaphragm to withstand the high filtration pressure (EL-AOUNI et al., 2006). The slit diaphragm, essentially a cell-cell connection between pedicels, is the most selective part of the filtration barrier. The proteins podocin and nephrin, both produced by the podocytes, are integral to maintaining the slit diaphragm architecture (ROSELLI et al., 2004; WARTIOVAARA et al., 2004; KHOSHNOODI et al., 2003). The glomerular basement membrane and the slit diaphragms each provide roughly half of the hydraulic resistance of the filtration barrier (DRUMOND and DEEN, 1994). The components of the glomerular filtration barrier retain blood particle components in a size- and charge-dependent manner.

2.2.3 Morphology and pathogenesis of glomerular and tubular lesions in diabetic nephropathy

In 1936, Kimmelstiel and Wilson first described eight cases of patients presenting with hyalinization of the glomeruli. They noted that the homogeneous mass they observed did not contain amyloid or fat, and that it belonged to the intercapillary connective tissue. Marked arteriosclerosis and fatty degeneration of arterioles were found in all cases. Further observations included slightly thickened glomerular basement membranes, decreased number of capillaries and hyalin-like masses lying between the bowman's capsule and the glomerulus. Kimmelstiel and Wilson noted that all patients reported long standing diabetes in their histories, and showed albuminuria and signs of renal insufficiency (KIMMELSTIEL and WILSON, 1936). The lesions described by Kimmelstiel and Wilson are now referred to as mesangial expansion and glomerulosclerosis. Glomerulosclerosis is now defined as a degenerative process with scarring of glomerulus. Microscopically, mesangial expansion, thickening of the glomerular basement membrane, adhesion of the glomerulus to the bowman's capsule or hyalinosis of the arterioles can be observed (LIZICAROVA et al., 2014). In humans, glomerulosclerosis often presents as a nodular sclerosis of the glomerulus. This nodular sclerosis is commonly called a Kimmelstiel-Wilson lesion (BERKMAN and RIFKIN, 1973).

Figure 2.1 Schematic drawing of the glomerulus

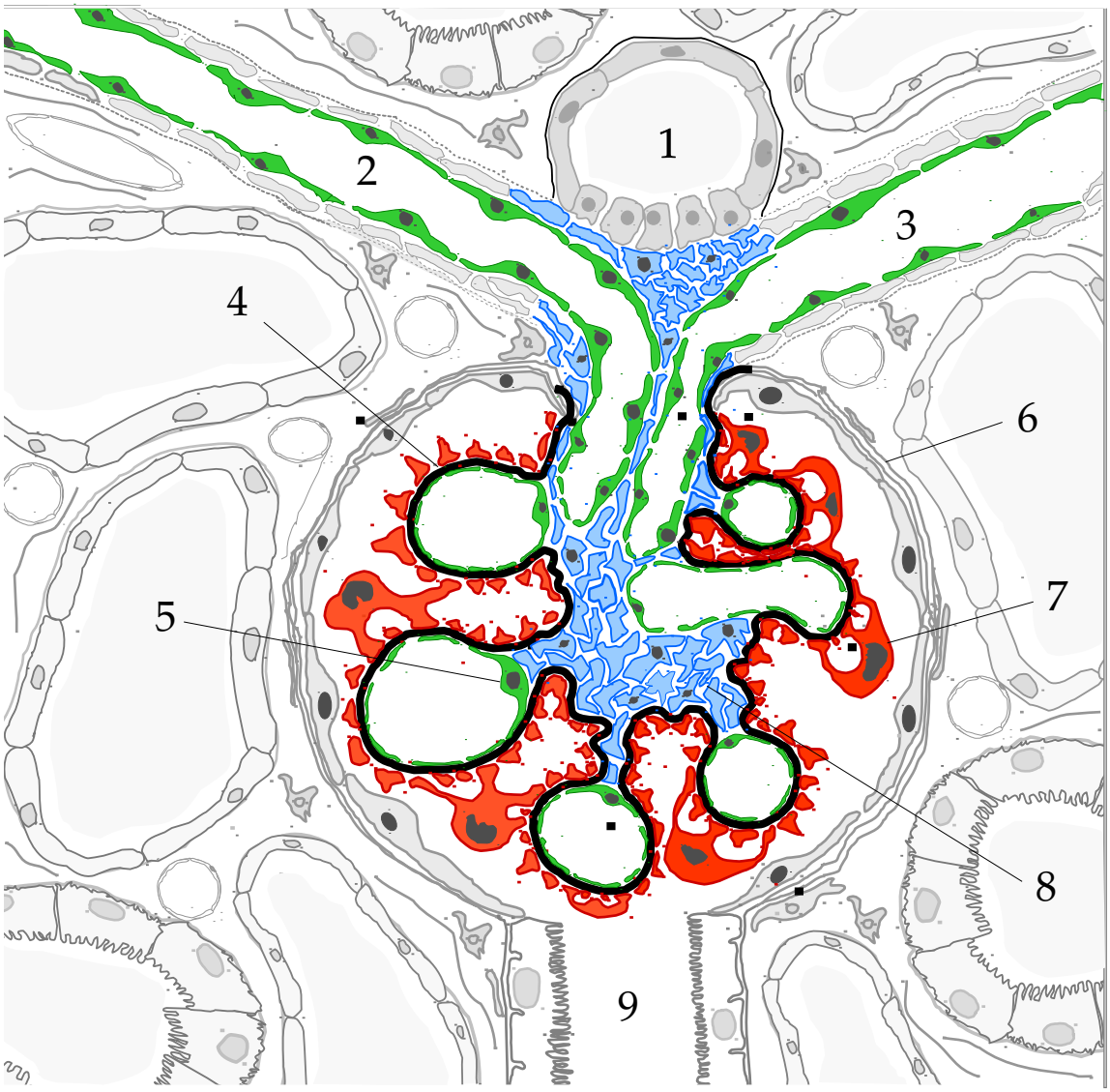

1: Macula densa, **2**: afferent arteriole, **3**: efferent arteriole, **4**: GBM (black), **5**: endothelial cells (green), **6**: Bowman's capsule, **7**: podocyte (red), **8**: mesangium (turquoise), **9**: proximal tubule. Picture courtesy of Dr. Andreas Blutke, Institute of Veterinary Pathology, LMU München.

Several factors play a role in the development of glomerular lesions associated with diabetes mellitus. One important feature in the development of DN is podocyte and glomerular injury through various metabolic changes. High glucose concentrations, nonenzymatically glycated proteins, mechanical stress and proteinuria

Figure 2.2 Schematic drawing of the glomerular filtration barrier

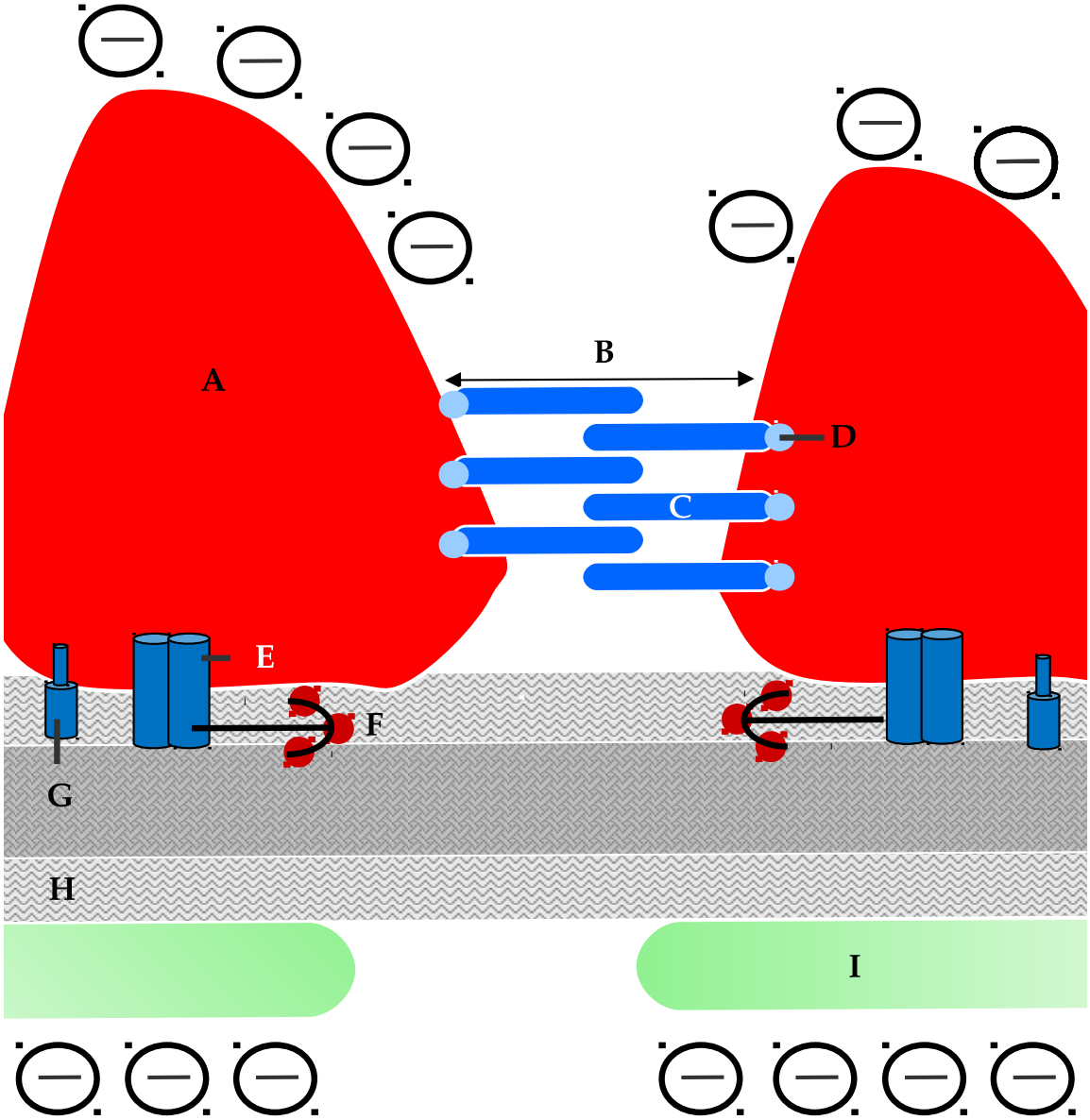

A: Podocyte foot process, **B**: Slit diaphragm, **C**: Nephrin, **D**: Podocin, **E**: $\alpha 3\beta 1$-Integrin, **F**: Laminin, **G**: Dystroglycan, **H**: Glomerular basement membrane, **I**: Glomerular endothelial cell. Picture courtesy of Dr. Andreas Blutke, Institute of Veterinary Pathology, LMU München.

can stimulate angiotensin II production. Locally high angiotensin II concentrations induce a reduction in nephrin production and induce the production of TGF-$\beta 1$, a fibrogenic growth factor which can promote renal hypertrophy (ZIYADEH

Table 2.1 Pathologic classification of DN in humans by TERVAERT et al. (2010)

Class	Description	Inclusion Criteria
I	Mild or nonspecific LM changes and EM-proven GBM thickening	GBM >395nm in female and >430nm in male individuals 9 years of age and older
IIa	Mild mesangial expansion	Mild mesangial expansion in >25% of the observed mesangium
IIb	Severe mesangial expansion	Severe mesangial expansion in >25% of the observed mesangium
III	Nodular sclerosis (Kimmelstiel-Wilson lesion)	At least one convincing Kimmelstiel-Wilson lesion
IV	Advanced diabetic glomerulo-sclerosis	Global glomerular sclerosis in >50% of glomeruli

DN: diabetic nephropathy, **LM**: light microscopical, **EM**: electron microscopical, **GBM**: glomerular basement membrane

and WOLF, 2008; SHARMA and ZIYADEH, 1994) and increases the production of podocyte-derived vasoendothelial growth factor (VEGF). TGF-β1 has great impact on podocyte metabolism and has been shown to suppress the genes coding for nephrin and podocin in the podocytes and can induce podocyte apoptosis (MITU et al., 2007) via MAP kinase p38 and caspase 3 (SCHIFFER et al., 2001). Changes in podocyte metabolism have a profound effect on podocyte morphology and function. TGF-β1 can also decrease podocyte adhesion to the GBM by reducing $\alpha 3\beta 1$ integrin production (DESSAPT et al., 2009). Combined with podocyte foot process effacement as a result of the reduction in nephrin production, decreased adhesion to the GBM increases the likelihood of podocyte loss. Podocyte loss through either detachment, apoptosis or necrosis is the most important aspect in the progressive destruction of the glomerular filtration barrier, eventually leading to the proteinuria and renal failure that is characteristic for the clinical presentation of DN. Podocyte hypertrophy and thickening of the glomerular basement membrane (GBM) has been shown to precede the development of glomerular hypertrophy and glomerulosclerosis in mice (TERVAERT et al., 2010; HERBACH et al., 2009). A thickening of the GBM, as a consequence of increased matrix protein deposition, is associated with ultrasturctural changes in GBM architecture that make the GBM more, rather than less, porous (ISOGAI et al., 1999). Hyperglycemia can induce increased glomerular matrix protein deposition in the glomerulus through various metabolic pathways, with transforming growth factor β1 (TGF-β1) as one of the

most important downstream mediators (ZIYADEH, 2004; SHARMA and ZIYADEH, 1994; ZIYADEH et al., 1994). The accumulation of extracellular matrix might be associated with a decrease in the capillary surface area available for filtration (MAUER et al., 1984). Glomerular hypertrophy also leads to reduced relative podocyte density, forcing the podocytes to further increase in size to maintain the glomerular filtration barrier. One of the most important risk factors for the development of glomerular lesions in human patients, aside from hyperglycemia, is hypertension (GANGADHARIAH et al., 2014; MOGENSEN, 1998). Diabetics suffering from DN are more likely to report a family history of hypertension, than diabetics who do not develop DN (ROGLIC et al., 1998). Increased intracapillary pressure in the glomerulus is thought to lead to hyperfiltration and subsequent scarring of the glomerulus as a result of endothelial and mesangial injury (BRENNER et al., 1988; BRENNER, 1983). The cases of two patients suffering from both diabetes mellitus and unilateral renal artery stenosis seem to support this theory, as both developed signs of DN in the initially healthy kidney, but not in the kidney affected by renal artery stenosis (BERONIADE et al., 1987; BERKMAN and RIFKIN, 1973). Common features of DN also include protein reabsoption into the proximal tubular epithelial cells, tubular hypertrophy, tubular basement membrane thickening and tubular atrophy (AN et al., 2015; HABIB, 2013). Most tubulointerstitial lesions are related to proteinuria and hyperfiltration, as protein erroneously filtrated into the interstitium has been shown to have a nephrotoxic effect (MARSHALL and WILLIAMS, 1998; REMUZZI et al., 1995; BRENNER, 1983). Renal interstitial fibrosis, mediated by TGFβ1 via multiple cytokines like tumor necrosis factor (TNF-α) and connective tissue growth factor (SAKAI et al., 2013) and epithelial-mesenchymal transformation (EMT) of tubular epithelial cells into myofibroblasts, are important features of human DN that animal models largely fail to reproduce. In kidneys with advanced DN, mononuclear cell infiltration as an inflammatory response to proteinuria can be observed and contributes to the progression of DN (TESCH, 2007; CHOW et al., 2004a,b).

2.3 Murine models of diabetes mellitus

In the following chapter, some of the most widely-used mouse models of diabetes mellitus on commonly used genetic backgrounds will be described. Mouse models of diabetes mellitus include genetically modified animals, spontaneously mutated animals and mice with dietary induced diabetes mellitus. Genetically modified mice can be subdivided into transgenic mice, knockout mice and mouse mutants. In transgenic mice, an exogenous gene (transgene) has been inserted randomly into the mouse genome. Mice in which a gene has been inactivated, are called knockout mice. Mouse mutants are generated by exposing the germ cells of male mice to mutagenic substances (i.e. ethylnitrosourea), causing random mutations in the genome of their offspring. The range and severity of symptoms displayed by different mouse models can vary drastically, depending on the genetic modification. The genetic background on which the different mutations and and knocked out genes are examined has been shown to have a great influence on the severity of the symptoms (BROSIUS, 2010; GURLEY et al., 2010; XU et al., 2010; BROSIUS et al., 2009; QI et al., 2005). Some mouse strains are more susceptible to the development of diabetic lesions, while other mouse strains carrying the same mutation display only mild diabetes mellitus. So far, no single mouse model of diabetes displays the entire range of symptoms, or the same severity of the disease, as human patients (BROSIUS et al., 2009; BREYER et al., 2005b). Mouse models of DN are described in chapter 2.4.

2.3.1 Streptozotocin-induced diabetes

Streptozotocin-induced diabetes mellitus is a popular model of diabetes mellitus type 1. Streptozotocin (STZ) is an antibiotic naturally produced by Streptomyces achromogenes, with a high toxicity for pancreatic beta cells (LEITER, 1982). Any genetic background can be used in this model of diabetes, though strains differ in their susceptibility to STZ. Disadvantages of the STZ-model include suspected non-specific toxicity of STZ and the need for different STZ regimes depending on the mouse strain and its susceptibility. To lower the risk of non-specific toxic effects, using low-dose STZ regimes instead of high-dose STZ regimes

is often recommended (BREYER et al., 2005b). Low-dose and high-dose STZ treatments induce comparable levels of hyperglycemia in males of the same genetic background, but the level of hyperglycemia varies both in respect to gender and mouse strain (LEITER, 1982; ROSSINI et al., 1977). High-dose STZ regimes lead to albuminuria even in C57BL/6J mice, while low-dose STZ treatment leads to comparatively lower levels of albuminuria, depending on the background strain (compare Table 2.2, p.31).

2.3.2 Obese mouse (ob/ob)

The ob/ob mouse carries a spontaneous recessive autosomal mutation of the leptin gene, leading to leptin deficiency, occurring in an animal at the Jackson Memorial Laboratory in 1950 (INGALLS et al., 1950). Leptin is a small adipokine that lowers appetite by binding to leptin receptors in the hypothalamus. On a C57BL/6J background, animals present with massive adipositas, mild hyperglycemia and hyperinsulinemia. On other available backgrounds, the obesity is observed to be less severe while diabetic symptoms are massively increased (BREYER et al., 2005b).

2.3.3 Diabetes mouse (db/db)

Db/db mice carry a point mutation of the leptin receptor and are available on the C57BL/6J, the C57BLKS/J and the DBA/2J background. They begin to develop hyperinsulinemia as early as 10d of age, with hyperglycemia beginning at approximately 1m of age. The progression to pancreatic islet cell degeneration takes between 5-6m. While it is possible to use db/db mice as a model of DN on the C57BLKS/J background, C57BL/6J mice display no noticeable signs of kidney insufficiency. More severe hyperinsulinemia and hyperglycemia develops on the DBA/2J background compared to the C57BL/6/J and C57BLKS/J (BREYER et al., 2005b).

2.3.4 Kuo Kondo mouse (KK/Ta)

Thought to be a polygenetic model of diabetes, the KK mouse was established by Kondo et al. in 1957 from native japanese mice. These mice exhibit obesity, mild insulin resistance and hyperglycemia, and increased pancreatic islet volume and number. Symptoms develop slowly over several months before stabilizing and finally reverting to normal at approximately one year of age. KK mice seem to be predisposed to renal lesions resembling DN, like mesangial expansion, mesangial cell proliferation and arteriole hyalinization (TOMINO et al., 2005).

2.3.5 Nagoya-Shibata-Yasuda mouse (NSY)

The inbred NSY mouse was created from outbred Jcl:ICR (ICR mice bred by CLEA Japan, Inc.) mice selected for glucose intolerance, and males reproducibly develop age related diabetes type 2. Unlike most mouse models of non-insulin-dependent diabetes mellitus, NSY mice are only moderately obese and hyperinsulinemic and do not show pancreatic islet hypertrophy. They display defects in both insulin secretion and insulin resistance (UEDA et al., 1995).

2.3.6 New Zealand obese mouse (NZO)

The NZO mouse is a polygenetic model of type 2 diabetes bred from two agouti mice, chosen from a mixed colony. It was first described in 1953. Animals present with obesity, insulin resistance, islet hypertrophy and hypercholesterolemia (BIELSCHOWSKY and BIELSCHOWSKY, 1956).

2.3.7 High fat diet (HFD) induced diabetes mellitus type 2

Different mouse strains exhibit diverging metabolic responses to HFD and several strains may develop glucose intolerance (MONTGOMERY et al., 2013; SIMS et al., 2013; ANDRIKOPOULOS et al., 2005; NOONAN and BANKS, 2000). HFD-fed

C57BL/6J, FVB/N and DBA/2J display only mild hyperglycemia and glucose intolerance. The 129X1 strain is the most glucose intolerant (MONTGOMERY et al., 2013) of all investigated mouse strains, when fed a HFD, and displays an increase in blood glucose concentration of 284% compared to control mice during an intraperitoneal glucose tolerance test. On the other hand, the C57BLKS/J strain, though closely related to the C57BL/6J mice, reacts to high fat diets by becoming more physically active and feeds self-restrictively. Thus, C57BLKS/J mice do not gain weight as quickly or develop insulin resistance (SIMS et al., 2013). The BALB/c strain is another strain that is unresponsive to HFD. BALB/c mice fail to develop adipositas or hyperglycemia (MONTGOMERY et al., 2013).

2.4 Murine models of diabetic nephropathy

In the following chapter, some of the most promising mouse models of diabetic nephropathy will be described shortly. While db/db and KK/Ta mouse models of diabetes mellitus type 2, described in chapter 2.3, can be utilized as models of DN, crossbreeding to create mouse models with several mutations or backcrossing of promising genetic variations on strains especially prone to the development of kidney lesions can be useful to better mimic human DN in the mouse model (BROSIUS et al., 2009; BREYER et al., 2005a). Mice with fasting blood glucose concentrations of more than 200-300mg/dl, depending on the source (MARRERO et al., 2013; FOX, 2007), are considered to be diabetic. No definition of DN in mice currently exists. Generally, mice display albuminuria, hyperfiltration and a varying collection of the histopathologic changes present in human patients with DN. No mouse model of DN achieves renal failure, which may point to either an insufficient duration of diabetes at the time of examination or an intrinsic resistance to kidney disease in the currently used mouse strains.

2.4.1 Bradykinin receptor deficient Ins2$^{Akita/+}$ mouse

Ins2$^{Akita/+}$ mice are a model for Mutant Ins-Gene Induced Diabetes of Youth (MIDY]. MIDY is a form of of permanent neonatal diabetes (LIU et al., 2010). These

mice develop hyperglycemia and albuminuria due to a spontaneous mutation in the Ins2 gene, which causes misfolding of insulin. They also show many signs of DN, like glomerulosclerosis and tubulointerstitial fibrosis, thickening of the glomerular basement membrane and detachment of podocyte foot processes (CHANG and GURLEY, 2012). Ins2$^{Akita/+}$ mice are available on a number of different genetic backgrounds. Ins2$^{Akita/+}$ on a FVB/N background display average blood glucose levels of 798$\pm$58 mg/dl, insulin levels of 0.11$\pm$0.08 μmol/l, a systolic blood pressure of 115$\pm$2 mmHg and 9.8 times higher albumin excretion compared to a control group. They display interstitial fibrosis scores of approximately 0.4, and glomerulosclerosis indices of 1 (KAKOKI et al., 2010).

Ins2$^{Akita/+}$ with a homozygous deletion of the Bdkrd2 gene (B2R-null Akita) on a C57BL/6J or C57BLKS/J background are used as a model of bradykinin 2 receptor (B2R) deficiency. BRKO(bradykinin receptor knockout mice)-Ins2$^{Akita/+}$ lack both B2R and B1R and display even more severe lesions of the kidney. Bradykinin is an endogenous polypeptide produced by the vascular kinin-kallikrein system that acts as a vasodilatator by stimulating the release of NO, prostacyclin or endothelium-derived hyperpolarizing factor. Additionally, B2R activation has a negative effect on the collagen I and IV synthesis stimulated through hyperglycemia, TGFβ and epithelial growth factor (BLAES et al., 2012) Clinical findings in B2R-null Akita deficient include stable blood pressure, comparable blood glucose and insulin levels, increased oxidative stress compared to Ins2$^{Akita/+}$ retaining both bradykinin receptors. Albuminuria is increased 1.8-fold in B2R-null Akita and 2.7-fold in BRKO Akita compared to Ins2$^{Akita/+}$. Semiquantitative measurements of interstitial fibrosis and glomerulosclerosis, are severely increased compared to wild-type controls. The interstitial fibrosis scores are approximately 1.4 and 3.3 and glomerulosclerosis indices approximately 1.5 and 2.3 respectively for B2R-null and BRKO Akita. All histological signs of DN present in the Ins2$^{Akita/+}$ mouse are found increased in severity in BRKO mice (KAKOKI et al., 2010).

2.4.2 Renin-overexpressing mouse with STZ-induced diabetes

Currently, several models of renin-overexpression exist on the 129S6/SvEvTac co-isogenic background. The genetic variations RenTgARE, RenTgKC and RenTgMK

display higher than normal plasma renin levels, leading to cardiovascular disease and nephropathy. Diabetes mellitus is induced either through low-dose STZ treatment or the Ins2$^{Akita/+}$ mutation (BREYER et al., 2005b). Blood glucose levels are dependent of the manner of diabetes induction. Albumin excretion varies from normal up to 10-fold increased, systolic blood pressure can reach up to 150mmHg. Histological observations include normal to severe glomerulosclerosis indices with inflammatory cell infiltration and tubulointerstitial fibrosis, according to unpublished observations (S.B.G. et al, found in (BROSIUS et al., 2009).

2.4.3 OVE26-transgenic FVB/N (FVB-OVE26) mouse

OVE26-transgenic FVB/N mice overexpress a calmodulin mini gene regulated by the rat insulin 2 promotor. The overexpression of calmodulin in the pancreatic β cells causes β cell toxicity, leading to severe early-onset type 1 diabetes. Due to a small population of surviving β cells, FVB-OVE 26 mice are not insulin dependent. Two month old FVB-OVE26 display average blood glucose levels of 594$\pm$11 mg/dl. Systolic blood pressure does not exceed 100mmHg. FVB-OVE26 develop pronounced albuminuria. At the age of nine months, albumin excretion exceeds 15000 μg/d, compared to approximately 2000μg/d in F1 hybrids of FVB-OVE26 and C57BL/6J mice. GFR, measured by FITC inulin clearance, decreases from 600μl/min at 3m, to just above 500μl/min at 9m (ZHENG et al., 2004). Histological alterations include glomerular hypertrophy, glomerulosclerosis, considerable tubulointerstitial fibrosis and GBM thickening (BREYER et al., 2005b). Mesangial volume is increased by factor 4 compared to the non-diabetic control in 10m old animals (ZHENG et al., 2004).

2.4.4 eNOS$^{-/-}$ mouse

Vascular endothelial nitric oxide synthase (eNOS) acitivity is lowered in this mouse model through polymorphisms in the NOS3 gene. Nitric oxide (NO) plays an important role in the management of vascular permeability and vasodilatation. Low NO levels lead to severe alterations in the kidneys of diabetic mice. This model has been established both on a C57BL/6J and C57BLKS/J background, with

diabetes being induced through various STZ-regimes. High-dosage STZ-diabetic B6-eNOS$^{-/-}$ develop more robust glomerulosclerotic and tubulointerstitial lesions, however, this is likely due to a direct toxic effect of the STZ on the kidneys. To avoid direct nephrotoxic effects, low-dosage STZ-regimes should be used (BREYER et al., 2005b). Although C57BL/6J-Ins2$^{Akita/+}$eNOS$^{-/-}$ die shortly after weaning, (C57BL/6J x 129SvEv)F1 hybrids carrying eNOS$^{-/-}$ and Ins2$^{Akita/+}$ are viable and show similar clinical alterations. As a model of type 2 diabetes, BKS-eNOS$^{-/-}$ mice have been crossbred with BKS-db/db mice (BREYER et al., 2005b). After a low-dose STZ-regime, 30w old eNOS deficient C57BL/6J develop severely increased blood glucose levels of about 650mg/dl, an increased systolic blood pressure of ca. 127mmHg and a 10-fold increase in albuminuria compared to wild.type controls. Unlike wild-type STZ-treated mice, eNOS$^{-/-}$ mice do not develop hyperfiltration. All mice displayed mild glomerular mesangial expansion, cell proliferation and mesangiolysis, 4.6% displayed global glomerulosclerosis (KANETSUNA et al., 2007).

2.4.5 Kuo Kondo - Agouti (KK-A^{y}/Ta) mouse

Established in 1969 by Nishimura et al., the KK-A^{y} was bred from KK mice and mice heterozygous for a mutation of the agouti gene called mouse lethal yellow (A^{y}). A^{y} mice are obese and insulin resistant (MICHAUD et al., 1994; HELLERSTROM and HELLMAN, 1963) KK-A^{y}/Ta mice display obesity, hyperinsulinemia and hyperglycemia, but no increase in blood pressure. Blood glucose levels average at 447$\pm$19 mg/dl casual and 84$\pm$2 mg/dl fasting blood glucose at the age of 20w. KK-A^{y} develop albuminuria with >400mg/g urinary albumin to creatinin ratio (WILLIAMS et al., 2007). Symptoms of DN like glomerular hypertrophy, moderate GBM thickening, podocyte fusion, podocyte loss, interstitial fibrosis and glomerulosclerosis are present, but no stereological data was made available (TOMINO, 2012; MACEDO et al., 2007; ITO et al., 2006; CHEN et al., 2002).

2.4.6 NONcNZO10/LtJ mouse

The NONcNZO10/LtJ is a congenic strain (definition in chapter 2.5) bred from nonobese nondiabetic mice (NON/LtJ) and the New Zealand obese mouse (NZO/HlLt) and is a polygenic model of type 2 diabetes. NONcNZO10/LtJ mice are only moderately obese compared to ob/ob or db/db mice. After weaning, NONcNZO10/LtJ mice are fed a diet containing 10% fat to promote the development of diabetes mellitus. Blood glucose levels of 24w old NONcNZO10/LtJ mice are averaging at approximately 466±35 mg/dl. The mice develop mild glomerulosclerosis and show increased PAS staining of the GBM (LEITER and REIFSNYDER, 2004). Though the renal alterations displayed by this strain can be severe, several features such as intracapillary glomerular lipid deposits and immunoglobulin deposits occur in the NON strain as well as in NONcNZO10/LtJ mice and are unrelated to diabetes (BREYER et al., 2005b; WATANABE et al., 1991).

2.4.7 Decorin deficient ($Dcn^{-/-}$) mouse with STZ-induced diabetes

The small leucine-rich proteoglycan decorin has the ability to bind to TGF-β and other growth factors that play a role in the development of mesangial expansion. In the tubulus, decorin can bind to the insulin-like growth-factor I receptor and prevent apoptosis of tubular epithelium caused by hyperglycemia (SCHONHERR et al., 2005). Decorin deficient mice are available on the C57BL/6J background. Mice are treated with standard STZ-regimes to induce diabetes mellitus. Blood glucose levels do not differ from those of wild-type STZ-induced diabetic mice. Compared to wild-type mice, $Dcn^{-/-}$ mice show 50% increased albuminuria, starting 6m after STZ treatment, and renal function is decreased by 23%. TGF-β levels are increased, and mononuclear infiltration can be observed. Mesangial matrix expansion is 1.5 times higher compared to wild-type diabetics and apoptosis of tubular epithelium can occur. Nodular glomerular sclerosis or tubulointerstitial fibrosis does not occur in this model (MERLINE et al., 2009; WILLIAMS et al., 2007).

2.4.8 Mice expressing a dominant negative glucose-dependent insulinotropic polypeptide receptor (GIPR^{dn}-tg mice)

Function of glucose-dependent insulinotropic polypeptide (GIP) and the GIP receptor

Glucose-dependent insulinotropic polypeptide, originally named gastric inhibitory polypeptide, is an incretin synthesized by K cells in the duodenum and proximal jejunum (BUCHAN et al., 1978). It consists of 42 amino acids, derived from its preprohormone precursor by proteolytic processing (GALLWITZ et al., 1996). The amino acid sequence of GIP is highly conserved and shows 90% homology for humans, pigs, cattle and rats. GIP is released after the consumption of carbohydrates and lipids. The amount of GIP released is directly proportionate to the amount of lipids and carbohydrates absorbed. The effectiveness of lipids in the stimulation of GIP secretion depends on species and dietary habits, lipids being a far more potent stimulant of GIP secretion in species with a high percentage of fat in their diet (i.e. humans). GIP binds to the GIP receptor expressed mainly on beta cells in the pancreas. The GIP receptor is a G-protein linked receptor of the secretin/VIP receptor family with seven transmembrane domains. The binding of the ligand to the N-terminal domain activates a heterotrimeric G-protein, and thus an adenylat-cyclase (GELLING et al., 1997). The adenylat-cyclase produces cAMP, which causes a Ca^{2+} influx through voltage-gated calcium channels. The increase of intracellular Ca^{2+} stimulates insulin excytosis (LU et al., 1993). GIPR is present in a variety of different tissues and cells, including pancreas, fat tissue, intestines, heart, adrenal cortex, hypothalamus, hippocampus, pituary, olfactory bulb, bone marrow stromal cells, osteoblasts and macrophages (NYBERG et al., 2005; KAPLAN and VIGNA, 1994; USDIN et al., 1993). In the presence of high plasma glucose levels, especially after oral administration, GIP stimulates insulin secretion from the beta cells of the endocrine pancreas. If, on the other hand, plasma glucose levels are low, GIP increases the secretion of glucagon. Thus it plays an important role in stabilizing blood glucose levels in healthy individuals. GIP also seems to influence beta cell number during post-natal islet neogenesis and apoptosis of beta cells in mice, as mice and pigs expressing a negative GIP receptor display decreased beta cell mass and decreased beta cell replication (HERBACH et al., 2011; RENNER et al.,

2010). Research has shown, that in diabetics, the effect of GIP on insulin secretion is impaired. Diabetic patients display a significantly decreased and delayed postprandial early phase and almost missing late phase reaction to GIP (VILSBØLL et al., 2002). Possible causes include impaired or missing GIP receptor functionality or postreceptor defects. While variances in the genetic sequence of the GIP receptor have been found, a clinical significance of the mutations is doubted. However, a reduced effectiveness of GIP has been shown in 50% of first degree relatives of diabetic patients (VILSBØLL et al., 2002). An inappropriate glucagon response in the presence of hyperglycemia and hyperinsulinemia has been discussed as a factor for the apparent reduced effectiveness of GIP in diabetics (CHRISTENSEN et al., 2013; DUNNING and GERICH, 2007). Another factor that might play a role in GIP effectiveness might be the by approximately 50% decreased amount of GIPR mRNA present in the beta cells of diabetic animals with persistent hyperglycemia (NOGI et al., 2012; XU et al., 2007). In the presence of insulin, GIP has a variety of effects on fat tissue. It stimulates fatty acid synthesis and the incorporation of fatty acids into triglycerides or adipose tissue, increases insulin receptor affinity for insulin, and can exacerbate conditions like obesity and fatty liver syndrome (YIP and WOLFE, 2000; YIP et al., 1998; WASADA et al., 1981). GIP receptor knockout ($GIPR^{-/-}$) mice do not display diet-induced obesity or insulin resistance, whereas mice overexpressing GIPR are prone to it. Part of this effect might be caused by a higher energy expenditure of GIPR deficient mice and a preference for using fat as an energy source. As GIP seems to act in concert with insulin, it also works contrary to glucagon and decreases glucagon-induced lipolysis. Furthermore, it stimulates the secretion and activity of adipose lipoprotein-lipase (LPL), which in turn further increases the uptake of triglycerides into adipose tissue. Additionally, GIP has a profound effect on bone density. Age-related bone density loss correlates with decreased GIPR mRNA in bone marrow stromal cells. $GIPR^{-/-}$ mice showed reduced bone mass, transgenic mice overexpressing GIP showed increased bone mass (DING et al., 2008).

$GIPR^{dn}$-tg mice on the outbred CD1 background

$GIPR^{dn}$-transgenic mice were generated on outbred CD1 stock and carry mutated GIP receptor cDNA. The loss of function of the mutated human GIP receptor

under the control of the rat proinsulin 2 promotor was demonstrated in vitro previously (VOLZ, 1997). Transgenic GIPR^{dn}-tg CD1 developed casual blood glucose levels of over 700mg/dl by the age of 6m. The 24h urine volume of GIPR^{dn}-tg CD1 was about 6-fold increased compared to controls. Albumin excretion per day was increased 7.7-fold compared to wild-types. Both GIPR^{dn}-tg and wild-type CD1 mice were endowed with 30000 nephrons and GIPR^{dn}-tg CD1 showed no signs of pathological nephron loss. Glomerular basement membrane thickness was significantly increased. GIPR^{dn}-tg mice displayed moderate to severe glomerulosclerosis and marked glomerular hypertrophy with mesangial expansion, enlarged capillary diameter and podocyte hypertrophy (POPPER, 2013; HERBACH et al., 2009).

GIPR^{dn}-tg mice on the inbred BALB/c background

To better understand the influence of the genetic background on the development of diabetes and DN, GIPR^{dn}-CD1 mice were backcrossed unto the inbred BALB/c strain. The BALB/c strain is one of the three most commonly used inbred mouse strains and popular as a general purpose strain in many different disciplines of basic research. GIPR^{dn}-tg BALB/c displayed casual blood glucose levels of 700mg/dl and higher by the age of 6m. BALB/c mice display a significantly higher baseline of ca. 127mmHg systolic blood pressure irrespective of transgenic status, compared to most other mouse strains (POPPER, 2013; SCHLAGER and WEIBUST, 1967). GIPR^{dn}-tg BALB/c produce only about one third of the 24h urine volume of GIPR^{dn}-tg CD1 mice. Only mild albuminuria, with 2.6 times increased albumin excretion in 24h, was be observed in GIPR^{dn}-tg BALB/c mice compared to GIPR^{dn}-tg CD1 mice. The glomerulosclerosis index of GIPR^{dn}-tg BALB/c mice was considerably lower compared to GIPR^{dn}-tg mice on a CD1 background. Nephron number was lower in BALB/c mice compared to CD1 mice, but no difference between wild-type and GIPR^{dn}-tg BALB/c animals could be observed. No measurable increase in glomerular basement membrane thickness was apparent in GIPR^{dn}-tg BALB/c mice vs. wild-type BALB/c mice. The mean glomerular volume of wild-type BALB/c mice was approximately 50% smaller than that of wild-type CD1 mice. GIPR^{dn}-tg BALB/c mice also showed a smaller percentile increase in mean glomerular volume compared to BALB/c-wt mice, than GIPR^{dn}-tg CD1 mice vs. CD1-wt mice.

The comparatively low glomerulosclerosis index displayed by GIPR^{dn}-tg BALB/c compared to GIPR^{dn}-tg CD1 mice might be due to the lower mean glomerular volume displayed by BALB/c mice compared to CD1 mice (POPPER, 2013).

2.5 Influence of the genetic background on the susceptibility to diabetes mellitus and diabetic nephropathy

2.5.1 Inbred and congenic mouse strains and outbred stock

A mouse strain is considered inbred if it can be traced to a single ancestral breeding pair and has been mated brother to sister for at least twenty consecutive generations (BECK et al., 2000). After those twenty generations, an average of 98.6% of loci are homozygous in each mouse of that strain. As all mice share the two ancestors initially used for breeding, they are also isogenic, which means they are virtually genetically identical (MOUSEGENOMEINFORMATICS). Many long established inbred mouse strains, i.e. C57BL/6J, FVB/N, BALB/c or DBA/2J, have been bred for more than a hundred generations and are now homozygous in all loci. Most inbred mouse strains have been bred for specific genotypes and the resulting specific phenotypes. The degree of genetic relationship between inbred mouse strains and substrains can differ significantly and depends on the subspecies of mice used to create the original founding strains and the amount of time that has passed since the divergence of substrains (WATERSTON et al., 2002; BECK et al., 2000). The distinct groups are the C57-related mice (i.e. C57BL/6, C57BLKS), the Castle's mice which split of from the C57 group during the early 20th century (i.e. 129/Sv, DBA/2), Swiss mice (i.e. FVB/N), mouse strains derived from Japan and China (i.e. KK/Ta) and mice derived from wild mice. Two more groups are comprised of "other" inbred strains with no relationship to each other or any of the previously described groups (i.e. A^{y}) and mouse strains descended from several inbred mouse strains (BECK et al., 2000). Genetic variation between inbred mouse strains has been measured by determining the number of single nucleotide polymorphisms (SNPs) present in various mouse strains. An average SNP density

of 1 in 500-700bp in C57BL/6J vs. 129S1, C3H and BALB/c mice (WATERSTON et al., 2002) was determined. Genealogically, C3H, 129S1 and BALB/c mice all belong to the Castle group of mouse strains, which split off from the C57BL/6 group, while FVB/N mice belong to the Swiss mouse group (BECK et al., 2000). The Swiss group of mice have had no contact whatsoever with C57BL/6 or Castle mice since they were founded (BECK et al., 2000). Considering the difference in contributing subspecies between C57BL/6J and FVB/N mice and the almost nonexistent degree of relationship, the number of SNPs of FVB/N versus C57BL/6J mice can be assumed to be considerably higher. Another important feature to be kept in mind when maintaining and using inbred mice is the high rate of genetic drift in a closed off livestock. A colony of inbred mice separated from a founding colony for 20 generations, spontaneously occurring mutations, residual heterozygosity and copy number variations can cause enough genetic drift to lead to substrain divergence. If possible, mice from the livestock of the original provider of a colony's animals should be crossed into that colony on a regular basis to reduce genetic drift (BAILEY, 1977).

In mouse genetics, "congenic" is a term used to describe organisms with a high genetical similarity. Congenic mice differ in only one locus, or even just one allele. If an interesting allele present in one inbred mouse strain, the so-called donor mouse strain, is supposed to be transferred to another inbred mouse strain, the recipient mouse strain, a special breeding scheme called backcrossing is used to produce a congenic mouse strain (GV-SOLAS, 2011). Conventional backcrossing requires ten generations (N10), while speed-congenic backcrossing, using a marker assisted selection protocol can reach the same level of homozygosity in seven generations. These breeding methods enable the investigation of the impact of a certain allele on different genetic backgrounds.

Outbred mouse stocks (i.e. CD1, NMRI) on the other hand, maintain genetic diversity and heterozygosity. Outbred mouse stocks are defined as a colony of genetically diverse mice closed off for at least four generations. For example, HsdWin:NMRI are outbred NMRI mice from a colony maintained by Harlan Sprague Dawley, Inc. (Hsd) since 1998. The founding animals of this colony were obtained from the colony at Winkelmann Versuchstierzucht GmbH & Co (Win). Crl:NMRI mice are outbred NMRI mice as well, but from a colony maintained by the Charles River Laboratories and genetically different from HsdWin:NMRI mice.

A rotational breeding scheme prevents to much inbreeding from occurring and aims to create maximum heterozygosity. Unlike inbred mice, outbred mice can vary greatly in phenotype as a reflection of their genetical heterozygosity.

2.5.2 C57BL/6J strain

All mice of the C57 group go back to the stock first bred by Miss Lathrop in 1921 (BECK et al., 2000) and have been inbred over many generations (current generation: F226PF235). Like most laboratory mice strains, the C57BL/6J strain is descended from several (sub)species of mice. Additionally to the usual subspecies Mus musculus musculus, Mus musculus domesticus and Mus musculus castaneus, remnants of genetic material of Mus spretus can be found in C57BL/6J mice (D. H. PERCY, 2007). The genome of C57BL/6J mice has been almost completely sequenced (WATERSTON et al., 2002) and the relationship to several other inbred mouse strains has been evaluated. It is currently the most commonly used mouse strain used in scientific research around the world. Several studies have noted the failure of diabetic C57BL/6J mice to develop anything more than mild renal lesions, even in the presence of severely increased blood glucose levels, but do not offer any insight as to the cause of that apparent insusceptibility (GURLEY et al., 2006). When fed a diet high in fat and carbohydrates, they are prone to develop a non-insulin dependent diabetes mellitus and high blood pressure (MILLS et al., 1993). According to data made available through the mouse phenome project, blood glucose levels of male 12w old C57BL/6J mice after a four hour fasting period average at 201mg/dl. The average systolic blood pressure of 10w old males was 113.7mmHg$\pm$3.2 (DESCHEPPER et al., 2004). BL/6 mice are known for their longevity (STORER, 1966).

2.5.3 FVB/N strain

FVB/N mice were bred from outbred albino swiss mice at the National Institute of Health (USA) and are characterized by their sensitivity to the B strain of the murine lymphoma virus (Friend virus). Unlike most strains of laboratory mice, swiss mice seem to be almost exclusively descended from Mus musculus domesticus

(D. H. PERCY, 2007). The large pronuclei of FVB/N mice make them ideal candidates for the direct microinjection of DNA for the production of transgenic animals (BECK et al., 2000). Several studies have noted that mouse models of DN displayed a significantly higher albumin excretion on the FVB/N background compared to almost any other genetic background. Severe albuminuria correlated with homozygosity for the FVB/N genotype in peaks on chromosomes 11, 13 and 19 in FVB-OVE26 x C57BL/6J crosses of the N2 generation. Also notably were the decreased mean glomerular volume and correspondingly decreased mesangial expansion and interstitial fibrosis displayed by FVB-OVE26 x C57BL/6J hybrids (XU et al., 2010). According to the Mouse Phenome Project Database (phenome.jax.org), blood glucose levels of male 12 week old FVB/N mice after a four hour fasting period average at 203mg/dl. The average systolic blood pressure of 10 weeks old males was 122.2mmHg$\pm$3.2 (DESCHEPPER et al., 2004).

2.5.4 Influence of the FVB/N and C57BL/6J genetic background on diabetes mellitus and diabetic nephropathy

The most likely factors to influence susceptibility to DN in transgenic mice are the degree of hyperglycemia, blood pressure, kidney architecture and the location and copy number of the inserted transgene. To investigate the influence of the FVB/N and C57BL/6J genetic background on diabetes mellitus and associated renal lesions, studies on DN using one or both of the strains were surveyed. The findings of this survey are listed in Table 2.2, p.31. A clear trend is immediately noticeable. Models of diabetes mellitus and DN using the FVB/N strain as a genetic background unfailingly develop severe hyperglycemia and albuminuria, and glomerulosclerosis is more severe compared to the same model on the C57BL/6J strain. In models of diabetes mellitus and DN using the C57BL/6J strain as a genetic background, the degree of hyperglycemia varies, with some models developing only very mild hyperglycemia and B2R$^{-/-}$ Ins2$^{Akita/+}$ C57BL/6J yielding the best results. Albuminuria does not reach the aim of a tenfold increase compared to wild-type controls in C57BL/6J mice, and only mild glomerular lesions were observed in the majority of models. None of the listed studies further addressed possible reasons for the observed differences in susceptibility to DN.

Table 2.2 FVB/N and C57BL/6J mice in DN research

Genetic back-ground	Mutations/diabetes induction	Blood glucose concentration (mg/dl)	Diabetes-associated renal lesions	Study
FVB/N	OVE26	803±30	(+) mesangial expansion	ZHENG et al.
			(+) glomerular hypertrophy	CARLSON et al.
			(+) increased GBM thickness	BREYER et al.
			(+) severe albuminuria (x12[1])	XU et al.
	db/db	300-400	(+) diffuse glomerular sclerosis	CHUA et al.
			(+) albuminuria (x10)	
	$Ins2^{Akita/+}$	700	(+) albuminuria (x10)	CHANG et al.
	STZ	570-610	(-) albuminuria (ACR)	QI et al.
			(+) albuminuria (UAE[2])	
			(+) mild mesangial expansion	
C57BL/6J	db/db	170-190	(+) glomerular hypertrophy (+22%)	HUMMEL et al.
			(+) mild glomerular sclerosis	SHARMA et al.
	$Ins2^{Akita/+}$	500	(+) albuminuria (x2.8)	GURLEY et al.
			(+) glomerular hypertrophy (+30%)	
			(+) mild glomerular glomerular sclerosis (0.95[3])	
	$B2R^{-/-}$, $Ins2^{Akita/+}$	798±58	(+) albuminuria (x4)	KAKOKI et al.
			(+) glomerulosclerosis (1.5)	
	$eNOS^{-/-}$, STZ	650	(+) mild mesangial expansion	KANETSUNA et al.
	$Os^{+/+}$[4], STZ	340±60	(+) mild sclerosis (0.83±0.26)	ZHENG et al.
			(-) glomerular hypertrophy	
	STZ	334±35	(+) albuminuria (34%)	GURLEY et al.
			(+) mild glomerular sclerosis (0.66±0.09)	
	HFD	138-259	none	NOONAN and BANKS

[1] increase compared to control group
[2] UAE: urinary albumin excretion (μg/24h)
[3] glomerulosclerosis index, between 0 (no alterations) and 4 (glomerulosclerosis with total tuft obliteration in all observed glomeruli).
[4] Os: oligosyndactyly mutation, that causes a 50% decrease in nephron number

3 Materials and methods

A list of the performed analyses and corresponding sample sizes is shown in Table 3.1, p.70. The animal experiments were conducted according to the specifications of the local ethics committee and the regional government of Upper Bavaria (55.2-1-54-2531.3-49-10).

3.1 Animals

3.1.1 Breeding

The C57BL/6J mice used for breeding were obtained from the Institute of Molecular Animal Breeding and Biotechnology of the LMU Munich (Germany) and were maintained in the Institute of Veterinary Pathology, LMU, München. Male $GIPR^{dn}$-transgenic mice on a CD1 background were breed to C57BL/6J wild-type females. The resulting male transgenic offspring was backcrossed on C57BL/6J wild-type females for six generations. $GIPR^{dn}$-transgenic males and their male wild-type litter mates of the sixth backcrossed generation (N6) were used for this study. Approximately 1.6% of the diploid genome of the CD1 background remains in the N6 generation of $GIPR^{dn}$-transgenic C57BL/6J mice.
The FVB/NJ mice were generously donated by the Medical Research Council (UK), via the University of North Carolina (USA) and the Laboratory for Functional Genome Analysis (LAFUGA), Gene Center of the LMU Munich (Germany). Male $GIPR^{dn}$-transgenic mice on a CD1 background (N37) were breed to FVB/N wild-type females (Figure 3.1, p.33). The resulting male $GIPR^{dn}$-transgenic offspring was backcrossed on FVB/NJ wild-type females over several generations to obtain

congenic animals. The transgenic males and their sex-matched wild-type litter mates of the N25 were used for this study. Approximately 2.98 x 10^{-4}% of the diploid genome of the CD1 background is still present in GIPR^{dn}-transgenic FVB/N mice of the N25.

Figure 3.1 Breeding scheme of GIPR^{dn}-tg FVB/N and C57BL/6J mice by backcrossing

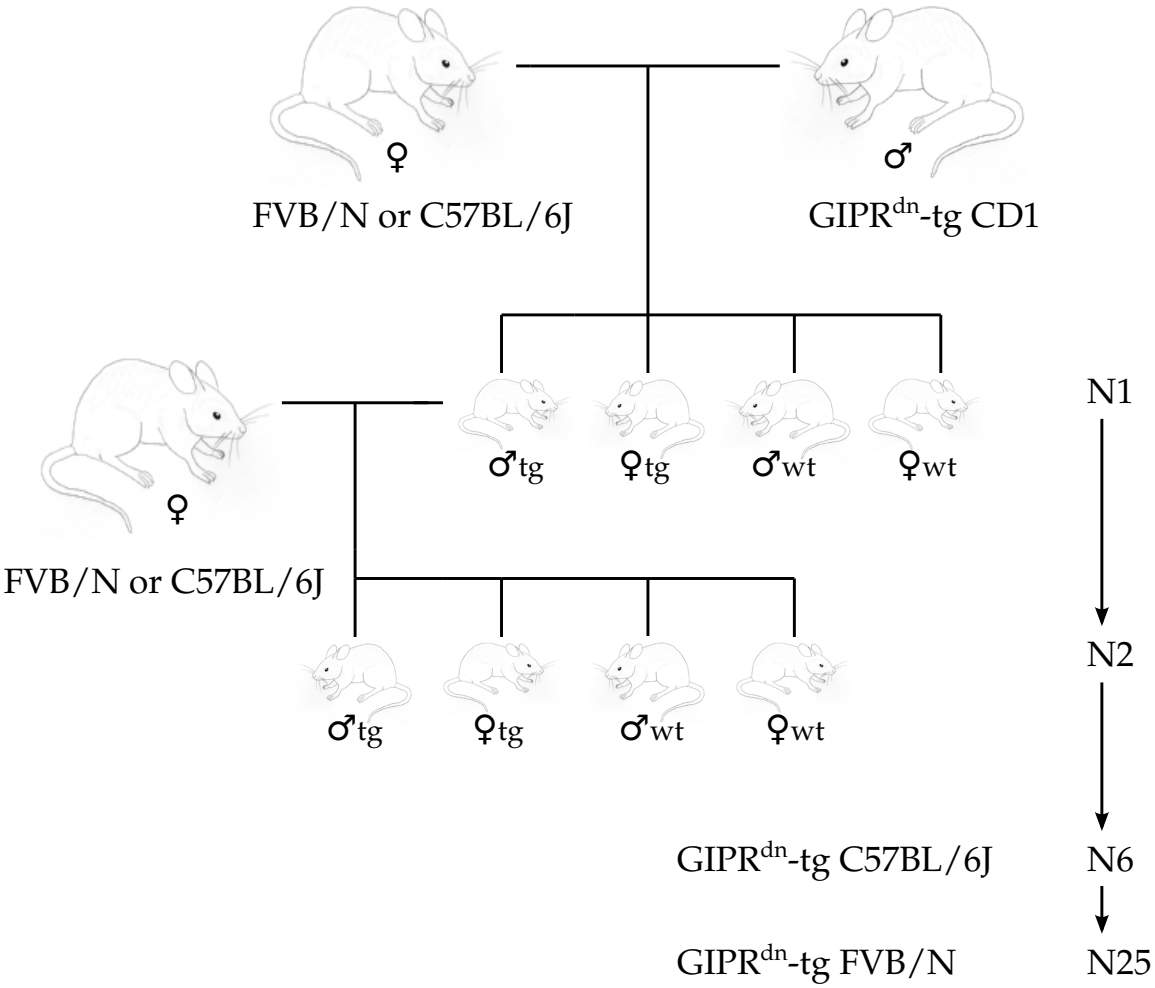

N1-25: number of backcrossed generations, **wt**: wild-type, **tg**: transgenic. Drawings of mice courtesy of Dr. Andreas Blutke, Institute of Veterinary Pathology, LMU München.

3.1.2 Animal husbandry

Environmental conditions were realized according to the guidelines by the Society for Laboratory Animal Science (BUSCH et al., 2014). A light cycle of 12 hours light, followed by 12 hours of darkness was implemented. The light intensity did not surpass 200 lux . The room temperature was kept within the range of $20° - 24°$C, the air humidity between 45% and 65%. Standard cages type II and III (Makrolon, Ehret, Germany) with hygienic animal bedding (Lignocel®, J. Rettenmaier & Söhne, Germany) were used to house mice. Environmental enrichment in the form of nesting material (cellulose paper) was offered to all animals. Tap water ad libitum and a standard diet for mice and rats (Altromin 1324, Germany) was provided. At the age of 3 weeks, the mice were weaned from their dams, separated by gender and marked through ear piercing.

3.1.3 Genotyping by polymerase chain reaction (PCR)

Genotyping was performed according to a protocol established in the Institute of Veterinary Pathology, LMU München (HERBACH, 2002), in which transgenic mice are identified via polymerase chain reaction from DNA extracted from tail tip biopsies.

DNA extraction

Tail tip biopsies of approximately 0.5cm length, obtained prior to perfusion from euthanized mice, were incubated with 400μl Mastermix in a heating block (Biometra TB1 Thermoblock, Whatman, Germany) over night, at 55C. Two minutes of centrifugation at 15.000 rpm (Sigma 1k15, Sigma, Germany) were used to separate digested from undigested material. The supernatant was transferred into a fresh 1.5ml reaction cup (Eppendorf, Roche, Germany). The DNA was precipitated by adding 400μl isopropanol (Roth, Germany) and vigorous shaking of the cups. Then the resulting DNA pellet was washed twice with 900μl of 70% ethanol (Roth, Germany). After the removal of the liquid phase, the pellet was dried at room temperature. Depending on the size of the dried DNA pellet, 100-200μl of TE buffer

were used to dissolve the DNA. Complete dissolution was ensured by storing the samples at 4° for 24h.

Mastermix

Cutting buffer	375μl
SDS 20% (Roth, Germany)	20μl
Proteinase K (20mg/ml) (Boehringer Ingelheim, Germany)	5μl

Cutting buffer

1M Tris-HCl (pH 7.5, Roth, Germany)	2,5ml
0.5M EDTA (pH 8.0, Sigma, Germany)	5.0ml
5M NaCl (Roth, Germany)	1.0ml
1M DTT (Roth, Germany)	250μl
Spermidine (500mg/ml, Sigma, Germany)	127μl
Aqua bidest.	ad 50ml

TE-buffer

10mM Tris-HCl (pH 8.0, Roth, Germany)
1mM EDTA
Storage at 4°C

Polymerase chain reaction (PCR)

All components were cooled on ice. The Taq DNA polymerase (Taq PCR Master Mix Kit, Qiagen, Germany) was stored at -20°C and defrosted directly prior to being added to the Mastermix. In PCR-analysis cups (Kisker, Germany), 1μl of the dissolved DNA was added to 19μl of the Mastermix. As positive and negative controls, DNA of mice of known status (wild-type and GIPR^{dn}-transgenic) were used. Distilled water served as an internal (no template) quality control. The PCR

was performed in a Biometra® Uno II Thermocycler (Biometra, Germany). Initially, the samples were heated to 94°C for 4min, followed by 35 cycles of 94°C for 1min, 60°C for 1min and 72°C for 2min. After 10 more minutes at 72°C, the thermocycler cooled down the samples to 4°C.

The following oligonucleotid primers were employed for the polymerase chain reaction:

-5'-ACA GNN TCT NAG GGG CAG ACG NCG GG-3' sense (Tra1)
-5'-CCA GCA GNC NTA CAT ATC GAA GG-3' antisense (Tra3)
(Synthesis, Ludwig-Maximilians-Universität, Munich, Germany)

The primers bind to the mutated human GIP receptor, but also to the murine GIP receptor. In the places where variations do occur, oligonucleotid synthesis, marked "N" in the primer sequence, was used to allow all nucleotides to attach (HERBACH (2002)). A difference in the number of base pairs allows for a differentiation of the mutant human (140bp) and endogenous murine (500bp) receptor.

Mastermix (Taq PCR Master Mix Kit, Qiagen, Germany)

1mM dNTP	4μl
10x Qiagen PCR buffer	2μl
$MgCl_2$	1.25μl
Primer sense (Tra1), 10pmol/μl	1μl
Primer antisense (Tra3), 10pmol/μl	1μl
RNase-free water	5.7μl
Q-solution	4μl
Taq-polymerase	0.125μl

Gel electrophoresis

The PCR products were separated by molecular size, weight and charge through gel electrophoresis. A TAE agarose gel (1,5%, 1,5g agarose (Gibco BRL, Germany)/100ml TAE buffer) in a Easy Cast® gel chamber (PeqLab, Germany) was

used. Both the TAE buffer used to make the gel and the TAE running buffer contained 9μl/l ethidiumbromide (0.1%, Merck, Germany). 4μl of 6x loading dye (MBI Fermentas, Germany) were added to each sample. The first well of each row was filled with 12μl of a size standard (PUC Mix Marker, MBI Fermentas, Germany). Remaining wells were each filled with 24μl of the samples. The electrophoresis was run at 90 V and 200 mA (Biorad Power PAC 300, Biorad, USA) for 45 minutes. The bands then were made visible under UV light (306 nm, Eagle Eye II, Stratagene, Germany) and the result was documented.

TAE buffer

Tris base (Roth, Germany)	2.42g
Glacial acetic acid (Sigma, Germany)	0.571ml
EDTA 0.5M, pH 8.0 (Sigma, Germany)	1ml
Aqua bidest.	ad 500ml

3.1.4 Blood pressure measurement

Noninvasive blood pressure measurements were performed on six months old mice. Prior to the blood pressure measurement, the animals were acquainted thoroughly to the automatic system over a timespan of two weeks. The system consisted of an occlusion tail cuff and a pressure recording sensor (CODA System, Kent Scientific, USA). The measurement of systolic, diastolic and mean blood pressure were performed on three consecutive days, between 8am and 11am. The results of one measurement cycle per day, consisting of 10 separate measurements, were averaged.

3.1.5 Quantitative and semiquantitative determination of glucose concentrations in urine and blood

All animals were tested for glucosuria, using diagnostic dipsticks for glucose detection (Macherey-Nagel, Germany). Urine was collected by gently stroking the animal's abdomen to encourage spontaneous micturition and caught with a

plastic cup (Eppendorf, Roche, Germany). The dipsticks were used according to the manufacturer's instructions. At six months of age, casual blood glucose levels were determined. At 3pm, blood was drawn from the tail vein into a 10μl capillary (Hirschmann, Germany) by incising the tail tip. The samples were immediately transferred into plastic cups (Eppendorf Roche, Germany) filled with 500μl haemolysing solution (Hitado, Germany). After calibration with a control solution of known glucose concentration, all samples were analyzed with the Super GLeasy automatic system (Hitado, Germany).

3.1.6 Serum parameter measurements: Creatinine, urea, triglyceride, protein and ion concentrations

Serum was collected from 6 months old male mice by drawing blood from an incision in the tail tip into a capillary (Brand, Germany). The drawn volume (170-190μl) did not exceed 10% of the animals' blood volume, calculated as 6.6% of the animals' body weight (MORTON et al., 1993; FURUHAMA and ONODERA, 1983). The blood was transferred into a plastic cup (1.5ml Eppendorf, Roche, Germany) and centrifugated for 10min at 10.000 x g (Sigma 1k15, Sigma, Germany). The serum was separated from the solid phase and stored at -80°C. Determination of serum creatinine, urea, triglycerides, total protein, albumin, chloride and sodium concentrations was graciously performed by the City Clinic Munich, Schwabing, Germany (Architect ci8200 Autoanalyser, Abbott, Germany).

3.1.7 Cystatin C serum concentration

For the determination of cystatin C serum concentrations, the mouse cystatin C ELISA kit (BioVendor, Czech Republic) was used according to the manufacturer's instructions. All steps were performed at room temperature. Next to a coated microtiter plate, the kit contains all required solutions, standards, quality controls and antibodies ready to use. First, 100μl each of the provided standards, high and low quality controls and the samples (diluted 1:500 with dilution buffer), as well as a blank (pure dilution buffer) were pipetted into their assigned wells in

duplicate. The plate was incubated on a microplate shaker (Corning® LSE^{TM} digital microplate shaker) at 300rpm for 1 hour. Then, three rounds of washing, using 350μl of washing solution, were performed. 100μl of biotin-labeled antibody were added to the wells and again left to incubate the microplate shaker for 1 hour, before repeating three washing steps. 100μl of streptavidin-horseradish-peroxidase conjugate were added to each well to incubate for 30 minutes on the microplate shaker. After another three washing steps, 100μl substrate solution were added and incubated under an opaque cover for 10 minutes. 100μl stop solution were added and the plate was immediately measured at a wavelength of 450 nm and 630 nm in a microplate reader (Magellan, Tecan AG, Germany). A standard curve was plotted automatically by the microplate reader program. Following to the manufacturer's manual, the reading at 630 nm was subtracted from the 450 nm measurement and the results of the duplicate readings were averaged.

3.1.8 Urine parameter measurements

Urine creatinine, urea and ion concentrations

Urine collected over a time period of 24h was centrifugated for 10 min at 10.000 x g (Sigma 1k15, Sigma, Germany) to remove impurities and stored at -80°C. Creatinine, urea, sodium and chloride concentration were determined with the Architect ci8200 Autoanalyser (Abbott, Germany) in the City Clinic Munich, Schwabing, Germany.

Urine albumin concentration

The mouse albumin ELISA kit Bethyl E90-134 (Bethyl, USA) was used in compliance with the manufacturer's recommendations to determine the urine albumin concentrations. Urine samples of 6 months old mice were collected from metabolic cages over a 24h period. First, the plate (Nunc C bottom Immunoplate 96 wells, Nunc A/S, Denmark) was coated with goat anti-mouse albumin capture antibody (1mg/ml A90-134A). 1μl of antibody was diluted with 100μl of coating buffer and the plate was incubated at room temperature for 1h. Three rounds of washing were

performed by pipetting and then aspiring 200μl of washing solution into each well. Unspecific binding sites were blocked with 200μl of blocking solution left in the wells for 30min. After the removal of the blocking solution, the plate was washed three times. Standard dilutions of mouse albumin were produced according to the manufacturer's directions (7.8 - 500 ng/ml). The predicted albumin concentration of the urine samples was used to calculate a dilution with a concentration that would fall within the range of the standards. Ultimately, samples were diluted with sample diluent between 1:200 and 1:6400. Every sample was analyzed in duplicate, and the second sample was diluted by the factor two compared to the first sample. 100μl of standard and samples respectively were pipetted into the wells. Aqua dest. served as a negative control. The plate was incubated for one hour and then washed five times. 100μl of horseradish peroxidase conjugate (1mg/ml goat anti-mouse albumin HRP-conjugate, A90-134P-22), diluted 1:100.000 in conjugate diluent, were pipetted into each well and incubated under an opaque cover for 60min. Another five rounds of washing were performed. Then, 100μl of substrate solution (TMB/H_2O_2, Kirkegaard and Perry, USA), an equal mixture of substrate reagents A and B, were added. The plate was placed under a light-tight cover for an incubation period of 7min. The reaction was stopped by adding 100μl of 1M H_3PO_4 (Roth, Germany). A computer-assisted microplate reader (Magellan, Tecan AG, Germany) measured the light absorption at 450 nm. The results of the duplicate readings were averaged and a standard curve (Magellan, Tecan AG, Germany) calculated for each plate. The value of the water's colour intensity was subtracted from the averaged sample values. Only values within in the range of the linear part of the standard curve were accepted.

Materials used for ELISA

Coating buffer

0.05M Carbonate-bicarbonate (Sigma, Germany) adjusted to pH 9.6

Washing solution

50mM TRIS (Roth, Germany)

0.14M NaCl (AppliChem, Germany)
0.05% Tween 20 (Roth, Germany)
adjusted to pH 8.0

Blocking solution

50mM Tris (Roth, Germany)
0.14M NaCl (AppliChem, Germany)
1% Bovine serum albumin in Tris buffered saline (Sigma Chemical, Germany)
adjusted to pH 8.0

Sample- /conjugate diluent

50mM Tris (Roth, Germany)
0.14M NaCl (AppliChem, Germany)
1% Bovine serum albumin in Tris buffered saline (Sigma Chemical, Germany)
0.05% Tween 20 (Roth, Germany)
adjusted to pH 8.0

Urine albumin to creatinine ratio (UACR)

UACR (mg/g) was calculated by dividing the urine albumin concentration (mg/dl) through the urine creatinine concentration (g/dl).

Estimated glomerular filtration rate (eGFR)

The glomerular filtration rate is calculated as the volume of the primary urine divided by the time in which it was filtrated. The estimated glomerular filtration rate uses creatinine clearance as a measure of actual GFR.

Equation 1:

$$eGFR = \frac{c_{crea\ urine} \times V_{urine}}{c_{crea\ serum} \times t}$$

$eGFR$: estimated glomerular filtration rate
$c_{crea\ urine}$: creatinine concentration in the urine
V_{urine}: urine volume
$c_{crea\ serum}$: creatinine concentration in the serum
t: time in which the urine volume was produced

3.1.9 Food and water consumption and 24h urine collection

To determine the food and water consumption and collect 24h urine samples, 180d old mice were kept in metabolic cages (Techniplast, Germany) over 24 hours. Before the start and after the end of the 24 hours, the body weight of the mice and the weight of feed and water were measured to the nearest 0.1g on a precision scale (Kern 440-43, Kern & Sohn GmbH, Germany). The obtained urine samples were stored at -80°C, protected from evaporation.

3.2 Perfusion fixation and processing of kidneys

3.2.1 Vascular perfusion fixation of the kidneys

Orthograde vascular perfusion was performed on eight 6 month-old mice per group. A system with two bottles containing buffer and paraformaldehyde, suspended approximately 1.2m above the working space and connected via a three-way valve to a perfusion needle, was used for the perfusion (Figure 3.2, p.43). Due to the set-up, a constant hydrostatic pressure was maintained (WANKE, 1996). The animals were killed by cervicocranial dislocation. The abdominal and thoracical cavities were opened with scissors. A gauge 20 needle (Sterican® Gr.1, B. Braun Melsungen AG, Germany) was used to pierce the left ventricle (Figure 3.3, p.44). Approximately 2ml Lidocain (Lidocainhydrochloride 2%, bela-pharm, Germany), inserted via the

three-way valve, were perfused first to dilate the vascular system. At the start of the perfusion process, the Vena cava caudalis was severed within the thoracic cavity to maintain a steady pressure and enable the perfusate to drain out. For the following two minutes PBS (pH 7.4, 37°C) was perfused by hydrostatic pressure, until all blood was removed from the circulation and the perfusate discharge appeared clear. The system was then switched to 4% paraformaldehyde (Serva, Germany) dissolved in PBS (pH 7.4, 37°C) for 5 minutes.

Figure 3.2 Cardial perfusion setup

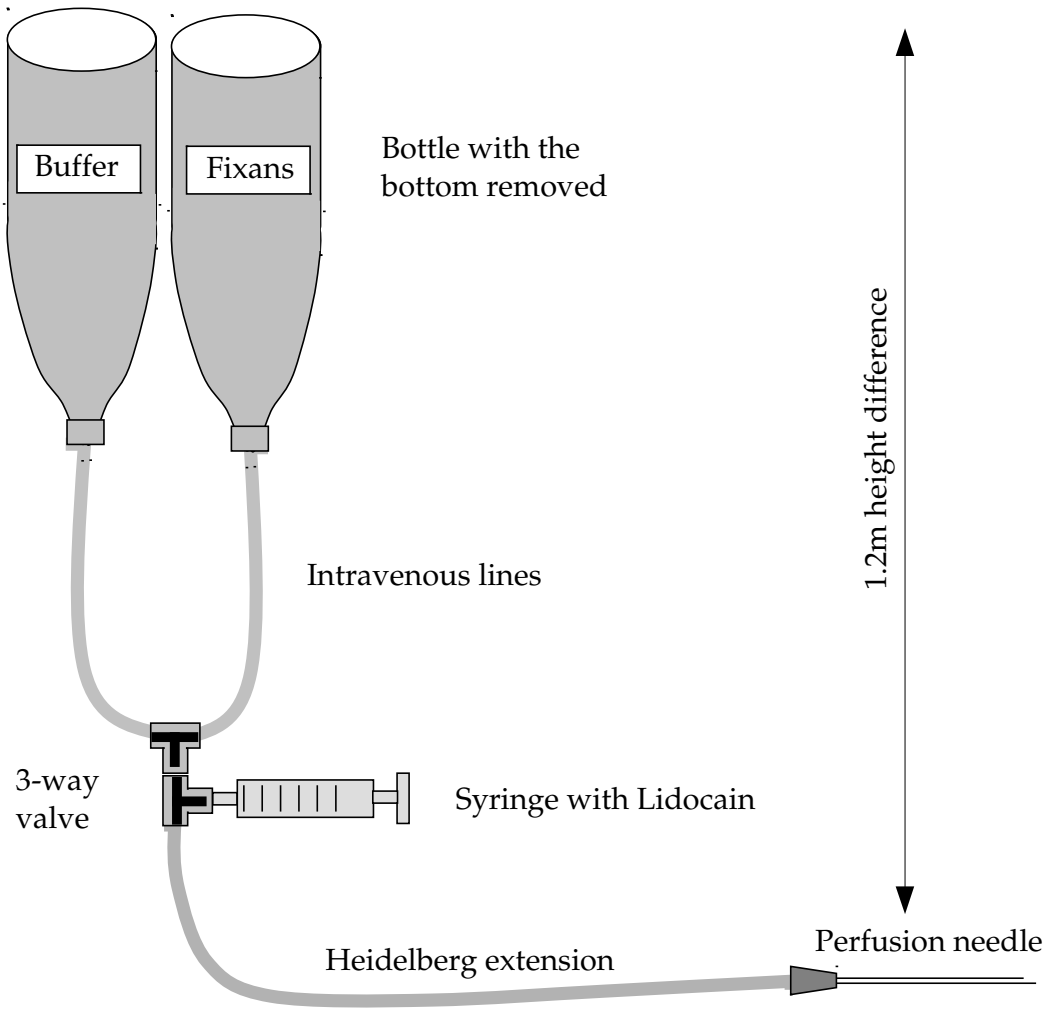

IV: intravenous. Picture courtesy of Dr. Andreas Blutke, Institute of Veterinary Pathology, LMU München

Figure 3.3 Perfusion of a mouse

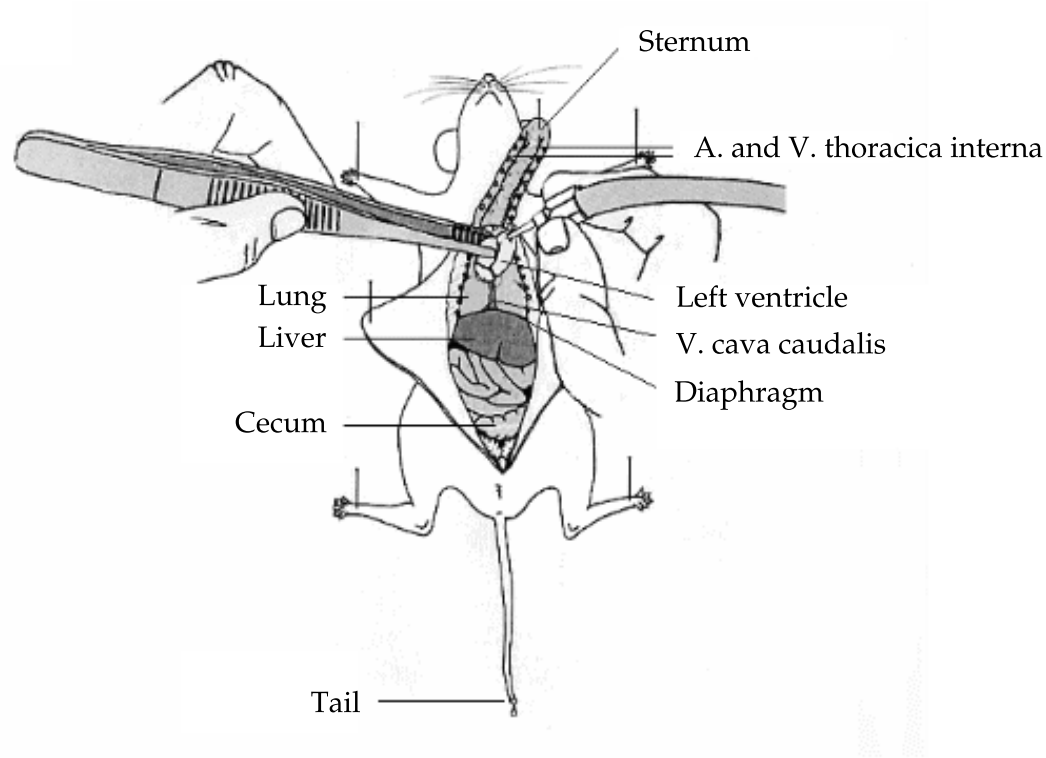

Picture courtesy of Dr. Andreas Blutke, Institute of Veterinary Pathology, LMU München

Materials used for kidney perfusion

Phosphate-buffered saline (PBS)

Sodium chloride (AppliChem, Germany)	8.0g
Potassium chloride (AppliChem, Germany)	0.2g
Potassium dihydrogen phosphate (AppliChem, Germany)	0.27g
Disodium hydrogen phosphate dihydrate (AppliChem, Germany)	1.78g
ad 1l Aqua dest.	
adjusted to pH 7.4	

4% Paraformaldehyde (PFA) in PBS (pH 7.4)

Paraformaldehyde (Serva, Germany)	40g

PBS pH 7.4	1l

3.2.2 Kidney processing for histology, immunohistochemistry and quantitative stereology

The entrails were removed and the carcass with the kidneys was submerged in 200ml 4% paraformaldehyde solution for 24 hours. The kidneys were blotted dry on paper, stripped of their capsules and weighed separately to the nearest milligram on a precision scale (Mettler AE200, Germany). A caliper gauge (Mannesmann, Germany) was used to measure the longitudinal length of each kidney. Every kidney was laminated vertically to the longitudinal axis by a microtome blade with the help of a laminator (design: Dr. Andreas Blutke, Figure 3.4, p.46). To facilitate the cutting of even, 1mm thick slices, the kidneys were embedded in agar (Bacto^{TM} agar, BD, USA). With the help of a dot matrix and random numbers, three locations in the cortex of each kidney were chosen by systematic random sampling (NYENGAARD, 1999) for epon embedding (Figure 3.5, p.47). The tissue samples of approximately 1mm diameter were obtained using a self-designed tissue punch and stored in plastic cups (Eppendorf, Roche, Germany) filled with 4% PFA solution in PBS (Figure 3.5, p.47). From each kidney, two slices were chosen randomly for paraffin embedding and placed in embedding capsules (Engelbrecht, Germany). They were fixed inside the capsules with pieces of sponge (Bio Optic, Italy). In the same manner, all remaining slices went on to GMA/MMA embedding.

3.2.3 Paraffin embedding and detection of glomerular matrix proteins and TGFβ1 by immunohistochemistry

After 24h of fixation in 4% paraformaldehyde, the samples were processed in a Histomaster 2050 (Bavimed, Germany, protocol p.47) and embedded in paraffin with the TBS 88 Paraffin Embedding System (Medite, Germany). Approximately 3-5μm thick sections were cut from the paraffin blocks with a HM 315 rotary microtome (Microm, Germany), put in a water bath (60°C, Daglef Patz, Germany) to unfold, and mounted on coated glass slides (Starfrost, Engelbrecht, Germany).

Figure 3.4 Lamination of kidneys

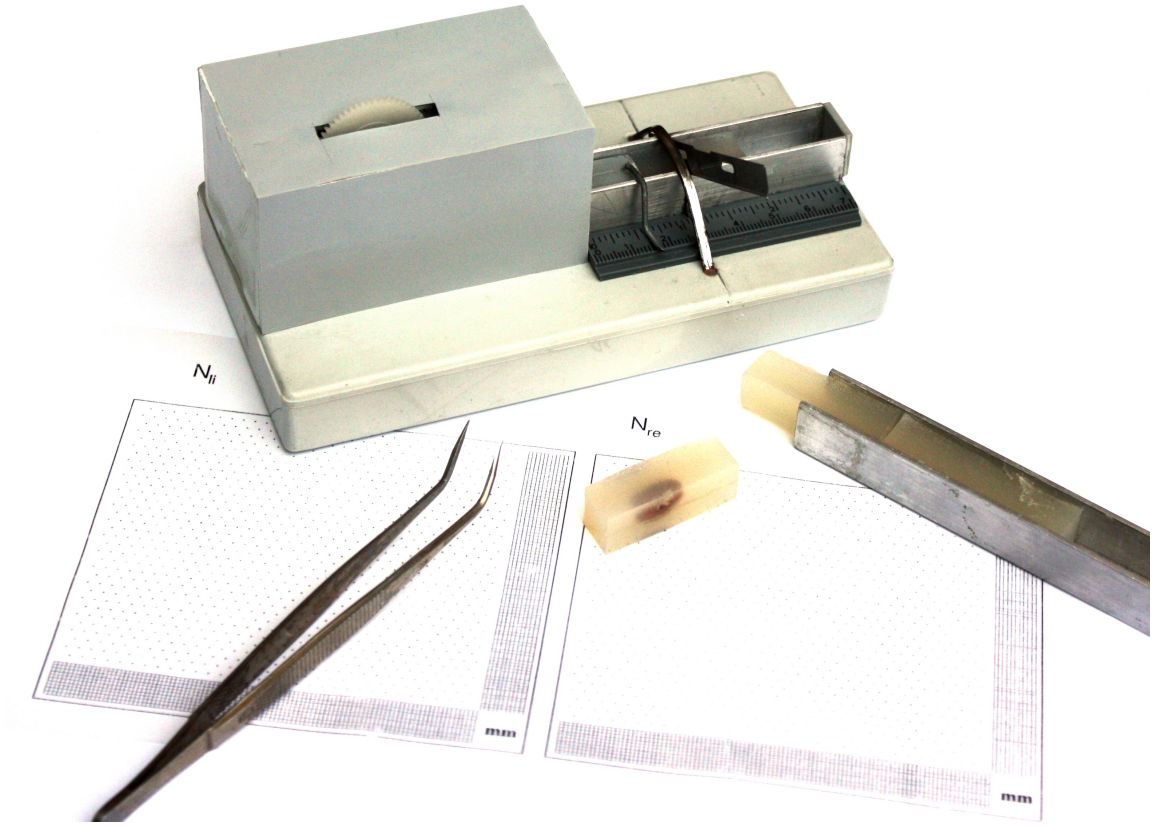

Finally, the sections were dried in a heating cabinet (Memmert, Germany) at 40°C for 24h. For the detection of laminin, fibronectin, collagen IV and TGFβ1, three animals per group were selected randomly.

Dehydration and paraffin embedding of kidney sections

30min Aqua dest.
2 x 1.5h 70% Ethanol (Bundesmonopolverwaltung für Branntwein (BfB), Germany)
2 x 1.5h 96% Ethanol (BfB, Germany)
2 x 1.5h 100% Ethanol (BfB, Germany)
1.5h Xylol (SAV LP, Germany)
2h Paraffin (60°C, Sherwood Medical, USA)

Figure 3.5 Sampling for epon embedding

Sampling of kidney slices with the help of a dot matrix and a tissue punch

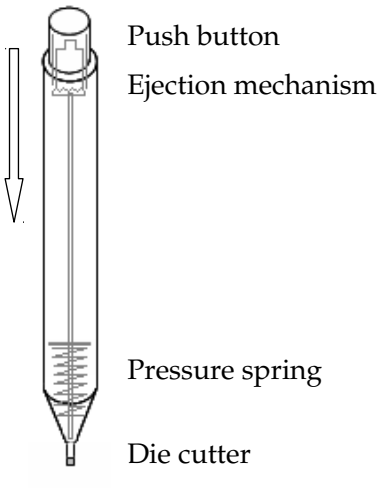

Tissue punch

Picture of the tissue puncher courtesy of Dr. Andreas Blutke, Institute of Veterinary Pathology, Ludwig-Maximilians-Universität München

3h Paraffin (60°C)

Materials used for immunohistochemistry

Tris buffer (TBS) pH

Tris (Roth, Germany)	6.05g
NaCl (AppliChem, Germany)	9g
Aqua dest.	ad 1000ml
adjust to pH 7.6	

Detection of laminin and fibronectin by immunohistochemistry

After drying overnight in a heating cabinet (37°C), the sections were deparaffinised and rehydrated by being immersed in xylol for 20 minutes and passing through a descending series of ethanol (100%, 96% and 70%) and Aqua dest. To block the endogenous peroxidase in the samples, they were then rinsed in 1% H_2O_2 for 15min, then rinsed again in TBS for 10min. Proteinase K (Dako Diagnostika, Germany) was used to facilitate tissue penetration (antigen retrieval) by completely covering the sections with the ready-to-use solution. The sections in their humidity chamber were placed in an incubator (Memmert, Germany) at 37°C for 30min. Another 10min of rinsing in TBS preceded the blocking of unspecific binding sites with normal serum (pig serum, 10% in TBS) for 30 minutes. The sections were tilted to remove the serum and then covered with the primary antibody (rabbit anti-mouse laminin, 4.1g/l (DAKO, Germany) and rabbit anti-mouse fibronectin 5.1g/l (DAKO, Germany) respectively), diluted 1:100 in TBS. Again, the humidity chamber with the sections was incubated at 37°C for 2 hours. The slides were washed in TBS for 10 minutes. Then, the section were covered with the secondary antibody, polyclonal swine anti-rabbit IgG (Dako, Denmark), diluted 1:100 in TBS containing 5% normal mouse serum. The sections were incubated at 37°C for 1 hour. Sections were rinsed in TBS for 10 minutes prior to target antigen detection with 3,3'-Diaminobenzidine (DAB, Sigma, Germany). Previously, the DAB pellet had been dissolved in 5ml of Aqua dest. beneath an opaque cover. Immediately before application, 1% H_2O_2 was added to the DAB. Depending on the strength of the reaction, the DAB was left on the sections for up to 5 minutes, then it was washed off in Aqua dest. for 2 minutes. The kidney sections were counterstained at room temperature with Hemalaun diluted 1:10 in Aqua dest. for 20-60 seconds, rinsed off briefly in cold tap water and dehydrated in 70%, 96% and 100% ethanol solutions. After immersion in xylol, the sections were mounted with glass cover slides. As a negative control, the primary antibody was replaced by TBS in an additional section. A positive control was deemed unneccessary, as kidneys naturally contain laminin and fibronectin.

Detection of collagen IV by immunohistochemistry

The protocol for collagen IV is identical to the protocol for laminin and fibronectin, except for antibodies and antibody concentrations. As a primary antibody, rabbit anti-human placental type IV collagen (Quartett, Germany) was used in a dilution of 1:40 in TBS. The secondary antibody (polyclonal swine anti-rabbit IgG, Dako, Denmark) was diluted 1:50 with TBS containing 5% mouse normal serum. As a negative control, the primary antibody was replaced by TBS in an additional section. No additional positive control was considered necessary, as kidney tissue can be used for that purpose.

Detection of transforming growth factor β1 (TGFβ1) by immunohistochemistry

The avidin-biotin peroxidase method, coupled with tyramin amplification was used to detect TGFβ1. All preparation steps up to the blocking with normal serum were performed as described for the detection of laminin and fibronectin. Instead of pig, 10% normal goat serum was used. The primary antibody, 200μg/ml rabbit anti-TGFβ1 (Santa Cruz Biotechnology, USA), was diluted 1:400 in TBS. Incubation at 37°C lasted for 2 hours. After washing in TBS, the secondary antibody, biotinylated goat anti-rabbit IgG (Vector Laboratories, USA) diluted 1:200 in TBS with 10% normal mouse serum, was applied for 1 hour at 37°C. The sections were rinsed in TBS for 10 minutes, before avidin-biotin complex (Vectastain ABC kit, Vector, USA) was added in a dilution of 1:100 for 30 minutes at room temperature. Again, the sections were rinsed in TBS for 10 minutes. Biotinylated Tyramin (0.5%, ProteoChem, USA) and H_2O_2 (1%) in TBS were added to the sections for 15 minutes. Avidin-biotin complex (1:100 in TBS) was applied to the sections and left to incubate at room temperature for 15 minutes. Antigen detection and counterstaining were carried out as specified before. As a negative control, the primary antibody was replaced by TBS in an additional section. Murine uterine tissue was used as a positive control.

Biotinylating of tyramin for TGF-β1 immunohistochemistry

NHS-LC-Biotin (ProteoChem, USA)	100mg
Borate buffer, pH 9.0 (Sigma, Germany)	40ml
Tyramine hydrochloride (Sigma, Germany)	30mg
shake for 12 hours	

3.2.4 Glycolmethylacrylate and methylmethacrylate (GMA/MMA) embedding and staining of GMA/MMA sections

After fixation, the tissue samples destined for glycolmethacrylate and methylmethacrylate (GMA/MMA) embedding were routinely processed in a Citadel 1000 tissue processor (Shandon, Germany) according to the protocol listed below. The embedding followed the protocol described by HERMANNS et al. (1981). All kidney sections were first immersed in a 1:1 2-hydroxymethylmethacrylate (Flika Chemie, Germany) : methylmethacrylate (Merck, Germany) solution and remained on a shaking plate (model 4010, Köttermann, Germany) for 24h at 4°C. Then the tissue samples were transferred into solution A and left to saturate at 4°C for 4 hours. Next, they were transferred in polyethylene cups (LDPE, Diagonal, Germany) and embedded in about 40ml of solution A, to which 60μl of dimethylanilin had been added. The polyethylene cups were transferred into a water bath of 4°C overnight for polymerization. After the removal of the polyethylene cups, 1.0μm thick sections were cut from the blocks with a Mikrom HM 360 rotary microtome (Mikrom, Germany). Sections were allowed to stretch out in a water bath (60°C, Daglef Patz, Germany) and after mounting on glass slides (Engelbrecht, Germany), were left to dry on a heating plate (OTS 40, Meditel, Germany). To ensure adherence to the glass slides, the sections were kept in a heating cabinet (Memmert, Germany) at 64°C for a minimum of 24h before staining. Hematoxilin Eosin (HE) stain, periodic acid Schiff (PAS) stain and a periodic acid silver methenamine stain were performed according to the following listed protocols.

Materials and protocols used for GMA/MMA embedding and staining of GMA/MMA sections

Dehydration protocol for GMA/MMA embedding

3h rinsing solution
2x1h Ethyl alcohol 30% (BfB, Germany)
2x1h Ethyl alcohol 56% (BfB, Germany)
2x1h Ethyl alcohol 70% (BfB, Germany)
2h Ethyl alcohol 96% (BfB, Germany)
2x3h Ethyl alcohol 96% (BfB, Germany)

Rinsing solution

Cadodylic acid sodium-trihydrate (AppliChem)	16g
1N Hydrochloric acid (AppliChem)	6.23ml
Aqua dest.	1500ml
D+Saccharose (AppliChem)	105g
Calciumchloride dihydrate (Merck)	1.105g
Adjust to pH 7.2	

Solution A

Benzoylperoxide (Merck, Germany)	338mg
Methylmethacrylate	20ml
Hydroxymethylmethacrylate	60ml
Ethyleneglycol monobutylether (Merck, Germany)	16ml
Polyethyleneglycol 400 (Merck, Germany)	2ml

HE staining

1. Mayer's Hemalaun (AppliChem, Germany)	30min
2. Rinsing in tap water	10min

3. 1% HCl-alcohol (Roth, Germany) 1s
4. Rinsing in tap water 10min
5. Drying on a heating plate (60°C)
6. Eosine-Phloxin (Merck, Germany) 30min
7. Aqua dest. 3x1s
8. Drying on a heating plate (60°C)
9. Xylol
10. Mounting with glass cover slides (Menzel GmbH & Co KG, Germany) with Histofluid® (Superior, Germany)

Periodic acid-Schiff reaction (PAS)

1. 1% Periodic acid (AppliChem, Germany) 15min
2. Aqua dest. 3x3s
3. Schiff's reagent (Merck, Germany) 30-60min
4. Rinsing in tap water 30min
5. Drying on a heating plate (60°C)
6. Mayer's Hemalaun (AppliChem, Germany) 30min
7. Rinsing in tap water 10min
8. 1% HCl-alcohol (Roth, Germany) 1s
9. Rinsing in tap water 20min
10. Drying on a heating plate (60°C)
11. Xylol
12. Mounting the slides with glass cover slides (Menzel GmbH & Co KG, Germany) with Histofluid® (Superior, Germany)

Periodic acid-Schiff methenamine silver stain (PAS-MS)

1. 1% Periodic acid (AppliChem, Germany) 5min
2. Aqua dest. 3x1s
3. Silvermethenamin 25min (65°C)
4. Aqua dest. 3x1s
5. 0.1% Goldchloride 10-20s
6. Aqua dest. 3x1s

7. 2% Sodiumthiosulfat 1min
8. Aqua dest. 3x1s
9. Drying on a heating plate (60°C)
10. Schiff's reagent (Merck, Germany) 60min
11. Rinsing in warm tap water 30min
12. Drying on a heating plate (60°C)
13. Mayer's Hemalaun (AppliChem, Germany) 30min
14. Rinsing in tap water 10min
15. Drying on a heating plate (60°C)
16. Xylol
17. Mounting with glass cover slides (Menzel GmbH & Co KG, Germany) with Histofluid® (Superior, Germany)

3.2.5 Glycid ether (Epon) embedding, staining of glycid ether sections and sample processing for disector analyses and electron microscopy

The six tissue samples per animal (n=8 per group) selected for glycid ether embedding were washed for 3h in Sörensen phosphate buffer at room temperature. Next, they were postfixed in 1% osmium tetroxide (Merck, Germany) for 2h at 4°C, followed by another three washing steps of 2min each in Sörensen phosphate buffer at room temperature. Dehydration in acetone solutions (Roth, Germany) was performed at 4°C. The samples were first immersed in a 100% acetone and glycid ether mixture at room temperature for one hour, and then in pure glycid ether for one hour. The samples were then embedded in dried gelatin capsules (Plano, Germany) with epon embedding mixture. The polymerization occurred over 48h at 60°C. Trimming of the blocks was performed with a TM60 Reichert-Jung milling machine (Leica, Germany). 0.5 μm thick semithin sections were cut of the blocks with a Reichert-Jung Ultracut E microtome (Leica, Germany). The sections were stained with Azur II-Safranin according to the protocol listed below.

Dehydration

30% Acetone (Merck, Germany)	15min
50% Acetone (Merck, Germany)	15min
70% Acetone (Merck, Germany)	15min
90% Acetone (Merck, Germany)	15min
100% Acetone (Merck, Germany)	3x30min

Sörensen phosphate buffer (0.067M, pH 7.4)

Solution I	80.8ml
Solution II	19.2ml
Adjust to pH 7.4	

Solution I

Potassium dihydrogen phosphate (Roth, Germany)	9.08g
Aqua dest.	ad 1000ml

Solution II

Disodium hydrogen phosphate dihydrate (Roth, Germany)	11.88g
Aqua dest.	ad 1000ml

1% Osmium tetroxide solution

2% Osmium tetroxide (Merck, Germany)	5ml
Veronal acetate buffer (pH 7.6)	2ml
0.1M Hydrogen chloride (Merck, Germany)	2ml
Saccharose (Merck, Germany)	0.45g
Aqua dest.	1ml

Veronal acetate buffer (pH 7.6)

Sodium veronal (barbitone sodium, Merck, Germany)	2.95g
Sodium acetate (Merck, Germany)	1.94g
Aqua dest.	ad 100ml

Epon-embedding mix

Solution A	3.5ml
Solution B	6.5ml
Paradimethyl aminomethyl phenol (Serva, Germany)	0.15ml

Solution A

Glycid ether 100 (Serva, Germany)	62ml
2-Dodecenyl succiniacid anhydride (Serva, Germany)	100ml

Solution B

Glycid ether 100 (Epon 812, Serva, Germany)	100ml
Methyl nadic anhydride (Serva, Germany)	89ml

Azur II solution

Disodium tetraborate (Merck, Germany)	1g
Aqua dest.	100ml
Azur II (Merck, Germany)	1g
Stir for 2h	
37% Formaldehyde (Roth, Germany)	250μl

Safranin O solution

Disodium tetraborate (Merck, Germany)	1g

Aqua dest.	100ml
Safranin O (Chroma, Germany)	1g
Saccharose (Merck, Germany)	40g
Stir for 2h	
37% Formaldehyde (Roth, Germany)	250μl

Azur II-Safranin staining protocol

1. Azur II solution (55°C) 15-20s
2. Aqua dest. 3x1s
3. Drying on a heating plate (55°C, Meditel, Germany)
4. Safranin solution (55°C) 15-20s
5. Aqua dest. 3x1s
6. Drying on a heating plate (55°C, Meditel, Germany)
7. Cover with glass cover slips (Menzel GmbH & Co KG, Germany), using Histofluid®

Preparation of glycid ether embedded samples for electron microscopy

Ultrathin sections were cut from epon embedded tissue samples with a nominal thickness of 70nm with an Ultracut E microtome (Leica, Germany). The sections were mounted on uncoated copper grids (SSI, Science Services, Germany) and contrasted with lead citrate (Serva, Germany) in accordance with a long established protocol (REYNOLDS, 1963), by floating the sections on droplets of lead citrate for 15-30min.

3.3 Glomerulosclerosis Index

To semiquantitatively evaluate the severity of glomerulosclerotic lesions, two periodic acid-Schiff methenamine silver (PAS-MS) stained GMA/MMA sections per animal (n=8 per group) were selected randomly. 108±6.6 (100 -120) glomerular

profiles were analysed at a magnification of 400x. The glomerular profiles were chosen for analysis through systematic meander sampling according to the unbiased counting rule (GUNDERSEN, 1978). All profiles were classified according to the score by EL NAHAS et al. (1991). The glomerulosclerosis index was calculated by dividing the sum of the allocated scores by the total number of sampled glomerular profiles (EL NAHAS et al., 1991).

Stages of glomerulosclerosis according to EL NAHAS et al. **(1991)**

Stage 0: Normal glomeruli, no visible alterations
Stage 1: Mesangial expansion/thickening of the basement membrane
Stage 2: Mild/moderate segmental sclerosis/hyalinosis of up to 50% of the glom. profile
Stage 3: Diffuse glomerular sclerosis/hyalinosis of more than 50% of the glom. profile
Stage 4: Diffuse glomerular sclerosis with total tuft obliteration and collapse

3.4 Quantitative stereological analyses

3.4.1 Determination of the total kidney volume

The total kidney volume was calculated by dividing the total kidney weight by the specific mass density of paraformaldehyde perfusion-fixed murine kidney tissue of 1.05mg/mm^3 (WANKE, 1996).

3.4.2 Estimation of the total nephron number in both kidneys

The physical disector method was used to estimate the total nephron numbers in the mouse kidneys. The physical disector method is a three-dimensional sampling method that enables the user to sample structures in an unbiased way, by comparing pairs of parallel sections (termed reference section and look-up section) at a distance of approximately one third of the diameter of the structures in question (NYENGAARD, 1999; STERIO, 1984). Five mice per group were selected for analysis with the help of random numbers. Serial sections (n=100) with a

nominal thickness of 1.0μm were cut from 3-6 kidney slices per kidney. Exactly every 10th section (with a distance of 9μm) was mounted and stained with HE. Two more sections were randomly selected for section thickness measurements. Particular care was taken to ensure similar environmental conditions during the sectioning and only one experienced person handled the Microm HM 360 rotary microtome (Microm, Germany) for all serial cutting of GMA/MMA sections. Using random numbers, pairs of reference and look-up sections with a disector height of 20μm (distance 19μm, each containing several kidney sections), were chosen for each kidney. A systematic meander sampling was set up with the help of a computer-assisted stereology system (Visiomorph™ with newCAST™ software, Visiopharm Integrator System, Denmark) at 100x magnification. The efficiency was increased by interchanging the roles of reference and look-up sections. Glomeruli that showed up on the reference section, but disappeared on the look-up section (defined by counting frames, (GUNDERSEN, 1978)), were counted ($\sum Q^-$). The area (A) covered by kidney tissue within the counting frame was determined by point-counting. The sampled kidney volume was calculated by multiplying the area of the analysed kidney sections by the disector height (h). The numerical volume density (N_v) of glomeruli in the kidneys was calculated by dividing Q^- by the sampled tissue volume (NYENGAARD, 1999). By multiplying N_v by the reference volume (V_{Ref}), in this case the kidney volume, the total number of glomeruli (N) was calculated. An average of 57±6 (52-67) Q^- for wild-type mice and 53±2 (51-56) Q^- for transgenic mice were counted.

Equation 2:

$$N_{v(Glom/Kid)} = \frac{\sum Q^-_{(Glom)}}{2 \times h \times \sum A} \times f_s^3$$

$N_{v(Glom/Kid)}$: estimated numerical volume density of glomeruli in the kidney (tissue shrinkage corrected)
$\sum Q^-_{(Glom)}$: number of glomeruli counted within the sum of disectors
h: disector height (20μm)
$\sum A$: area of kidney tissue within the counting frame
f_s: linear tissue shrinkage correction factor for murine kidney tissue embedded in GMA/MMA (0.91, (WANKE, 1996))

Equation 3:

$$N_{(Glom,Kid)} = N_{v(Glom/Kid)_{(s)}} \times V_{Kid}$$

$N_{(Glom,Kid)}$: number of glomeruli in both kidneys
$N_{v(Glom/Kid)_{(s)}}$: estimated numerical volume density of glomeruli in the kidney (tissue shrinkage corrected)
$V_{(Kid)}$: volume of both kidneys

3.4.3 Estimation of the total glomerular volume in both kidneys

To estimate the total glomerular volume in both kidneys, 6-10 randomly selected HE stained GMA/MMA embedded kidney sections per mouse were examined at a 200x magnification. First, the volume fraction of glomeruli per kidneys ($V_{v(Glom/Kid)}$) was determined by point-counting with the computer-assisted stereology system (Visiomorph™ with newCAST™ software, Visiopharm Integrator System, Denmark) By multiplying the volume fraction of glomeruli per kidneys ($V_{v(Glom/Kid)}$) by the kidney volume ($V_{(Kid)}$), the total glomerular volume in both kidneys ($V_{(Glom,Kid)}$) was calculated. Between 157±25 (102-207) points hitting glomerular profiles and 6431±364 (6022-7286) points hitting kidney tissue were counted.

Equation 4:

$$V_{(Glom,Kid)} = V_{v(Glom/Kid)} \times V_{(Kid)}$$

$V_{(Glom,Kid)}$: total glomerular volume of all glomeruli in the kidneys
$V_{v(Glom/Kid)}$: volume fraction of glomeruli in the kidneys
$V_{(Kid)}$: volume of both kidneys

3.4.4 Estimation of the mean glomerular volume

To determine the mean glomerular volume ($\bar{v}_{(Glom)}$), a commonly used model-based method (WEIBEL and GOMEZ, 1962) was used. PAS stained GMA/MMA slides were analysed with a computer-based digital image analysis system (Videoplan®, Zeiss Kontron, Germany) and an attached microscope (Orthoplan, Leitz, Germany) with a video camera (CCTV WV-CD132E, Matsushita, Japan) at a 400x magnification. The system was calibrated, using an object micrometer (Zeiss, Germany). A systematic meander sampling (GUNDERSEN, 1978) was applied to select 182±11 (163-219) glomerular tuft profiles for area measurements per case. Their outlines were traced with a cursor on a digitising tablet. According to the equations by Weibel and Gomez (1962), the mean glomerular volume was calculated with the help of the arithmetic mean area. A shape coefficient (β) for spheres was divided by a size distribution coefficient (K), assuming a coefficient of variation of 15%. The result was multiplied with the mean glomerular profile by the power of 1.5 and then corrected for tissue shrinkage.

Equation 5:

$$\bar{v}_{(Glom)} = \frac{\frac{\beta}{k} \times (\bar{a}_{Glom})^{1.5}}{f_s^3}$$

$\bar{v}_{(Glom)}$: mean glomerular volume (tissue shrinkage corrected)
$\bar{a}_{Glom}$: arithmetic mean of the areas of analysed glomerular tuft profiles
β: shape coefficient (1.4, WANKE, 1996)
k: size distribution coefficient (1.04, WANKE, 1996)
f_s: linear tissue shrinkage correction factor for murine kidney tissue embedded in GMA/MMA (0.91)

3.4.5 Estimation of the podocyte number per glomerulus

The number of podocytes per glomerulus ($N_{(Pod,Glom)}$) was calculated by multiplying the numerical volume density of podocytes per glomerulus ($N_{v(Pod/Glom)}$)

by the mean glomerular volume ($\bar{v}_{(Glom)}$) (WANKE, 1996). The numerical volume density $N_{v(Pod/Glom)}$ was determined using the physical disector method (STERIO, 1984). Ten serial semithin sections with a nominal section thickness of 0.5μm were cut from glycid ether embedded kidney cortex tissue with an Ultracut E microtome (Leica, Germany). The first section was discarded, the remaining nine sections were stained according to protocol. One set of three sections with a distance of 1.5μm was chosen using random numbers. Glomerular tuft profiles, present on all three sections, were photographed at a 400x magnification with a Leica DFC 320 (Leica, Germany), connected to a light microscope (Orthoplan, Leitz, Germany). Every set of glomerular tuft profiles was counted in both directions, first to second and second to third section, making for a total of four disectors analysed per sample. Podocyte nuclei appearing in the reference section, but not in the look-up section, were counted as $Q^-_{(Pod)}$ (Figure 3.6, p.62). The pictures taken of the glomeruli were printed at 1000x magnification. An object micrometer (Zeiss, Germany) was photographed and printed under the same conditions for calibration. The areas of the glomerular tuft were measured planimetrically, using a computer-based digital image analysis system (Videoplan®, Zeiss Kontron, Germany) on printed pages, as previously described. Twelve glomeruli per animal were analysed. On average, 73±20 (42-107) $Q^-_{(Pod)}$ were counted.

Equation 6:

$$N_{v(Pod/Glom)} = \frac{\sum Q^-_{(Pod)}}{h \times A_{(Glom)}} \times f_s^3$$

$N_{v(Pod/Glom)}$: estimated numerical volume density of podocytes in the glomerulus (tissue shrinkage corrected)
$Q^-_{(Pod)}$: number of podocyte nuclei counted in the disector
$A_{(Glom)}$: area of the glomerular cross section
h: disector height (distance between reference and look-up section; 1.5μm)
f_s: linear tissue shrinkage correction factor for murine kidney tissue embedded in epon (0.95, (WANKE, 1996))

Equation 7:

$$N_{(Pod,Glom)} = N_{v(Pod/Glom)} \times \bar{v}_{(Glom)}$$

$N_{(Pod,Glom)}$: number of podocytes per glomerulus
$\bar{v}_{(Glom)}$: estimated mean glomerular volume

Figure 3.6 Stereological estimation of number of podocytes per glomerulus (physical disector method)

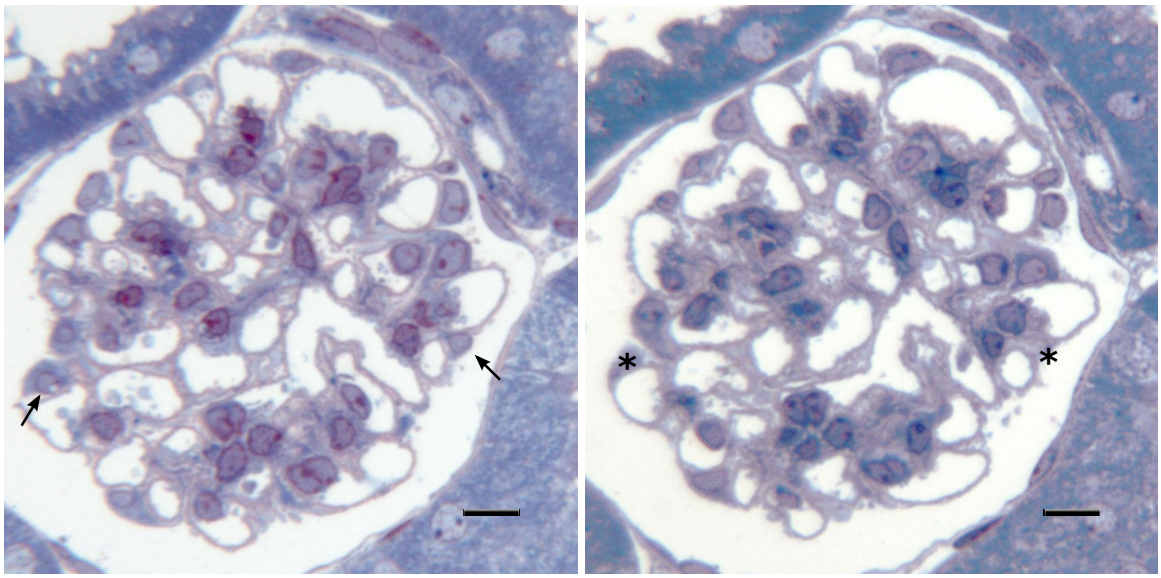

Reference section Look-up section

(*) marks Q^-, in this case podocyte nuclei present in the reference section, but missing in the look-up section. After all Q^- have been counted, the reference section becomes the look-up section and vice versa. Semithin sections, Azur II-Safranin, bar = 10μm.

3.4.6 Estimation of the mean podocyte volume

Pictures of glomerular profiles (n=12 per animal), already taken for the estimation of the podocyte number, were used to estimate the mean podocyte volume. The pictures were superimposed with a 2x2mm point matrix to determine the volume

fraction of podocytes per glomerulus ($V_{v(Pod/Glom)}$). It was differentiated between points hitting the glomerular tuft area ($p_{(Glom)}$) and the subset of points hitting podocyte section profiles ($p_{(Pod)}$). The volume fraction of podocytes per glomerulus ($V_{v(Pod/Glom)}$) was calculated by dividing $p_{(Pod)}$ by $p_{(Glom)}$. The mean volume of podocytes was calculated by dividing the volume fraction by the numerical volume density of podocytes in the glomerulus (NYENGAARD, 1999). On average, 222±55 (153-346) podocyte hits were counted, and 913±321 (509-1574) points hitting the glomerulus.

Equation 8:

$$V_{v(Pod/Glom)} = \frac{\sum p_{(Pod)}}{\sum p_{(Glom)}}$$

$V_{v(Pod/Glom)}$: volume fraction of podocytes in the glomerulus
$p_{(Pod)}$: number of points hitting podocytes
$p_{(Glom)}$: number of points hitting the glomerular tuft profile

Equation 9:

$$\bar{v}_{(Pod)} = \frac{V_{v(Pod/Glom)}}{N_{v(Pod/Glom)}}$$

$\bar{v}_{(Pod)}$: estimated mean podocyte volume
$V_{v(Pod/Glom)}$: volume fraction of podocytes per glomerulus
$N_{v(Pod/Glom)}$: numerical volume density of podocytes in the glomerulus

3.4.7 Estimation of the mean mesangial and capillary volume per glomerulus

The volume fractions of the mesangium ($V_{v(Mes/Glom)}$) and the glomerular capillaries ($V_{v(Cap/Glom)}$) were determined at 400x magnification in PAS stained GMA/MMA sections with a computed-assisted system (Visiomorph™ with newCAST™ software, Visiopharm Integrator System, Denmark). A systematic meander sampling of kidney cortex tissue was performed to select glomerular tuft profiles. A point grid was superimposed over all glomerular tuft profiles within the sampling frame. The points hitting the mesangium and the capillaries respectively were divided by the total number of points hitting the glomerular tuft profile. The mean mesangial and capillary volume per glomerulus were derived by multiplying the corresponding volume fractions with the mean glomerular volume ($\bar{v}_{(Glom)}$; (WANKE, 1996)). An average of 59±5 (52 - 78) glomerular tuft profiles were analysed. In FVB/N mice, 1446±142 (975 - 1794) points hitting the glomerular tuft area were counted. 883±93 (713 - 1107) points hitting the glomerular tuft area were counted in C57BL/6J mice.

Equation 10:

$$\bar{V}_{(x,Glom)} = V_{v(x/Glom)} \times \bar{v}_{(Glom)}$$

$V_{(x,Glom)}$: estimated mean volume of x (mesangium or capillaries) per glomerulus
$V_{v(x/Glom)}$: volume fraction of x in the glomerulus
$\bar{v}_{(Glom)}$: estimated mean glomerular volume

3.4.8 Estimation of the capillary length density in the glomeruli

A systematic meander sampling was set up with a stereology system (Visiomorph™ with newCAST™ software, Visiopharm Integrator System, Denmark), and HE stained GMA/MMA sections were analysed at 400x magnification. The number of capillary profiles ($Q_{(Cap)}$) in 54±2 (51-68) glomerular profiles was counted and

related to the cumulative area of the corresponding glomerular profiles, which were measured planimetrically. The resulting quotient was multiplied by two and corrected for tissue shrinkage (WANKE, 1996).

Equation 11:

$$L_{v(Cap/Glom)} = 2 \times \frac{\sum Q_{(Cap)}}{\sum A_{(Glom)}} \times f_s^2$$

$L_{v(Cap/Glom)}$: estimated capillary length density in the glomerulus (tissue shrinkage corrected)
$\sum Q_{(Cap)}$: sum of glomerular capillary profiles in the investigated glomeruli
$\sum A_{(Glom)}$: sum of areas of glomerular tuft cross sections in the investigated glomeruli
f_s: linear tissue shrinkage correction factor for murine kidney tissue embedded in GMA/MMA (0.91)

3.4.9 Estimation of the mean capillary length per glomerulus

The mean capillary length per glomerulus was obtained by multiplying the capillary length density per glomerulus ($L_{v(Cap/Glom)}$) by the mean glomerular volume.

Equation 12:

$$L_{(Cap,Glom)} = L_{v(Cap/Glom)} \times \bar{v}_{(Glom)}$$

$L_{(Cap,Glom)}$: estimated capillary length per glomerulus
$L_{v(Cap/Glom)}$: estimated capillary length density in the glomerulus (tissue shrinkage corrected)
$\bar{v}_{(Glom)}$: estimated mean glomerular volume

3.4.10 Determination of the filtration slit frequency (FSF)

To determine the filtration slit frequency, five mice per group were randomly selected for electron microscopic analysis. Six glomerular profiles per mouse, each from a different tissue sample, were selected from Azur II-Safranin stained semithin sections (3.2.5) using random numbers. The glycid ether embedded tissue samples containing the selected glomeruli were prepared for electron microscopy as previously described (3.2.5). Electron microscopic images of ultrathin sections (eight peripheral capillary loops per glomerulus) were taken with a Zeiss EM 10 transmission electron microscope (Zeiss, Germany) at a 8000x magnification in a predetermined manner by half turns of the stagehandle. A standard cross-grating grid (S107, TAAB, USA) with 2160 lines/mm was photographed at the same magnification for calibration. All images were printed with identical settings. The filtration slit frequency (FSF) was determined by counting the total number of filtration slits and dividing it by the total length of the peripheral capillary wall at the epithelial interface (JANI et al., 2002; REMUZZI et al., 1995). Length measurements were performed with a computer-assisted image analysis system (Videoplan®, Zeiss Kontron, Germany). On average, 1205±297 (593-1588) filtration slits per animal were counted.

3.4.11 Estimation of the true harmonic mean thickness of the glomerular basement membrane (GBM)

The previously printed electron microscopy pictures were used to determine the thickness of the glomerular basement membrane (GBM), using the orthogonal intercept method (EL-AOUNI et al., 2006; GUO et al., 2005; RAMAGE et al., 2002). A grid (2.5 x 2.5cm) was superimposed over the prints. At the intersections of grid lines and GBM, the shortest distance between the endothelial cytoplasmatic membrane and the outer edge of the lamina rara externa of the glomerular basement membrane beneath the podocytes' foot processes' cytoplasmatic membrane was measured with a transparent, logarithmic ruler. The logarithmic ruler, provided by Ewald Freitag (Institute of Thermodynamics, TU Munich) in accordance with the description by RAMAGE et al. (2002), uses the multiplier 0.75 for the harmonic value

for the divisions The ruler is divided into an initial division (A = 2mm, harmonic value: 1/A = 0.5mm), in which no measurement can be contained, and eleven classes, into which the measurements fall (n observations, Fig. 3.7, p.68). The limits of the classes are calculated as $1/(0.75^{n} \times 0.5)$, with n denoting the number of the respective class. A midpoint for each class is calculated as the arithmetic mean of the harmonic values of its limits (((1/lower limit of class n) + (1/lower limit of class n+1))/2).

Equation 13:

Apparent harmonic mean thickness I_h (mm):

$$I_h = \frac{\sum(n\ of\ observations)}{\sum(midpoints \times n\ of\ observations)}$$

Equation 14:

True harmonic mean thickness T_h (nm):

$$T_h = \frac{8}{3\pi} \times \frac{10^6}{magnification\ (m)} \times I_h$$

3.4.12 Shrinkage in GMA/MMA and glycid ether embedded kidney tissue and determination of thickness of GMA/MMA sections

To reduce the bias caused by linear tissue shrinkage during the embedding process, correction factors previously established for GMA/MMA and glycid ether embedded murine kidney tissue were used (WANKE, 1996). Spectral reflectance measurements (FILMETRICS-INC., 2012) of two sections per GMA/MMA block were made to determine the average section thickness of serial sections for the disector method. The sections were selected randomly during the consecutive sectioning of GMA/MMA embedded kidneys. Sections were mounted on standard glass slides (Menzel GmbH & Co KG, Germany) and reflected, absorbed and transmitted light (380-1050nm wavelength) were measured by a F20 thin-film

Figure 3.7 Estimation of the true harmonic mean thickness of the glomerular basement membrane with a logarithmic ruler

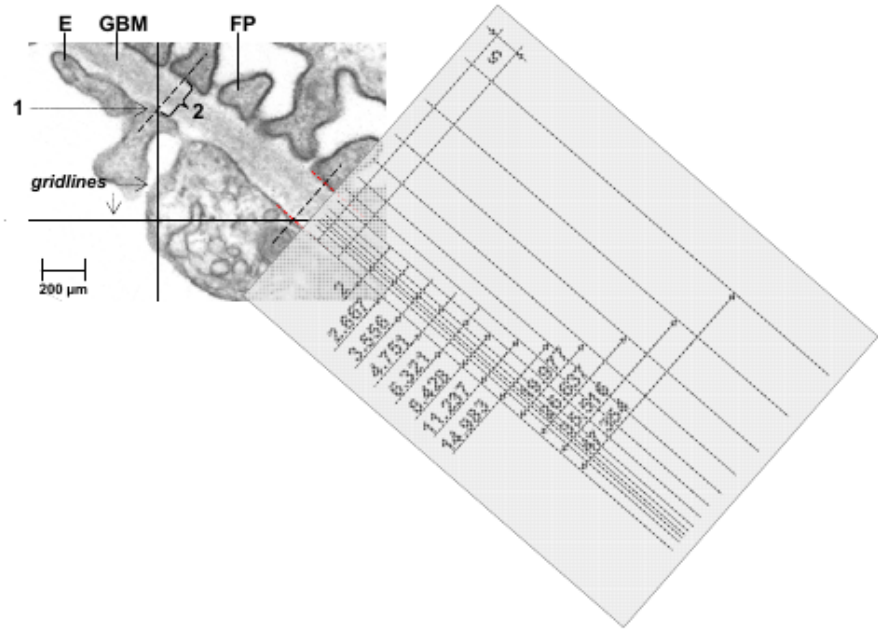

E: endothelial cell, **GBM**: glomerular basement membrane, **FP**: podocyte foot process, **1**: intersection of a grid line (transparent 2.5x2.5cm grid) with the GBM, **2**:shortest distance between the attachment of the endothelial cytoplasmatic membrane and the outer lining of the lamina rara externa of the glomerular basement membrane underneath the cytoplasmatic membrane of the epithelial foot process. The GBM-thickness is read off in terms of classes, here class 6
Picture courtesy of Dr. Andreas Blutke, Institute of Veterinary Pathology, LMU München

analyser (comprised of a regulated tungsten halogen light source, spectrometer and computer with a specialized software; kindly provided by Filmetrics Europe GmbH, Unterhaching).

3.5 Statistical analyses

Shapiro-Wilk-test and Levene-test were performed to test for normal distribution and equality of variance. For each parameter, either two-sample t-tests or Mann-Whitney U-tests were performed to test for significant differences between wild-type and $GIPR^{dn}$-transgenic animals of the FVB/N and C57BL/6J strain respectively. Strain-dependent differences between wild-type mice of the FVB/N background compared to the C57BL/6J background were tested in the same manner. Differences in the development of diabetes mellitus and diabetic nephropathy in $GIPR^{dn}$-tg mice on a FVB/N and C57BL/6 background were examined as well. Parametric data was tested for statistical significance by Student's t-test for independent samples in cases of equal variances. Welch-test was used in cases of non-equal variances. Non-parametric data sets were analysed with the Mann-Whitney U test. Analyses were performed with the statistical analysis software SPSS Statistics 21 (IBM, USA).

Table 3.1 Outline of performed analyses

Parameter	**Number of examined animals**			
	FVB/N		**C57BL/6J**	
	GIPR^{dn}-tg	**wt**	**GIPR^{dn}-tg**	**wt**
Blood pressure	8	8	8	8
Blood glucose conc.				
Fasting blood glucose	8	8	8	8
Casual blood glucose	8	8	8	8
Serum parameters				
Serum albumin conc.	5	5	5	5
Serum creatinin conc.	5	5	5	5
Serum cystatin c conc.	5	5	5	5
Serum total protein conc.	5	5	5	5
Serum triglycerides conc.	5	5	5	5
Serum sodium conc.	5	5	5	5
Serum chloride conc.	5	5	5	5
Urine parameters				
Urine albumin conc.	8	8	8	8
Urine creatinine conc.	5	5	5	5
Urine sodium conc.	5	5	5	5
Urine chloride conc.	5	5	5	5
Body weight	8	8	8	8
Food consumption	8	8	8	8
Water consumption	8	8	8	8
Urine volume	8	8	8	8
Immunohistochemistry				
Laminin	3	3	3	3
Fibronectin	3	3	3	3
Collagen IV	3	3	3	3
TGF β1	3	3	3	3
Glomerulosclerosis index	8	8	8	8
Total kidney volume	8	8	8	8
Total nephron number	5	5	5	5
Total glom. vol. per kidneys	8	8	8	8
Total mean glom. volume	8	8	8	8
Podocyte number per glom.	8	8	8	8
Mean podocyte vol. per glom.	8	8	8	8
Mean glom. mesangial vol.	8	8	8	8
Mean glom. capillary vol.	8	8	8	8
Cap. length density per glom.	8	8	8	8
Mean cap. length per glom.	8	8	8	8
Filtration slit frequency	5	5	5	5
Thickness of the GBM	5	5	5	5

4 Results

4.1 Clinical parameters

4.1.1 Body weight

There is no statistically significant difference in the body weights of GIPR^{dn}-tg FVB/N vs. FVB/N-wt mice or GIPR^{dn}-tg C57BL/6J vs. C57BL/6J-wt mice. Nor do GIPR^{dn}-tg FVB/N vs. GIPR^{dn}-tg C57BL/6J or FVB/N-wt vs. C57BL/6J-wt mice display any statistically significant differences in body weight.

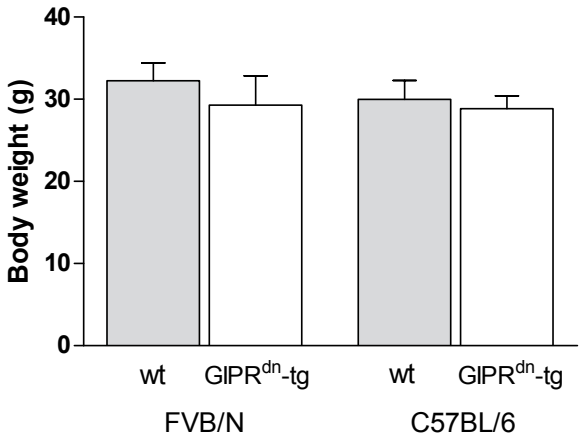

Figure 4.1 Body weight
Data are depicted as means ± SD, n=8. Significance calculated with Student's t-test. Level of significance is displayed as $* = p \leq 0.05, ** = p \leq 0.01$ and $*** = p \leq 0.001$. "A" marks significant differences between GIPR^{dn}-tg FVB/N and GIPR^{dn}-tg C57BL/6J animals, "B" between FVB/N-wt and C57BL/6J-wt animals. **wt**: non-transgenic wild-type littermate controls, **GIPR^{dn}-tg**: GIPR^{dn}-transgenic mice

4.1.2 Food consumption per day

The food consumption per day of GIPR^{dn}-tg FVB/N mice is statistically significantly increased by 38% compared to FVB/N-wt mice. The food consumption per day of GIPR^{dn}-tg C57BL/6J mice is statistically significantly increased by 45% compared to C57BL/6J-wt mice. Compared to GIPR^{dn}-tg C57BL/6J mice, the food consumption of GIPR^{dn}-tg FVB/N mice is increased by 30%. In FVB/N-wt mice, the food consumption per day is increased by 36% compared to C57BL/6J-wt mice.

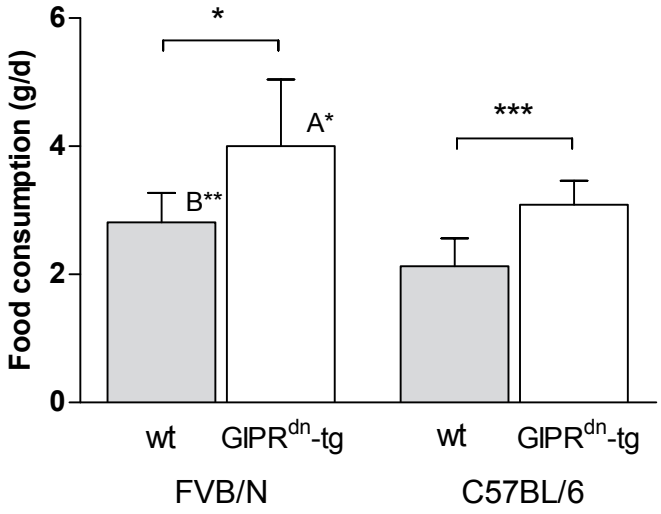

Figure 4.2 Food consumption per day
Data are depicted as means ± SD, n=8. Significance calculated with Student's t-test. Level of significance is displayed as $* = p \leq 0.05, ** = p \leq 0.01$ and $*** = p \leq 0.001$. "A" marks significant differences between GIPR^{dn}-tg FVB/N and GIPR^{dn}-tg C57BL/6J animals, "B" between FVB/N-wt and C57BL/6J-wt animals. **wt**: non-transgenic wild-type littermate controls, **GIPR^{dn}-tg**: GIPR^{dn}-transgenic mice

4.1.3 Food consumption per day and body weight

The food consumption per day and body weight of GIPR^{dn}-tg FVB/N mice is statistically significantly increased by factor 1.6 compared to FVB/N-wt mice. The food consumption per day and body weight of GIPR^{dn}-tg C57BL/6J mice is statistically significantly increased by factor 1.5 compared to C57BL/6J-wt mice. There is no statistically significant difference in the food consumption of GIPR^{dn}-tg FVB/N vs. GIPR^{dn}-tg C57BL/6J or FVB/N-wt vs. C57BL/6J-wt mice.

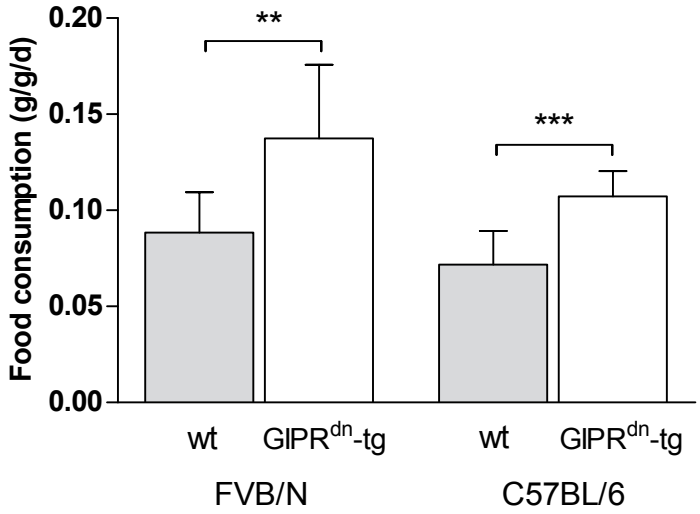

Figure 4.3 Food consumption per day and body weight
Data are depicted as means ± SD, n=8. Significance calculated with Student's t-test. Level of significance is displayed as $* = p \leq 0.05, ** = p \leq 0.01$ and $*** = p \leq 0.001$. "A" marks significant differences between GIPR^{dn}-tg FVB/N and GIPR^{dn}-tg C57BL/6J animals, "B" between FVB/N-wt and C57BL/6J-wt animals. **wt**: non-transgenic wild-type littermate controls, **GIPR^{dn}-tg**: GIPR^{dn}-transgenic mice

4.1.4 Water consumption per day

The water consumption per day of GIPR^{dn}-tg FVB/N mice is statistically significantly increased by factor 3.8 compared to FVB/N-wt mice. In GIPR^{dn}-tg C57BL/6J mice, the water consumption per day is statistically significantly increased by factor 1.9 compared to C57BL/6J-wt mice. The water consumption per day of GIPR^{dn}-tg FVB/N mice is statistically higher by factor 2.2 compared to GIPR^{dn}-tg C57BL/6J mice. No statistically significant difference appears in the water consumption of FVB/N-wt vs. C57BL/6J-wt mice.

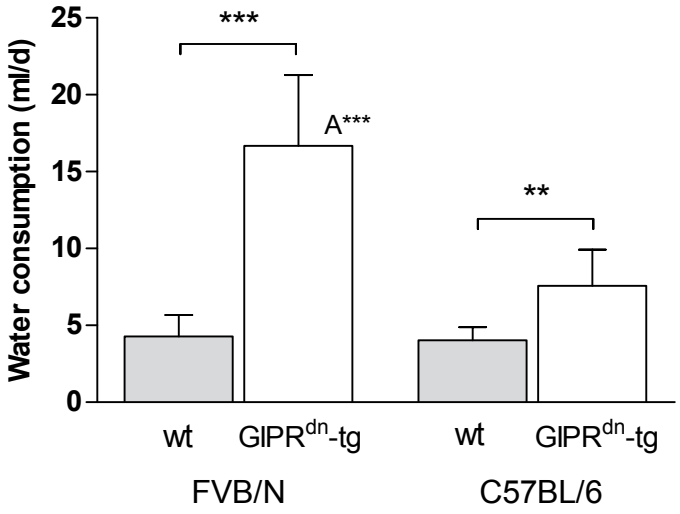

Figure 4.4 Water consumption per day
Data are depicted as means ± SD, n=8. Significance calculated with Student's t-test. Welch's correction was used for GIPR^{dn}-tg FVB/N vs. FVB/N-wt. Level of significance is displayed as $* = p \leq 0.05, ** = p \leq 0.01$ and $*** = p \leq 0.001$. "A" marks significant differences between GIPR^{dn}-tg FVB/N and GIPR^{dn}-tg C57BL/6J animals, "B" between FVB/N-wt and C57BL/6J-wt animals. **wt**: non-transgenic wild-type littermate controls, **GIPR^{dn}-tg**: GIPR^{dn}-transgenic mice

4.1.5 Water consumption per day and body weight

The water consumption per day and body weight of GIPR^{dn}-tg FVB/N mice is statistically significantly increased by factor 4.3 compared to FVB/N-wt mice. In GIPR^{dn}-tg C57BL/6J mice, the water consumption per day and body weight is statistically significantly increased by factor 2 compared to C57BL/6J-wt mice. The water consumption per day and body weight of GIPR^{dn}-tg FVB/N mice is statistically higher by factor 2.2 compared to GIPR^{dn}-tg C57BL/6J mice. No statistically significant difference appears in the water consumption of FVB/N-wt vs. C57BL/6J-wt mice.

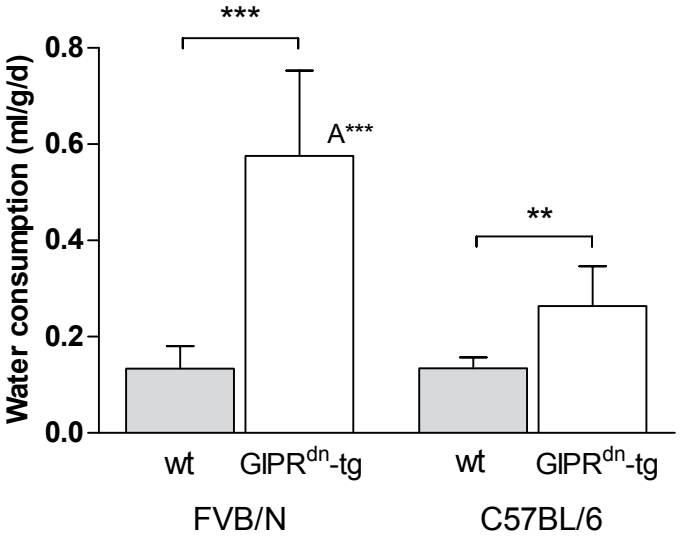

Figure 4.5 Water consumption per day and body weight
Data are depicted as means $\pm$ SD, n=8. Significance calculated with Student's t-test. Welch's correction was used for GIPR^{dn}-tg FVB/N vs. FVB/N-wt. Level of significance is displayed as $* = p \leq 0.05, ** = p \leq 0.01$ and $*** = p \leq 0.001$. "A" marks significant differences between GIPR^{dn}-tg FVB/N and GIPR^{dn}-tg C57BL/6J animals, "B" between FVB/N-wt and C57BL/6J-wt animals. **wt**: non-transgenic wild-type littermate controls, **GIPR^{dn}-tg**: GIPR^{dn}-transgenic mice

4.1.6 Daily urine volume

In GIPR^{dn}-tg FVB/N mice, the urine volume per day is statistically significantly increased by factor 6.2 compared to FVB/N-wt mice. Compared to C57BL/6J-wt mice, the urine volume per day of GIPR^{dn}-tg C57BL/6J mice is statistically significantly increased by factor 3.8. The urine volume per day of GIPR^{dn}-tg FVB/N mice is statistically significantly increased by factor 3.3 compared to GIPR^{dn}-tg C57BL/6J mice. There is no statistically significant difference in the urine volume of FVB/N-wt vs. C57BL/6J-wt mice.

4.1.7 Blood pressure

The systolic blood pressure of GIPR^{dn}-tg FVB/N mice is statistically significantly increased by 21% compared to FVB/N-wt mice. No statistically significant increase in systolic blood pressure of GIPR^{dn}-tg C57BL/6J vs. C57BL/6J-wt mice is observed. The systolic blood pressure of GIPR^{dn}-tg FVB/N mice is statistically significantly higher by 36% compared to GIPR^{dn}-tg C57BL/6J mice. In FVB/N-wt mice, the systolic blood pressure is statistically significantly higher by 29% compared to C57BL/6J-wt mice. There is no statistically significant difference in the diastolic blood pressure of GIPR^{dn}-tg FVB/N vs. FVB/N-w, GIPR^{dn}-tg C57BL/6J vs. C57BL/6J-wt or GIPR^{dn}-tg FVB/N vs. GIPR^{dn}-tg C57BL/6J mice. A by 12% statistically significantly higher diastolic blood pressure is observed in FVB/N-wt mice compared to C57BL/6J-wt mice.

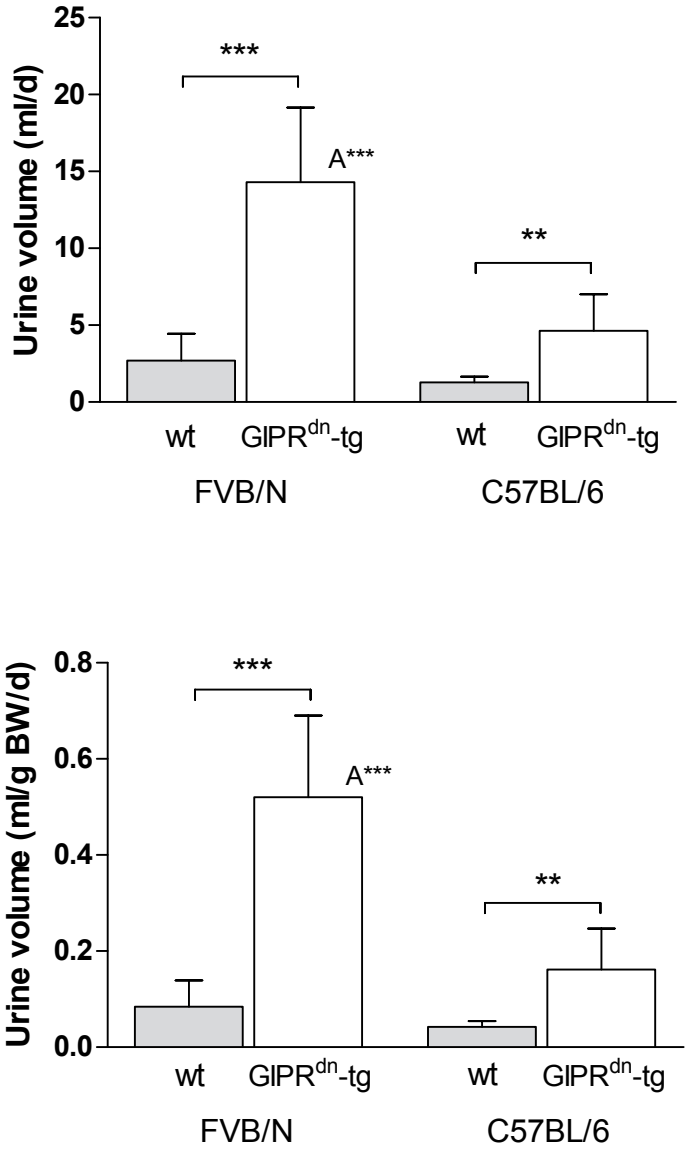

Figure 4.6 24h-urine volume
Data are depicted as means $\pm$ SD, n=8. Significance calculated with Student's t-test. Welch's correction was used for GIPR^{dn}-tg FVB/N vs. FVB/N-wt, GIPR^{dn}-tg C57BL/6J vs. C57BL/6J-wt and FVB/N-wt vs. C57BL/6J-wt. Level of significance is displayed as $* = p \leq 0.05, ** = p \leq 0.01$ and $*** = p \leq 0.001$. "A" marks significant differences between GIPR^{dn}-tg FVB/N and GIPR^{dn}-tg C57BL/6J animals, "B" between FVB/N-wt and C57BL/6J-wt animals. **wt**: non-transgenic wild-type littermate controls, **GIPR^{dn}-tg**: GIPR^{dn}-transgenic mice

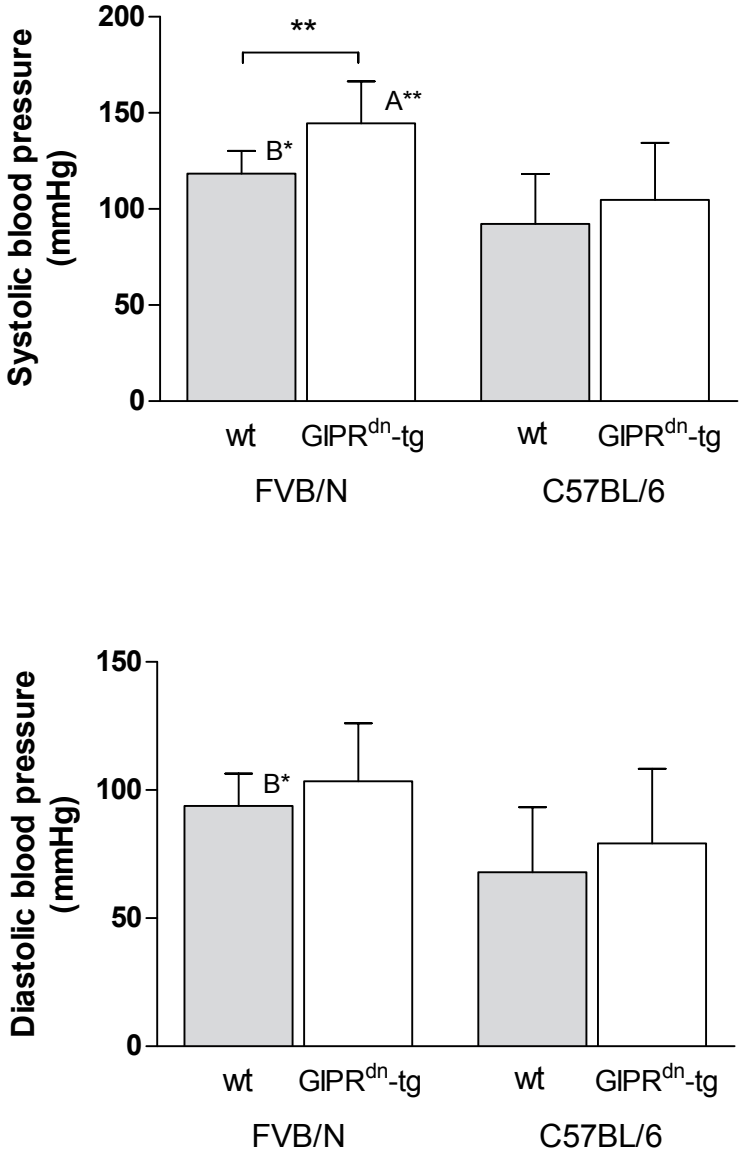

Figure 4.7 Blood pressure
Data are depicted as means ± SD, n=8. Significance calculated with Student's t-test. Welch's correction was used for systolic blood pressure FVB/N-wt vs. C57BL/6J-wt. Level of significance is displayed as $* = p \leq 0.05, ** = p \leq 0.01$ and $*** = p \leq 0.001$. "A" marks significant differences between GIPR^{dn}-tg FVB/N and GIPR^{dn}-tg C57BL/6J animals, "B" between FVB/N-wt and C57BL/6J-wt animals. **wt**: non-transgenic wild-type littermate controls, **GIPR^{dn}-tg**: GIPR^{dn}-transgenic mice

4.1.8 Blood glucose concentration

A statistically significant increase of the casual blood glucose concentration by the factor 4.3 is present in GIPR^{dn}-tg FVB/N mice compared to FVB/N-wt mice. The casual blood glucose concentration of GIPR^{dn}-tg C57BL/6J mice is statistically significantly increased by factor 2.8 compared to C57BL/6J-wt mice. In GIPR^{dn}-tg FVB/N mice, the casual blood glucose concentration is statistically significantly higher by factor 1.7 compared to GIPR^{dn}-tg C57BL/6J mice. The casual blood glucose concentration of FVB/N-wt is slightly, but statistically significantly lower compared to C57BL/6J-wt mice.

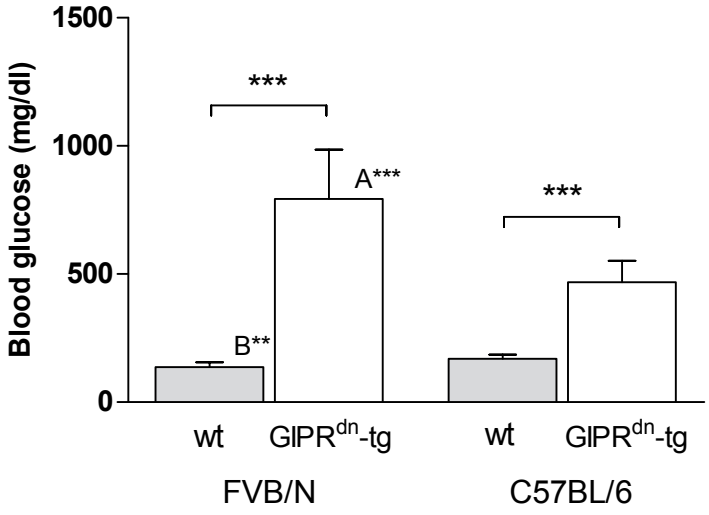

Figure 4.8 Blood glucose concentrations
Data are depicted as means ± SD, n=8. Significance calculated with Student's t-test. Welch's correction was used for casual blood glucose GIPR^{dn}-tg FVB/N vs. FVB/N-wt and GIPR^{dn}-tg C57BL/6J vs. C57BL/6J-wt. Level of significance is displayed as $* = p \leq 0.05, ** = p \leq 0.01$ and $*** = p \leq 0.001$. "A" marks significant differences between GIPR^{dn}-tg FVB/N and GIPR^{dn}-tg C57BL/6J animals, "B" between FVB/N-wt and C57BL/6J-wt animals. **wt**: non-transgenic wild-type littermate controls, **GIPR^{dn}-tg**: GIPR^{dn}-transgenic mice

4.1.9 Serum parameters

Serum creatinine concentration

A statistically significant increase of 99% is observed in the serum creatinine concentration of GIPR^{dn}-tg FVB/N mice compared to FVB/N-wt mice. The serum creatinine concentration GIPR^{dn}-tg C57BL/6J mice is statistically significantly increased by 46% compared to C57BL/6J-wt mice. Compared to GIPR^{dn}-tg C57BL/6J mice, the serum creatinine concentration of GIPR^{dn}-tg FVB/N mice is statistically significantly increased by 26%. There is no statistically significant difference in the serum creatinine concentration of FVB/N-wt vs. C57BL/6J-wt mice.

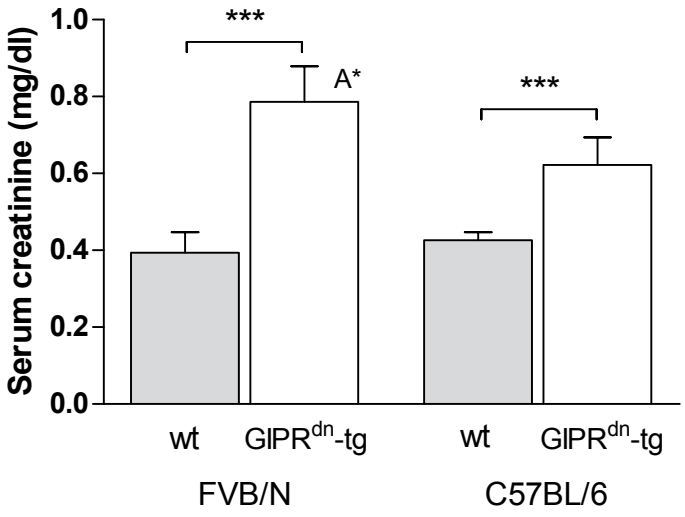

Figure 4.9 Serum creatinine concentration
Data are depicted as means ± SD, n=5. Significance calculated with Student's t-test. Welch's correction was used for FVB/N-wt vs. C57BL/6J-wt. Level of significance is displayed as $* = p \leq 0.05, ** = p \leq 0.01$ and $*** = p \leq 0.001$. "A" marks significant differences between GIPR^{dn}-tg FVB/N and GIPR^{dn}-tg C57BL/6J animals, "B" between FVB/N-wt and C57BL/6J-wt animals. **wt**: non-transgenic wild-type littermate controls, **GIPR^{dn}-tg**: GIPR^{dn}-transgenic mice

Serum urea concentration

There is no statistically significant difference in serum urea concentrations of GIPR^{dn}-tg FVB/N vs. FVB/N-wt, GIPR^{dn}-tg C57BL/6J vs. C57BL/6J-wt, GIPR^{dn}-tg FVB/N vs. GIPR^{dn}-tg C57BL/6J or FVB/N-wt vs. C57BL/6J-wt mice.

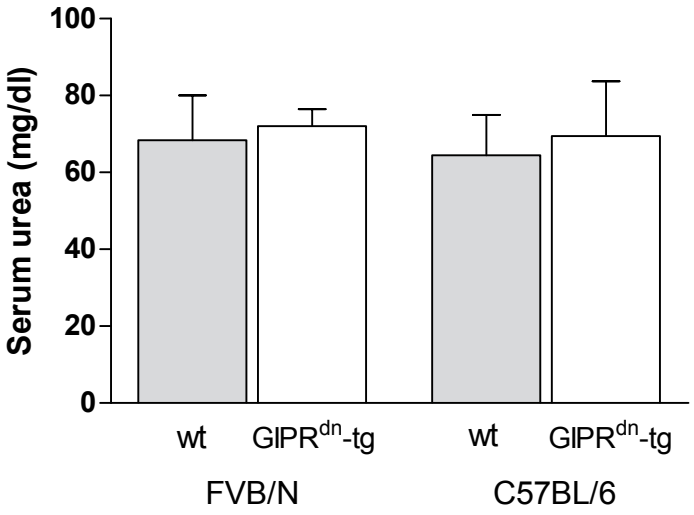

Figure 4.10 Serum urea concentration
Data are depicted as means ± SD, n=5. Significance calculated with Student's t-test (GIPR^{dn}-tg FVB/N vs. FVB/N-wt and FVB/N-wt vs. C57BL/6J-wt) and Mann-Whitney u-test (GIPR^{dn}-tg C57BL/6J vs. C57BL/6J-wt and GIPR^{dn}-tg FVB/N vs. GIPR^{dn}-tg C57BL/6J). Level of significance is displayed as $* = p \leq 0.05, ** = p \leq 0.01$ and $*** = p \leq 0.001$. "A" marks significant differences between GIPR^{dn}-tg FVB/N and GIPR^{dn}-tg C57BL/6J animals, "B" between FVB/N-wt and C57BL/6J-wt animals. **wt**: non-transgenic wild-type littermate controls, **GIPR^{dn}-tg**: GIPR^{dn}-transgenic mice

Serum triglyceride concentration

There is no statistically significant difference in serum triglyceride concentration of GIPR^{dn}-tg FVB/N vs. FVB/N-wt mice. The serum triglyceride concentration of GIPR^{dn}-tg C57BL/6J mice is statistically significantly increased by 52% compared to C57BL/6J-wt mice. In GIPR^{dn}-tg FVB/N mice, the serum triglyceride concentration is statistically significantly higher by factor 2.7 compared to GIPR^{dn}-tg C57BL/6J mice. Compared to C57BL/6J-wt mice, the serum triglyceride concentration of FVB/N-wt mice is statistically significantly higher by 3.6.

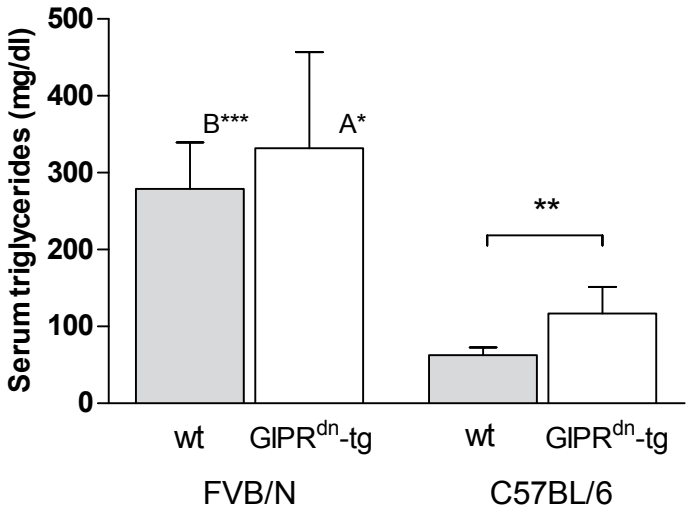

Figure 4.11 Serum triglyceride concentration
Data are depicted as means ± SD, n=5. Significance calculated with Student's t-test. Welch's correction was used for GIPR^{dn}-tg FVB/N vs. GIPR^{dn}-tg C57BL/6J and FVB/N-wt vs. C57BL/6J-wt. Level of significance is displayed as $* = p \leq 0.05, ** = p \leq 0.01$ and $*** = p \leq 0.001$. "A" marks significant differences between GIPR^{dn}-tg FVB/N and GIPR^{dn}-tg C57BL/6J animals, "B" between FVB/N-wt and C57BL/6J-wt animals. **wt**: non-transgenic wild-type littermate controls, **GIPR^{dn}-tg**: GIPR^{dn}-transgenic mice

Serum total protein concentration

There is no statistically significant difference in serum total protein concentrations of GIPR^{dn}-tg FVB/N vs. FVB/N-wt mice. GIPR^{dn}-tg C57BL/6J vs. C57BL/6J-wt mice show no statistically significant difference in serum total protein concentrations either. GIPR^{dn}-tg FVB/N vs. GIPR^{dn}-tg C57BL/6J or FVB/N-wt vs. C57BL/6J-wt mice do not significantly differ in respect to their serum total protein concentrations.

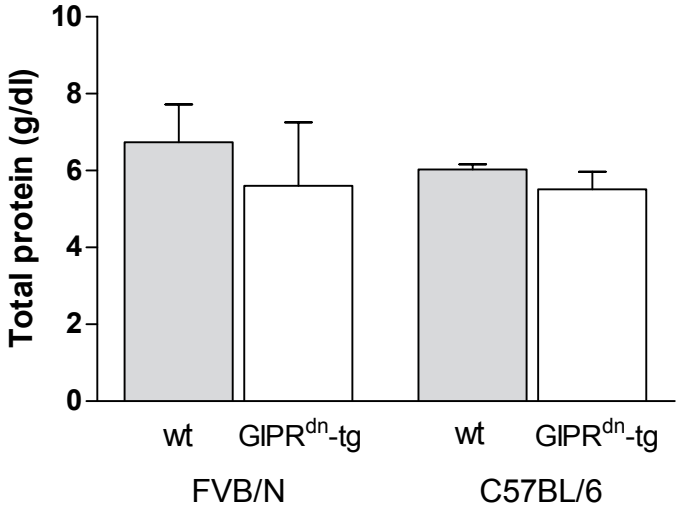

Figure 4.12 Serum total protein concentration
Data are depicted as means ± SD, n=5. Significance calculated with Mann-Whitney u-test. Level of significance is displayed as $* = p \leq 0.05, ** = p \leq 0.01$ and $*** = p \leq 0.001$. "A" marks significant differences between GIPR^{dn}-tg FVB/N and GIPR^{dn}-tg C57BL/6J animals, "B" between FVB/N-wt and C57BL/6J-wt animals. **wt**: non-transgenic wild-type littermate controls, **GIPR^{dn}-tg**: GIPR^{dn}-transgenic mice

Serum albumin concentration

The serum albumin concentration of GIPR^{dn}-tg FVB/N mice is statistically significantly decreased by 23% compared to FVB/N-wt mice. In GIPR^{dn}-tg C57BL/6J mice, the serum albumin concentration is statistically significantly decreased by 16% compared to C57BL/6J-wt mice. The serum albumin concentration of GIPR^{dn}-tg FVB/N mice is statistically significantly lower by 17% compared to GIPR^{dn}-tg C57BL/6J mice. There is no statistically significant difference of serum albumin concentrations of FVB/N-wt vs. C57BL/6J-wt mice.

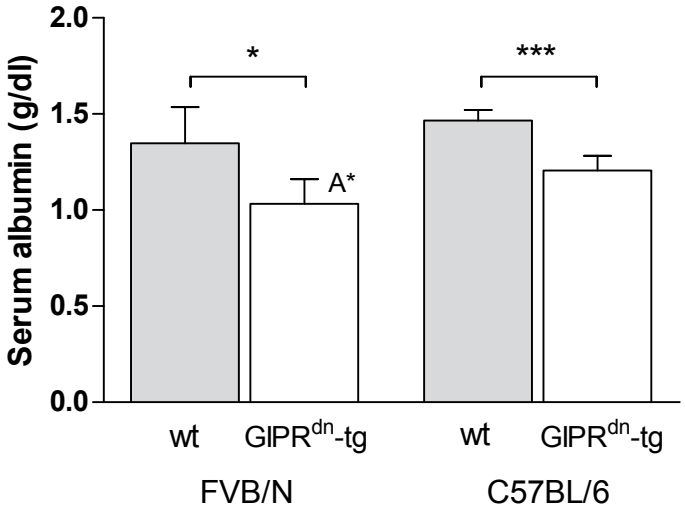

Figure 4.13 Serum albumin concentration
Data are depicted as means ± SD, n=5. Significance calculated with Student's t-test. Welch's correction was used for FVB/N-wt vs. C57BL/6J-wt. Level of significance is displayed as $* = p \leq 0.05, ** = p \leq 0.01$ and $*** = p \leq 0.001$. "A" marks significant differences between GIPR^{dn}-tg FVB/N and GIPR^{dn}-tg C57BL/6J animals, "B" between FVB/N-wt and C57BL/6J-wt animals. **wt**: non-transgenic wild-type littermate controls, **GIPR^{dn}-tg**: GIPR^{dn}-transgenic mice

Serum cystatin C concentration

There is no statistically significant difference in serum cystatin C concentrations of GIPR^{dn}-tg FVB/N vs. FVB/N-wt, GIPR^{dn}-tg C57BL/6J vs. C57BL/6J-wt, GIPR^{dn}-tg FVB/N vs. GIPR^{dn}-tg C57BL/6J or FVB/N-wt vs. C57BL/6J-wt mice.

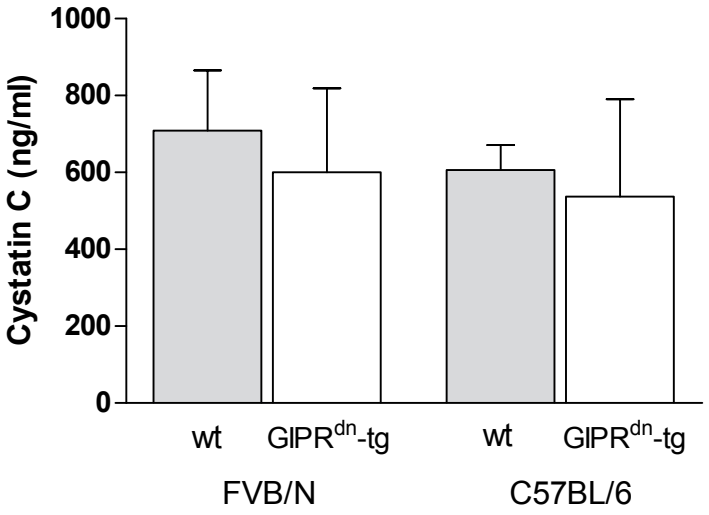

Figure 4.14 Serum cystatin C concentration
Data are depicted as means $\pm$ SD, n=5. Significance calculated with Student's t-test (GIPR^{dn}-tg C57BL/6J vs. C57BL/6J-wt and FVB/N-wt vs. C57BL/6J-wt) and Mann-Whitney u-test (GIPR^{dn}-tg FVB/N vs. FVB/N-wt and GIPR^{dn}-tg FVB/N vs. GIPR^{dn}-tg C57BL/6J). Level of significance is displayed as $* = p \leq 0.05, ** = p \leq 0.01$ and $*** = p \leq 0.001$. "A" marks significant differences between GIPR^{dn}-tg FVB/N and GIPR^{dn}-tg C57BL/6J animals, "B" between FVB/N-wt and C57BL/6J-wt animals. **wt**: non-transgenic wild-type littermate controls, **GIPR^{dn}-tg**: GIPR^{dn}-transgenic mice

Serum sodium concentration

There is no statistically significant difference in the serum sodium concentration of GIPR^{dn}-tg FVB/N vs. FVB/N-wt mice. The serum sodium concentration of GIPR^{dn}-tg C57BL/6J is slightly, but statistically significantly decreased compared to C57BL/6J-wt mice. No statistically significant difference in the serum sodium concentration of GIPR^{dn}-tg FVB/N vs. GIPR^{dn}-tg C57BL/6J mice was apparent. The serum sodium concentration of FVB/N-wt is slightly, but statistically significantly higher compared to C57BL/6J-wt mice.

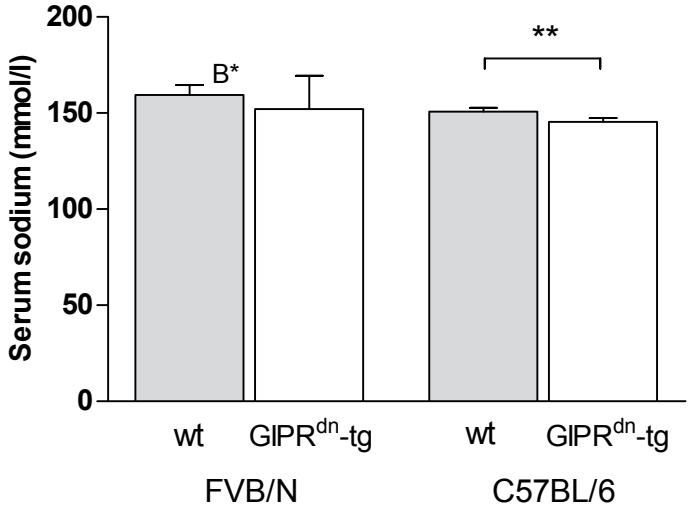

Figure 4.15 Serum sodium concentration
Data are depicted as means ± SD, n=5. Significance calculated with Student's t-test. Welch's correction was used for FVB/N-wt vs. C57BL/6-wt. Level of significance is displayed as $* = p \leq 0.05, ** = p \leq 0.01$ and $*** = p \leq 0.001$. "A" marks significant differences between GIPR^{dn}-tg FVB/N and GIPR^{dn}-tg C57BL/6J animals, "B" between FVB/N-wt and C57BL/6J-wt animals. **wt**: non-transgenic wild-type littermate controls, **GIPR^{dn}-tg**: GIPR^{dn}-transgenic mice

Serum chloride concentration

There is no statistically significant difference in the serum chloride levels of GIPR^{dn}-tg FVB/N vs. FVB/N-wt, GIPR^{dn}-tg FVB/N vs. GIPR^{dn}-tg C57BL/6J or FVB/N-wt vs. C57BL/6J-wt mice. The serum chloride concentration of GIPR^{dn}-tg C57BL/6J mice is slightly, but significantly decreased compared to C57BL/6J-wt mice.

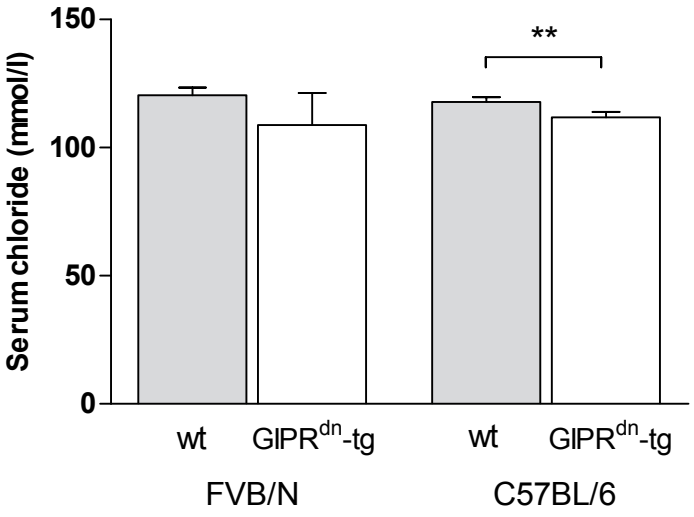

Figure 4.16 Serum chloride concentration
Data are depicted as means ± SD, n=5. Significance calculated with Student's t-test. Level of significance is displayed as $* = p \leq 0.05, ** = p \leq 0.01$ and $*** = p \leq 0.001$. "A" marks significant differences between GIPR^{dn}-tg FVB/N and GIPR^{dn}-tg C57BL/6J animals, "B" between FVB/N-wt and C57BL/6J-wt animals. **wt**: non-transgenic wild-type littermate controls, **GIPR^{dn}-tg**: GIPR^{dn}-transgenic mice

4.1.10 Urine analyses

Urine creatinine concentration

Compared to FVB/N-wt mice, the urine creatinine levels of GIPR^{dn}-tg FVB/N mice are statistically significantly decreased by 90% The urine creatinine levels of GIPR^{dn}-tg C57BL/6J mice are statistically significantly decreased by 71% compared to C57BL/6J-wt mice. In GIPR^{dn}-tg FVB/N mice, the urine creatinine levels are statistically significantly lower by 82% compared to GIPR^{dn}-tg C57BL/6J mice. The urine creatinine levels of FVB/N-wt mice are statistically significantly lower by 47% compared to C57BL/6J-wt mice.

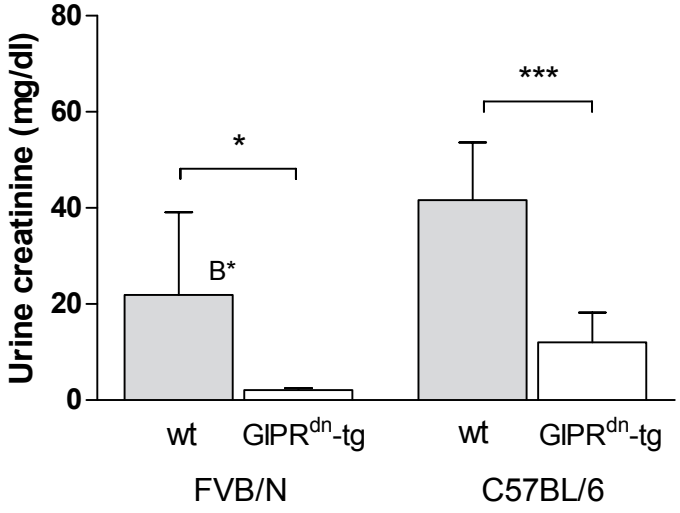

Figure 4.17 Urine creatinine concentration
Data are depicted as means ± SD, n=5. Significance calculated with Student's t-test. Welch's correction was used for GIPR^{dn}-tg FVB/N vs. FVB/N-wt and GIPR^{dn}-tg FVB/N vs. GIPR^{dn}-tg C57BL/6J. Level of significance is displayed as $* = p \leq 0.05, ** = p \leq 0.01$ and $*** = p \leq 0.001$. "A" marks significant differences between GIPR^{dn}-tg FVB/N and GIPR^{dn}-tg C57BL/6J animals, "B" between FVB/N-wt and C57BL/6J-wt animals. **wt**: non-transgenic wild-type littermate controls, **GIPR^{dn}-tg**: GIPR^{dn}-transgenic mice

Estimated glomerular filtration rate (eGFR)

There is no statistically significant difference in the eGFR of GIPR^{dn}-tg FVB/N vs. FVB/N-wt, GIPR^{dn}-tg FVB/N vs. GIPR^{dn}-tg C57BL/6J or FVB/N-wt vs. C57BL/6J-wt mice. The eGFR of GIPR^{dn}-tg C57BL/6J is slightly, but statistically significantly, decreased compared to C57BL/6J-wt mice.

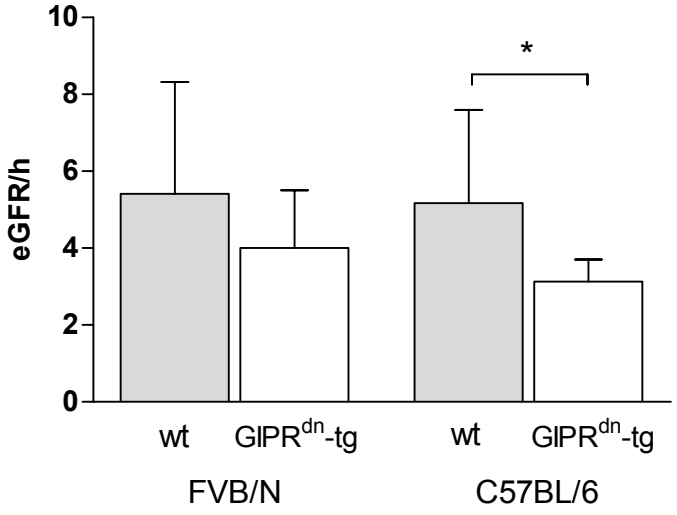

Figure 4.18 Estimated glomerular filtration rate (eGFR)
Data are depicted as means ± SD, n=5. Significance calculated with Student's t-test. Welch's correction was used for GIPR^{dn}-tg C57BL/6J vs. C57BL/6J-wt and GIPR^{dn}-tg FVB/N vs. GIPR^{dn}-tg C57BL/6J. Level of significance is displayed as $* = p \leq 0.05, ** = p \leq 0.01$ and $*** = p \leq 0.001$. "A" marks significant differences between GIPR^{dn}-tg FVB/N and GIPR^{dn}-tg C57BL/6J animals, "B" between FVB/N-wt and C57BL/6J-wt animals. **wt**: non-transgenic wild-type littermate controls, **GIPR^{dn}-tg**: GIPR^{dn}-transgenic mice

Urine urea concentration

Sample concentrations of several animals exceed the range of the autoanalyzer. Graphically, there appears to be no significant difference between the means of the accepted samples.

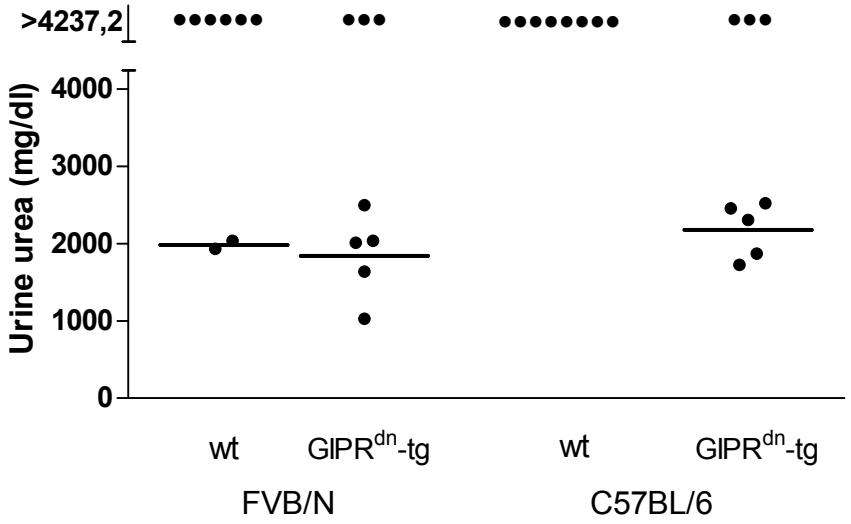

Figure 4.19 Urine urea concentration
Each dot represents one animal, n=8. **wt**: non-transgenic wild-type littermate controls, **GIPR^{dn}-tg**: GIPR^{dn}-transgenic mice

Urine sodium concentration

The urine sodium concentrations of a number of samples fall below the testing range of the autoanalyzer. The urine sodium concentration of GIPR^{dn}-tg FVB/N mice appears to be decreased compared to FVB/N-wt mice and the urine sodium concentration of GIPR^{dn}-tg C57BL/6J mice appears to be decreased compared to C57BL/6J-wt mice.

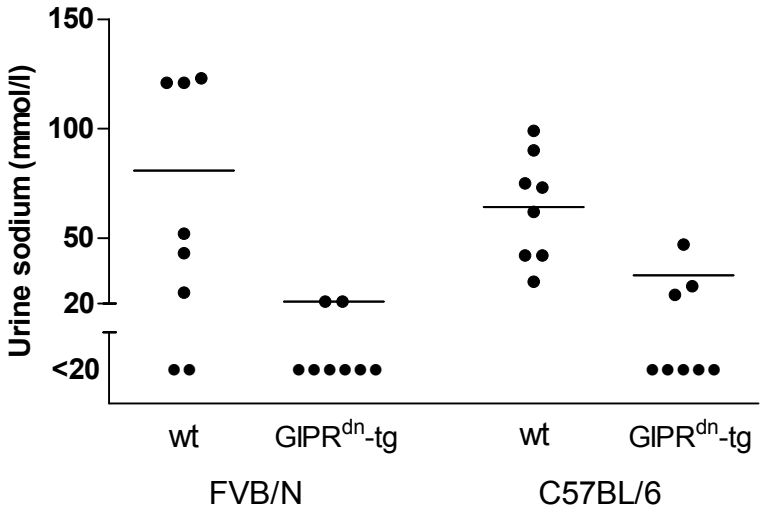

Figure 4.20 Urine sodium concentration
Each dot represents one animal, n=8. **wt**: non-transgenic wild-type littermate controls, **GIPR^{dn}-tg**: GIPR^{dn}-transgenic mice

Urine chloride concentration

In GIPR^{dn}-tg FVB/N mice, the urine chloride concentrations are statistically significantly decreased by 76% compared to FVB/N-wt mice. The urine chloride concentrations of GIPR^{dn}-tg C57BL/6J mice are statistically significantly decreased by 74% compared to C57BL/6J-wt mice. There is no statistically significant difference between the urine chloride concentrations of GIPR^{dn}-tg FVB/N vs. GIPR^{dn}-tg C57BL/6J or FVB/N-wt vs. C57BL/6J-wt mice.

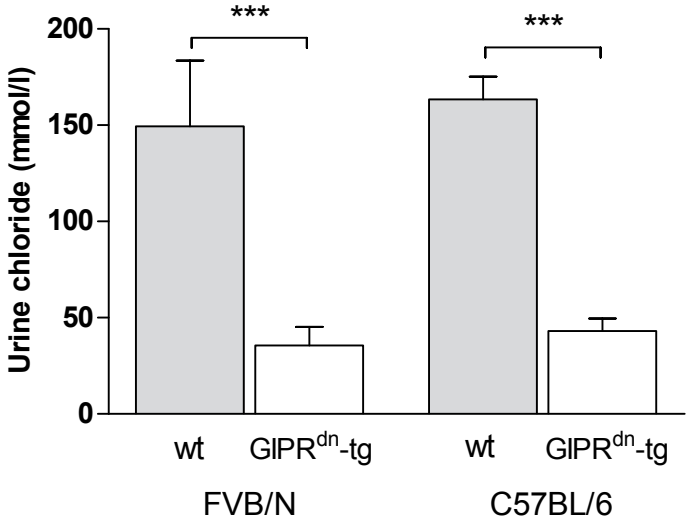

Figure 4.21 Urine chloride concentration
Data are depicted as means $\pm$ SD, n=5. Significance calculated with Student's t-test. Welch's correction was used for GIPR^{dn}-tg FVB/N vs. FVB/N-wt and FVB/N-wt vs. C57BL/6J-wt. Level of significance is displayed as $* = p \leq 0.05, ** = p \leq 0.01$ and $*** = p \leq 0.001$. "A" marks significant differences between GIPR^{dn}-tg FVB/N and GIPR^{dn}-tg C57BL/6J animals, "B" between FVB/N-wt and C57BL/6J-wt animals. **wt**: non-transgenic wild-type littermate controls, **GIPR^{dn}-tg**: GIPR^{dn}-transgenic mice

Urine albumin concentration

A statistically significantly increase of 98% in the urine albumin concentration is displayed by GIPR^{dn}-tg FVB/N mice compared to FVB/N-wt mice. The urine albumin concentration of GIPR^{dn}-tg C57BL/6J mice is statistically significantly decreased by 77% compared to C57BL/6J-wt mice. The urine albumin concentration of GIPR^{dn}-tg FVB/N mice is statistically significantly increased by factor 9.6 compared to GIPR^{dn}-tg C57BL/6J-mice. There is no statistically significant difference in the urine albumin concentration of FVB/N-wt vs C57BL/6J-wt mice.

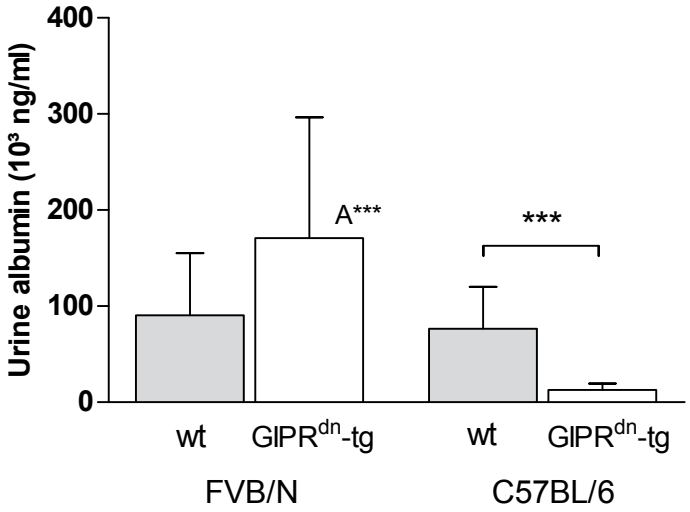

Figure 4.22 Urine albumin concentration
Data are depicted as means ± SD, n=8. Significance calculated with Student's t-test (GIPR^{dn}-tg FVB/N vs FVB/N-wt and FVB/N-wt vs. C57BL/6J-wt) and Mann-Whitney u-test (GIPR^{dn}-tg C57BL/6J vs. C57BL/6J-wt and GIPR^{dn}-tg FVB/N vs. GIPR^{dn}-tg C57BL/6J). Level of significance is displayed as $* = p \leq 0.05, ** = p \leq 0.01$ and $*** = p \leq 0.001$. "A" marks significant differences between GIPR^{dn}-tg FVB/N and GIPR^{dn}-tg C57BL/6J animals, "B" between FVB/N-wt and C57BL/6J-wt animals. **wt**: non-transgenic wild-type littermate controls, **GIPR^{dn}-tg**: GIPR^{dn}-transgenic mice

Daily albumin excretion

The albumin excretion per day of GIPR^{dn}-tg FVB/N mice is statistically significantly increased by the factor 11.9 compared to FVB/N-wt mice. There is no statistically significant difference in the albumin excretion per day of GIPR^{dn}-tg C57BL/6J vs. C57BL/6J-wt mice. The albumin excretion per day is statistically significantly higher by the factor 33.0 in GIPR^{dn}-tg FVB/N mice compared to GIPR^{dn}-tg C57BL/6J mice. Compared to C57BL/6J-wt mice, the albumin excretion per day of FVB/N-wt mice is statistically significantly higher by the factor 2.0.

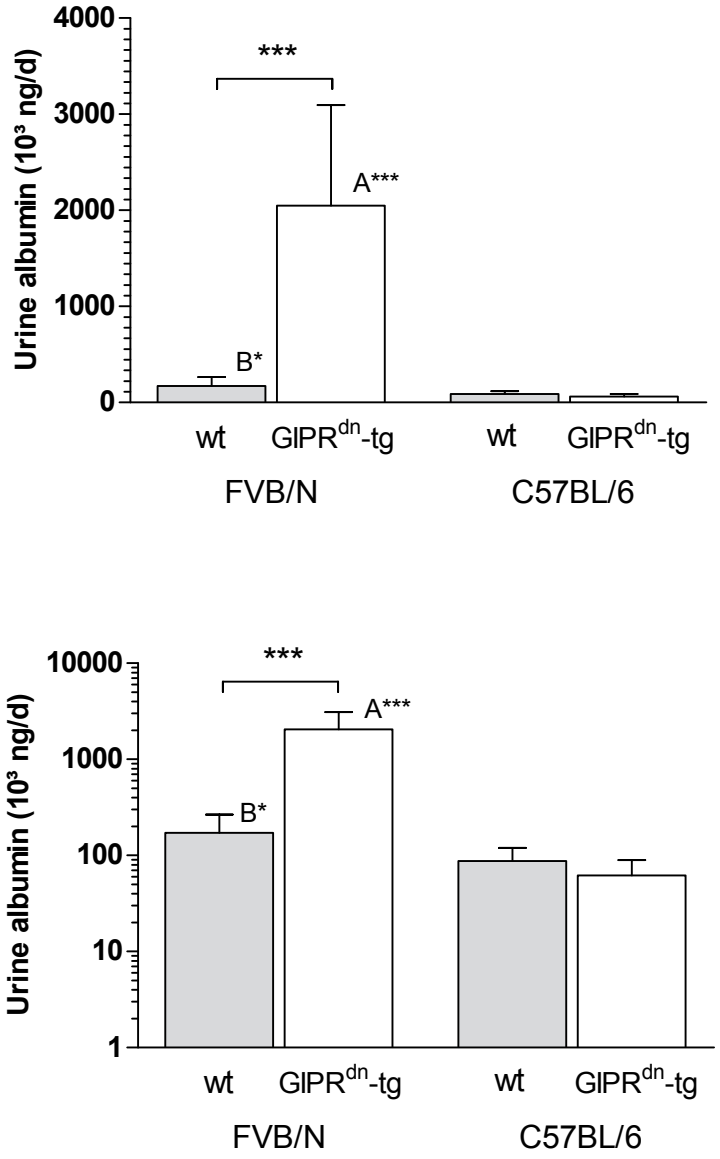

Figure 4.23 Albumin excretion
Data are depicted as means ± SD, n=8. Significance calculated with Student's t-test. Level of significance is displayed as $* = p \leq 0.05, ** = p \leq 0.01$ and $*** = p \leq 0.001$. "A" marks significant differences between GIPR^{dn}-tg FVB/N and GIPR^{dn}-tg C57BL/6J animals, "B" between FVB/N-wt and C57BL/6J-wt animals. **wt**: non-transgenic wild-type littermate controls, **GIPR^{dn}-tg**: GIPR^{dn}-transgenic mice

Urine albumin creatinine ratio (UACR)

The UACR of GIPR^{dn}-tg FVB/N mice is statistically significantly increased by the factor 8.3 compared to FVB/N-wt mice. There is no statistically significant difference in the UACR of GIPR^{dn}-tg C57BL/6J vs. C57BL/6J-wt mice. Compared to GIPR^{dn}-tg C57BL/6J mice, the UACR of GIPR^{dn}-tg FVB/N mice is statistically significantly higher by the factor 24.0. The UACR of FVB/N-wt mice is statistically significantly higher by the factor 2.1 compared to C57BL/6J-wt mice.

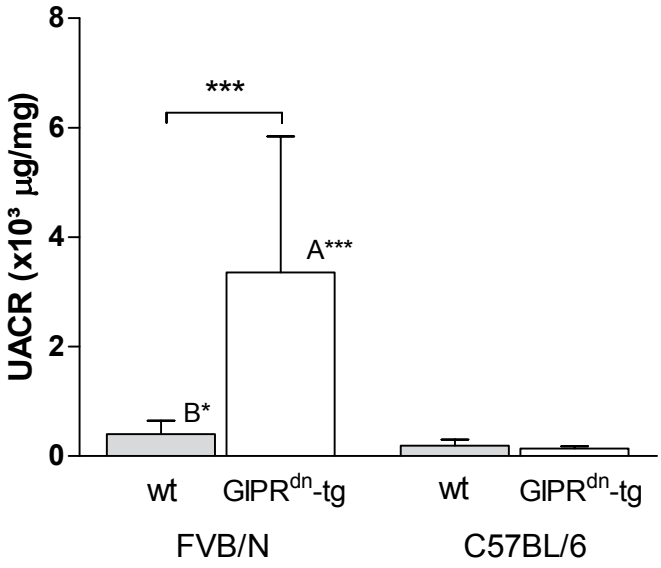

Figure 4.24 Urine albumin creatinine ratio
Data are depicted as means $\pm$ SD, n=5. Significance calculated with Student's t-test (FVB/N-wt vs. C57BL/6-wt) and Mann-Whitney u-test (GIPR^{dn}-tg FVB/N vs. FVB/N-wt, GIPR^{dn}-tg C57BL/6J vs. C57BL/6J-wt, GIPR^{dn}-tg FVB/N vs. GIPR^{dn}-tg C57BL/6J). Level of significance is displayed as $* = p \leq 0.05, ** = p \leq 0.01$ and $*** = p \leq 0.001$. "A" marks significant differences between GIPR^{dn}-tg FVB/N and GIPR^{dn}-tg C57BL/6J animals, "B" between FVB/N-wt and C57BL/6J-wt animals. **wt**: non-transgenic wild-type littermate controls, **GIPR^{dn}-tg**: GIPR^{dn}-transgenic mice

4.2 Qualitative histological findings

4.2.1 Glomerular tuft profiles of GIPR^{dn}-tg mice

HE stained glomerular tuft profiles

Typical glomerular tuft profiles of wild-type and GIPR^{dn}-tg FVB/N and C57BL/6J mice are displayed. Subjectively, mice on the FVB/N background appear to display a larger glomerular tuft areas compared to mice on the C57BL/6J background. In GIPR^{dn}-tg FVB/N mice in this study, dilated and distorted glomerular capillaries were a common finding, No significant number of dilated capillaries could be found in GIPR^{dn}-tg C57BL/6J mice.

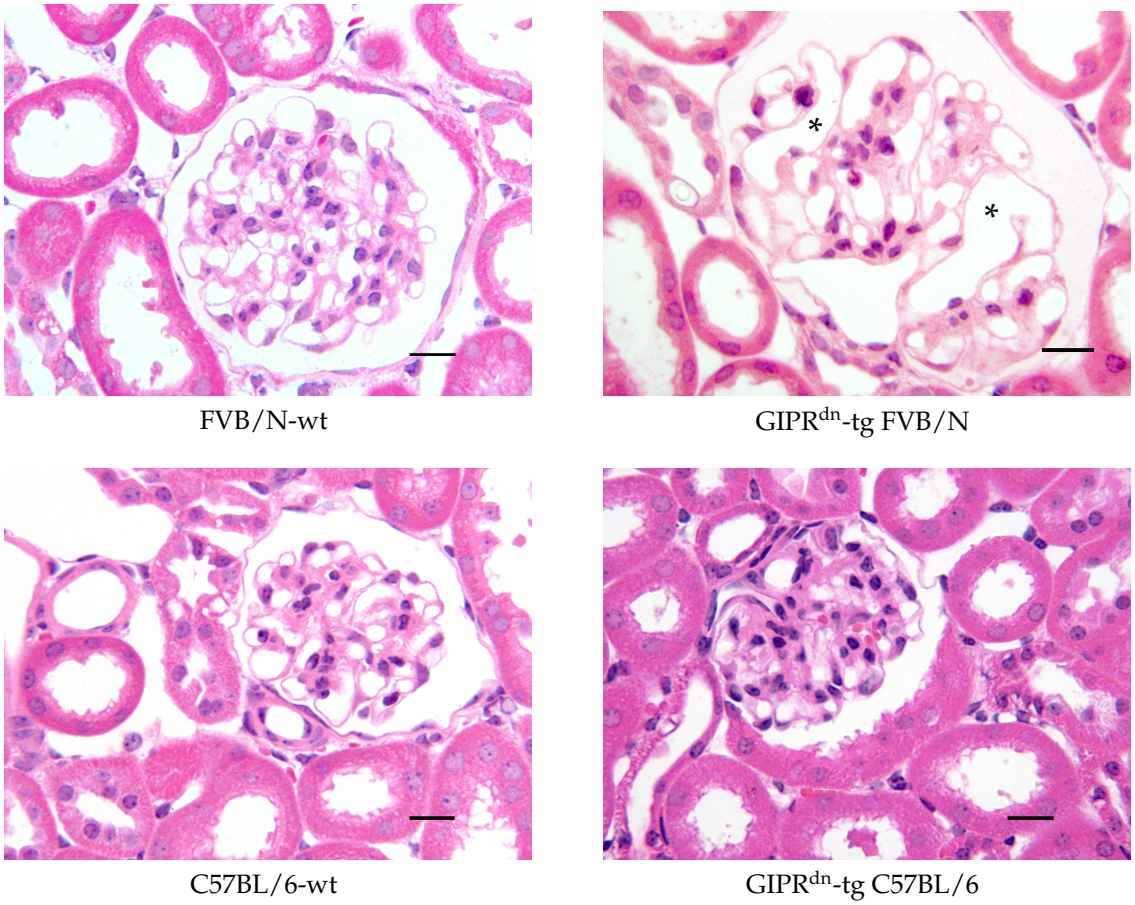

Figure 4.25 Glomerular histology of GIPR^{dn}-tg FVB/N and C57BL/6J mice in HE stained GMA/MMA-embedded kidney tissue. * Distorted capillaries. Bar 30μm.

PAS-MS stained glomerular tuft profiles

In the present study, FVB/N-wt and C57BL/6J-wt mice only occasionally mild glomerulosclerotic lesions. The glomerular tuft profiles of GIPR^{dn}-tg C57BL/6J mice sometimes display mild mesangial expansion, but do not differ significantly from those of C57BL/6J-wt mice. A number of glomerular tuft profiles of GIPR^{dn}-tg FVB/N mice shows segmental glomerulosclerosis or mesangial expansion.

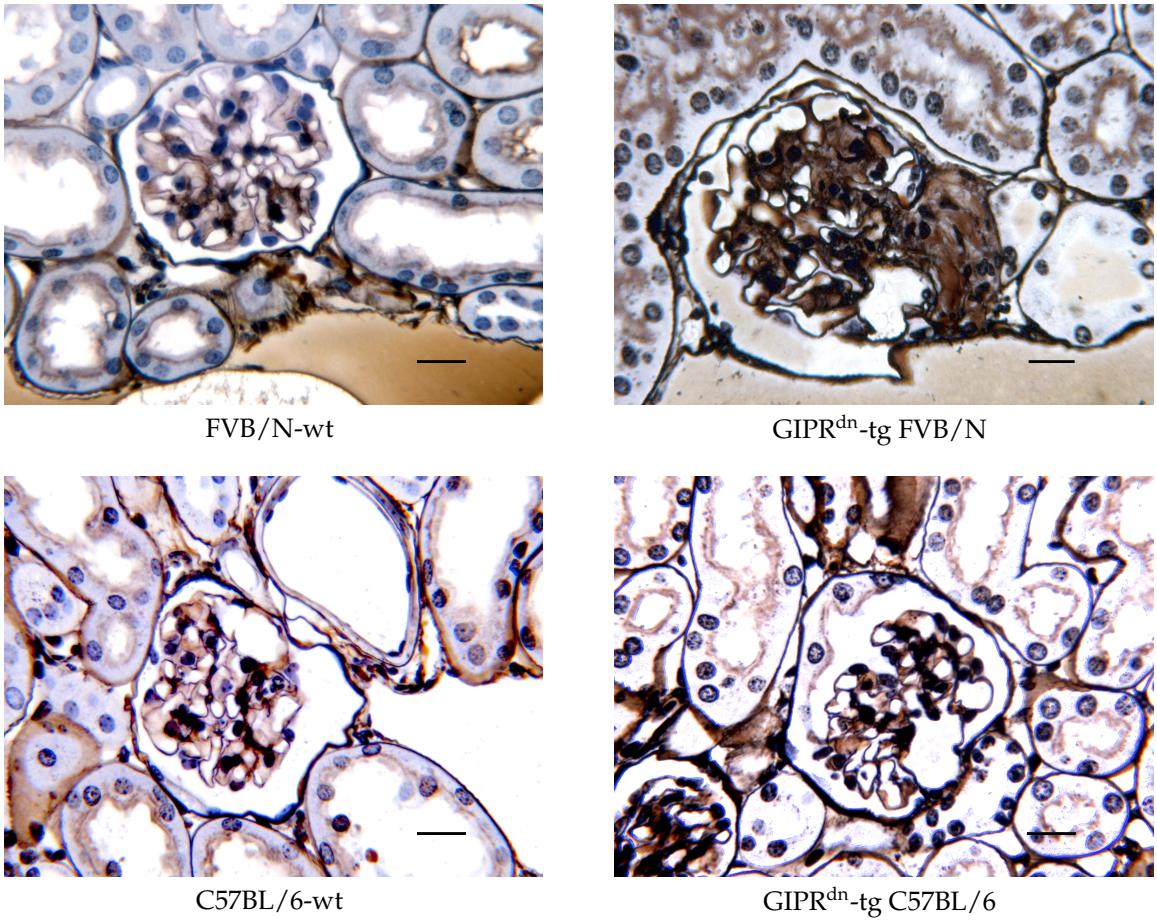

FVB/N-wt | GIPR^{dn}-tg FVB/N

C57BL/6-wt | GIPR^{dn}-tg C57BL/6

Figure 4.26 Kidney histology in PAS-MS stained GMA/MMA-embedded tissue of GIPR^{dn}-tg FVB/N and C57BL/6J mice. Bar 30μm.

4.2.2 Immunohistochemical detection of glomerular extracellular matrix proteins and TGF-β1

Immunohistochemical detection of collagen IV

GIPR^{dn}-tg FVB/N mice display increased glomerular immunostaining for collagen IV compared to FVB/N-wt mice. GIPR^{dn}-tg C57BL/6J mice display an only slightly increased immunostaining for collagen IV in the glomerulus compared to C57BL/6J-wt mice. GIPR^{dn}-tg FVB/N mice display more accumulation of collagen IV in the glomerulus than GIPR^{dn}-tg C57BL/6J mice. There is no difference in glomerular collagen immunostaining of FVB/N-wt vs. C57BL/6J-wt mice.

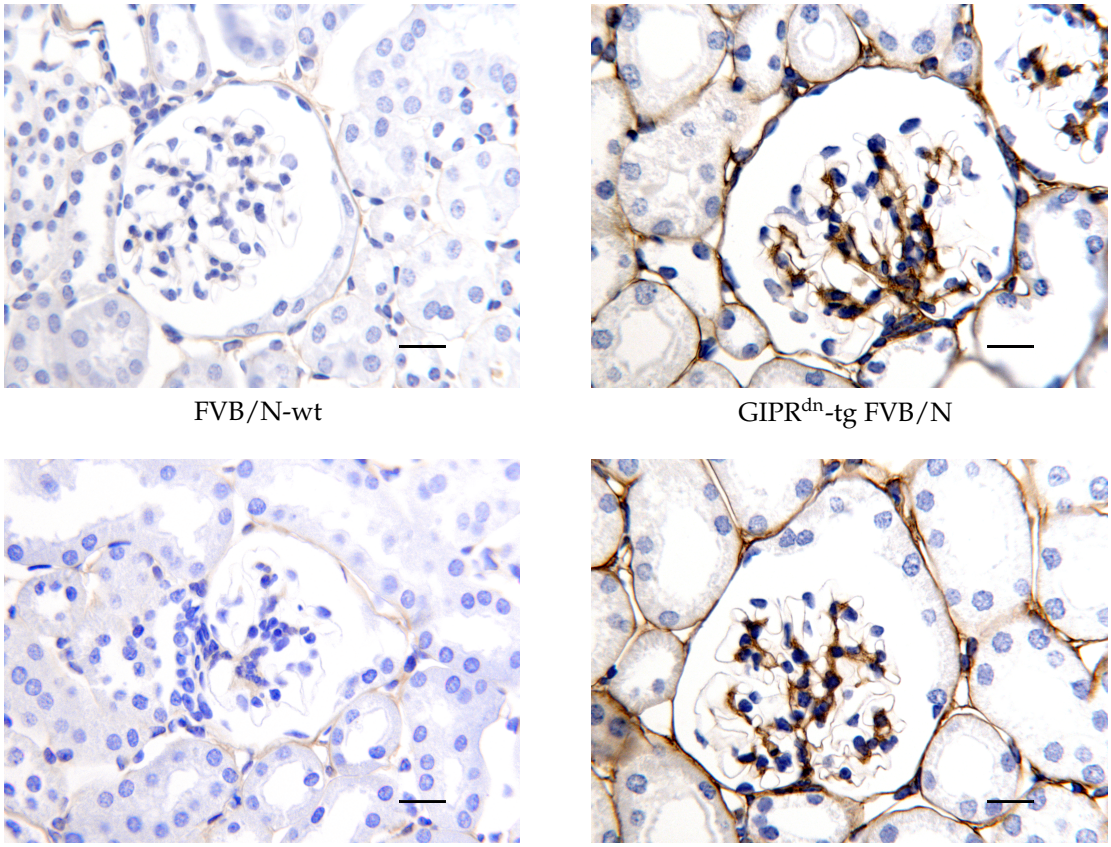

FVB/N-wt | GIPR^{dn}-tg FVB/N

C57BL/6J-wt | GIPR^{dn}-tg C57BL/6J

Figure 4.27 Immunohistochemical detection of collagen IV in paraffin-embedded tissue of GIPR^{dn}-tg mice. Bar 30μm.

Immunohistochemical detection of laminin

GIPR^{dn}-tg FVB/N display increased glomerular immunostaining of laminin compared to FVB/N-wt mice. GIPR^{dn}-tg C57BL/6J display increased glomerular immunostaining of laminin compared to C57BL/6J-wt mice. There is no difference in glomerular laminin immunostaining of GIPR^{dn}-tg FVB/N vs. GIPR^{dn}-tg C57BL/6J or FVB/N-wt vs. C57BL/6J-wt mice.

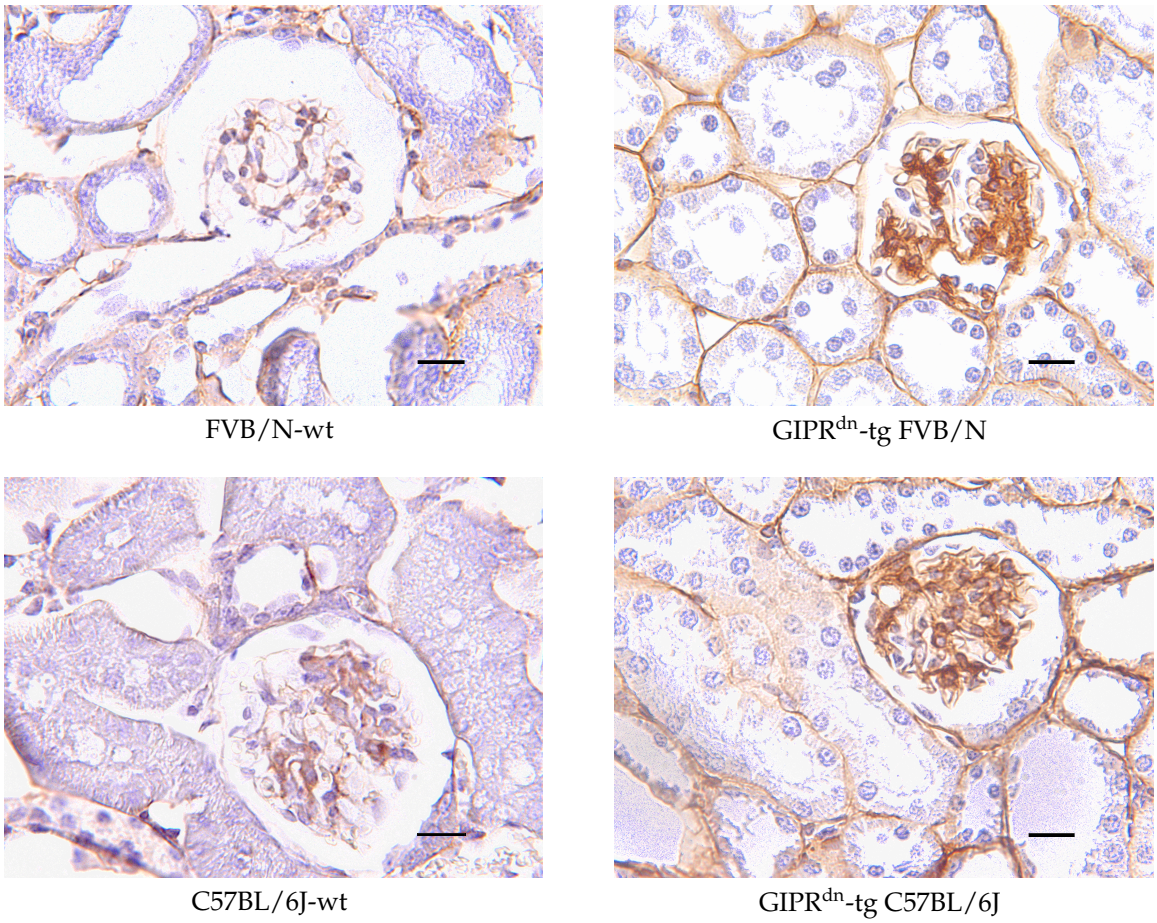

Figure 4.28 Immunohistochemical detection of laminin in paraffin-embedded tissue of GIPR^{dn}-tg mice. Bar 30μm.

Immunohistochemical detection of fibronectin

GIPR^{dn}-tg FVB/N display increased immunostaining of fibronectin in the glomerulus compared to FVB/N-wt mice. GIPR^{dn}-tg C57BL/6J mice display increased glomerular immunostaining of fibronectin compared to C57BL/6J-wt mice. GIPR^{dn}-tg FVB/N mice display more intense immunostaining of fibronectin in the glomerulus compared to GIPR^{dn}-tg C57BL/6J. There is no difference in the fibronectin immunostaining intensity in the glomeruli of FVB/N-wt vs. C57BL/6J-wt mice.

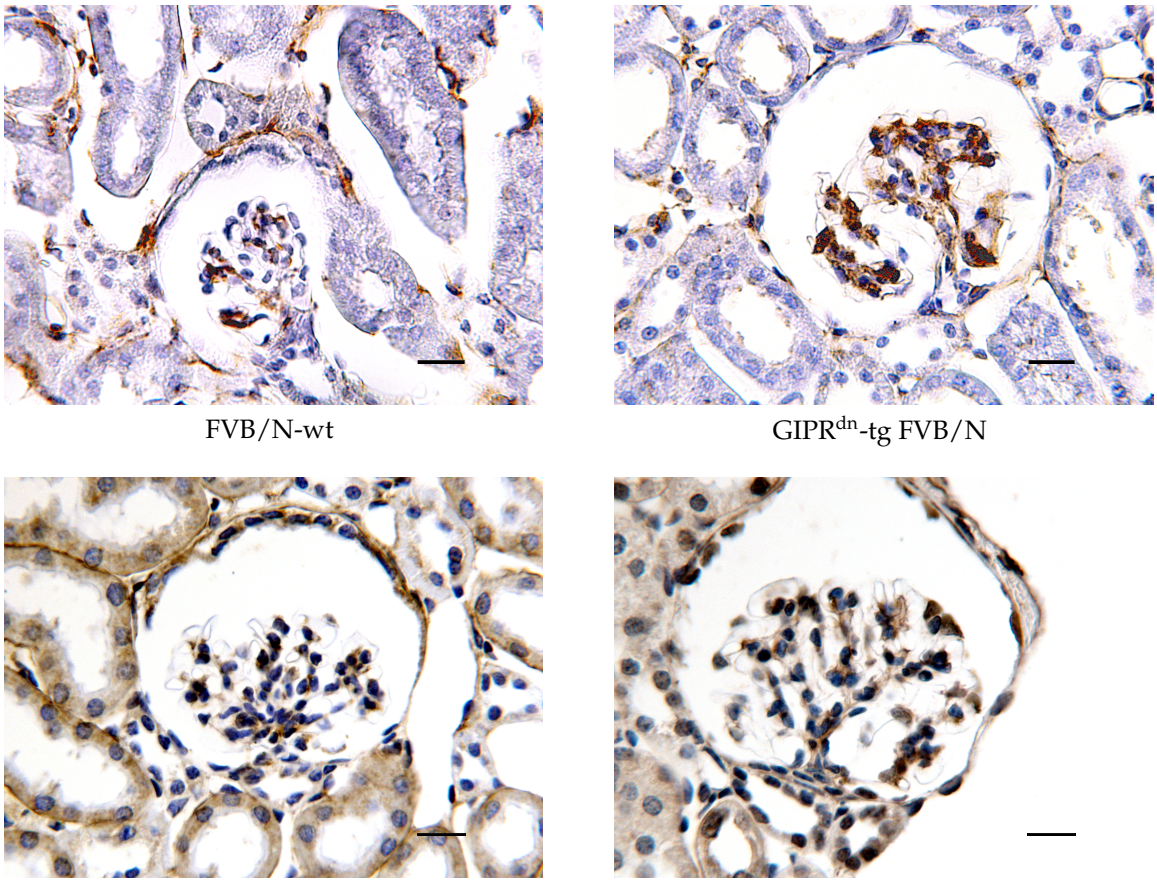

FVB/N-wt | GIPR^{dn}-tg FVB/N

C57BL/6J-wt | GIPR^{dn}-tg C57BL/6J

Figure 4.29 Immunohistochemical detection of fibronectin in paraffin-embedded tissue of GIPR^{dn}-tg mice. Bar 30μm.

Immunohistochemical detection of TGF-β1 in the glomerulus

Podocytes of GIPR^{dn}-tg FVB/N display TGF-β1 immunostaining, unlike FVB/N-wt, GIPR^{dn}-tg C57BL/6J and C57BL/6J-wt mice.

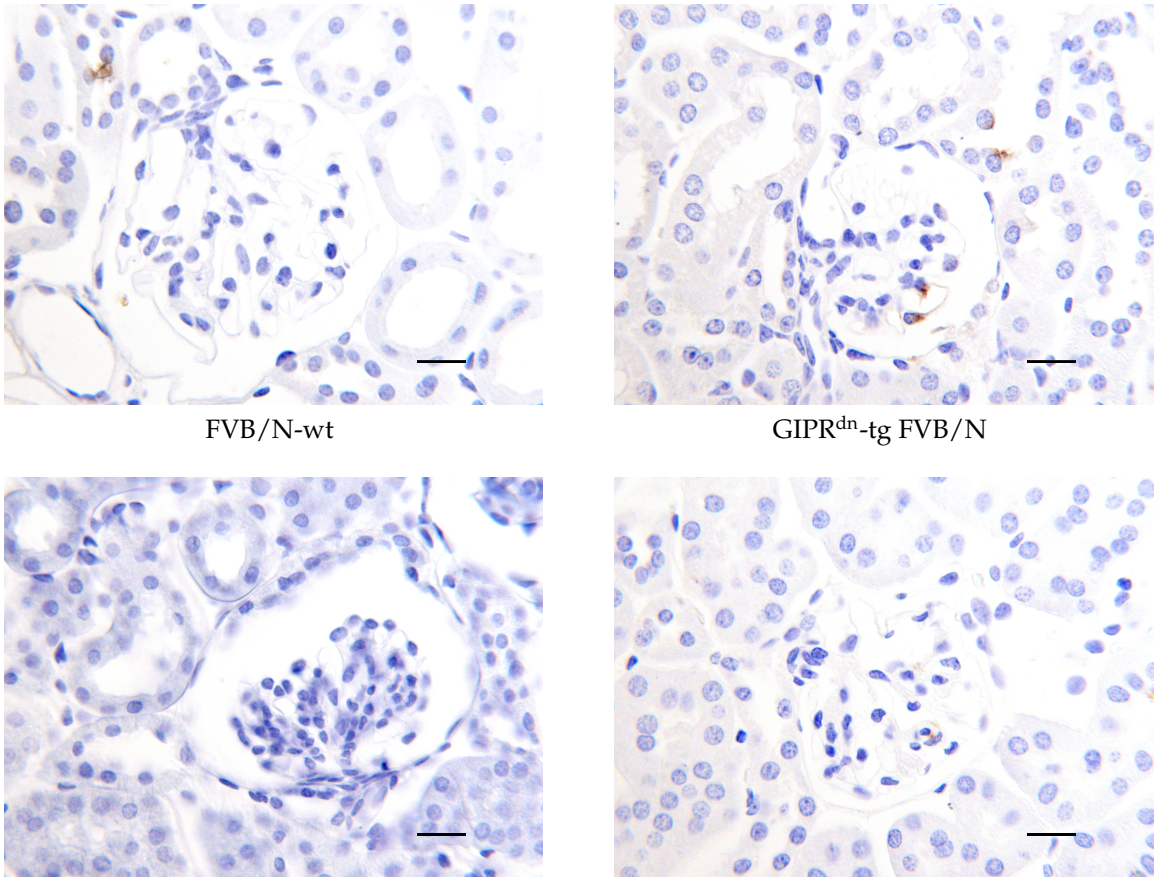

FVB/N-wt | GIPR^{dn}-tg FVB/N

C57BL/6J-wt | GIPR^{dn}-tg C57BL/6J

Figure 4.30 Immunohistochemical detection of TGF-β1 in paraffin-embedded tissue of GIPR^{dn}-tg mice. Bar 30μm.

4.3 Glomerulosclerosis index

The glomerulosclerosis index of GIPR^{dn}-tg FVB/N mice is statistically significantly increased by the factor 3.5 compared to FVB/N-wt mice. The glomerulosclerosis index of GIPR^{dn}-tg FVB/N mice is statistically significantly higher by the factor 3.8 compared to GIPR^{dn}-tg C57BL/6J mice. There is no statistically significant difference in the glomerulosclerosis index of GIPR^{dn}-tg C57BL/6J vs. C57BL/6J-wt or FVB/N-wt vs. C57BL/6J-wt mice.

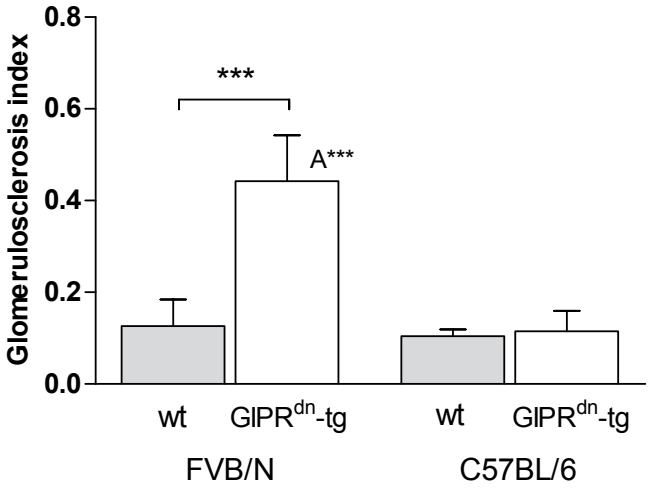

Figure 4.31 Glomerulosclerosis index
Data are depicted as means ± SD, n=8. Significance calculated with Student's t-test. Welch's correction was used for GIPR^{dn}-tg C57BL/6J vs. C57BL/6J-wt, GIPR^{dn}-tg FVB/N vs. GIPR^{dn}-tg C57BL/6J and FVB/N-wt vs. C57BL/6J-wt. Level of significance is displayed as $* = p \leq 0.05, ** = p \leq 0.01$ and $*** = p \leq 0.001$. "A" marks significant differences between GIPR^{dn}-tg FVB/N and GIPR^{dn}-tg C57BL/6J animals, "B" between FVB/N-wt and C57BL/6J-wt animals. **wt**: non-transgenic wild-type littermate controls, **GIPR^{dn}-tg**: GIPR^{dn}-transgenic mice

4.4 Quantitative stereological parameters

4.4.1 Total volume of both kidneys

Compared to FVB/N-wt mice, the total volume of both kidneys of GIPR^{dn}-tg FVB/N mice is statistically significantly increased by 29%. In GIPR^{dn}-tg C57BL/6J mice, the total volume of both kidneys is statistically significantly increased by 12% compared to C57BL/6J-wt mice. The total volume of both kidneys of GIPR^{dn}-tg FVB/N mice is statistically significantly increased by 65% compared to GIPR^{dn}-tg C57BL/6J mice, while the kidney volume-to-body weight ratio is increased by 64%, compared to GIPR^{dn}-tg C57BL/6J mice. The total volume of both kidneys of FVB/N-wt mice is statistically significantly increased by 42%, compared to C57BL/6J-wt mice. The kidney volume-to-body weight ratio is increased by 33% in FVB/N-wt mice compared to C57BL/6J-wt mice.

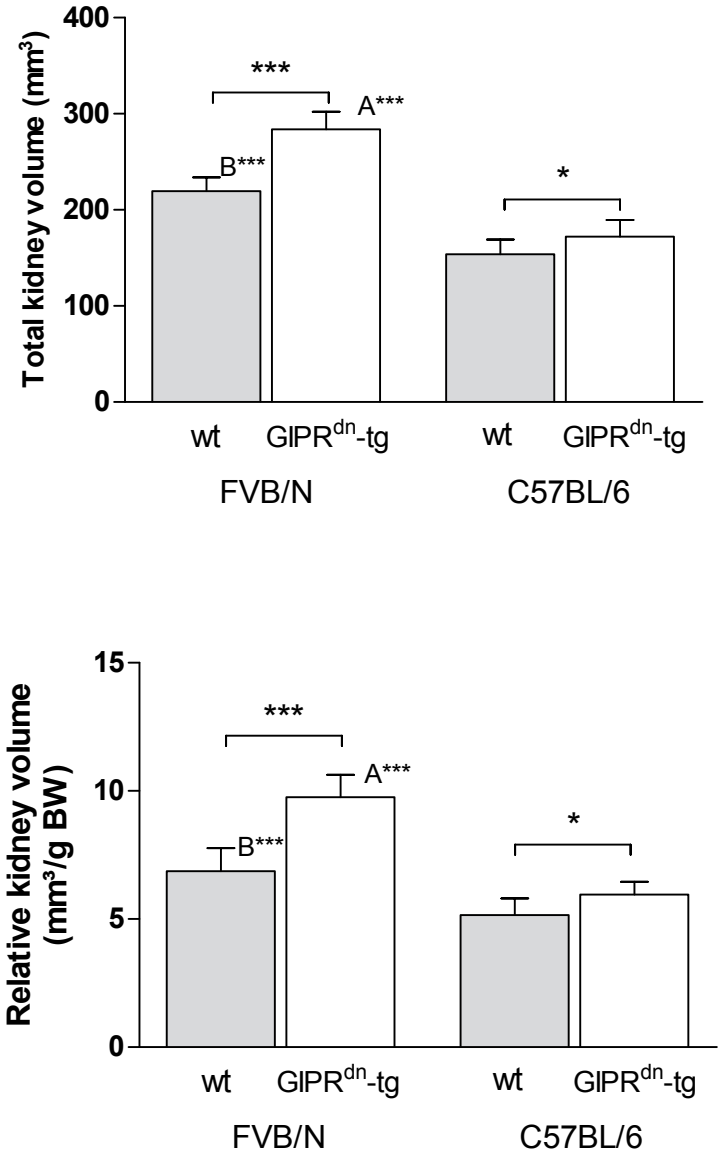

Figure 4.32 Total volume of both kidneys
Data are depicted as means ± SD, n=8. Significance calculated with Student's t-test. Level of significance is displayed as $* = p \leq 0.05, ** = p \leq 0.01$ and $*** = p \leq 0.001$. "A" marks significant differences between GIPR^{dn}-tg FVB/N and GIPR^{dn}-tg C57BL/6J animals, "B" between FVB/N-wt and C57BL/6J-wt animals. **wt**: non-transgenic wild-type littermate controls, **GIPR^{dn}-tg**: GIPR^{dn}-transgenic mice

4.4.2 Total number of nephrons in both kidneys

There is no statistically significant difference in the total nephron number in both kidneys of GIPR^{dn}-tg FVB/N vs. FVB/N-wt, GIPR^{dn}-tg C57BL/6J vs. C57BL/6J-wt, GIPR^{dn}-tg FVB/N vs. GIPR^{dn}-tg C57BL/6J or FVB/N-wt vs. C57BL/6J-wt mice.

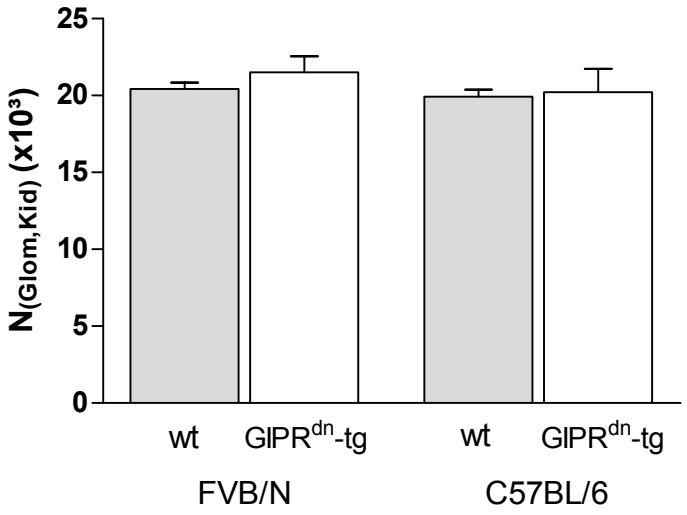

Figure 4.33 Total nephron number in both kidneys
Data are depicted as means ± SD, n=5. Significance calculated with Student's t-test. Welch's correction was used for GIPR^{dn}-tg C57BL/6J vs. C57BL/6J-wt. Level of significance is displayed as $* = p \leq 0.05, ** = p \leq 0.01$ and $*** = p \leq 0.001$. "A" marks significant differences between GIPR^{dn}-tg FVB/N and GIPR^{dn}-tg C57BL/6J animals, "B" between FVB/N-wt and C57BL/6J-wt animals. **wt**: non-transgenic wild-type littermate controls, **GIPR^{dn}-tg**: GIPR^{dn}-transgenic mice

4.4.3 Volume fraction of glomeruli in the kidneys

A statistically significant increase by 0.82 percentage points (more than one fourth) is displayed by GIPR^{dn}-tg FVB/N mice compared to the volume fraction of glomeruli in the kidneys of FVB/N-wt mice There is no statistically significant difference in the volume fraction of GIPR^{dn}-tg C57BL/6J vs. C57BL/6J-wt mice. The volume fraction of glomeruli in the kidneys of GIPR^{dn}-tg FVB/N mice is statistically significantly lower by 0.37 percentage points compared to GIPR^{dn}-tg C57BL/6J mice. The volume fraction of glomeruli in the kidneys of FVB/N-wt mice is statistically significantly higher by 0.83 percentage points compared to C57BL/6J-wt mice.

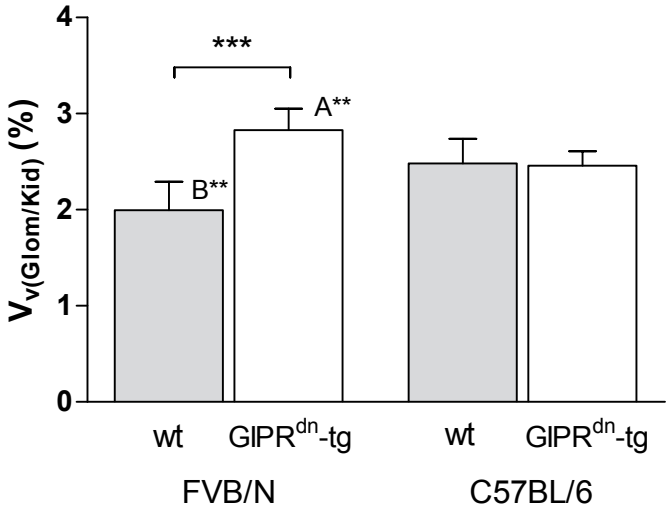

Figure 4.34 Volume fraction of glomeruli in both kidneys
Data are depicted as means ± SD, n=8. Significance calculated with Student's t-test. Level of significance is displayed as $* = p \leq 0.05, ** = p \leq 0.01$ and $*** = p \leq 0.001$. "A" marks significant differences between GIPR^{dn}-tg FVB/N and GIPR^{dn}-tg C57BL/6J animals, "B" between FVB/N-wt and C57BL/6J-wt animals. **wt**: non-transgenic wild-type littermate controls, **GIPR^{dn}-tg**: GIPR^{dn}-transgenic mice

4.4.4 Total glomerular volume in both kidneys

The total glomerular volume pertaining to both kidneys of GIPR^{dn}-tg FVB/N mice is statistically significantly increased by 84% compared to FVB/N-wt mice. The total glomerular volume pertaining to both kidneys of GIPR^{dn}-tg FVB/N mice is statistically significantly increased by 91% compared to GIPR^{dn}-tg C57BL/6 mice. There is no statistically significant difference in the total glomerular volume of GIPR^{dn}-tg C57BL/6 vs. C57BL/6-wt or FVB/N-wt vs. C57BL/6-wt mice.

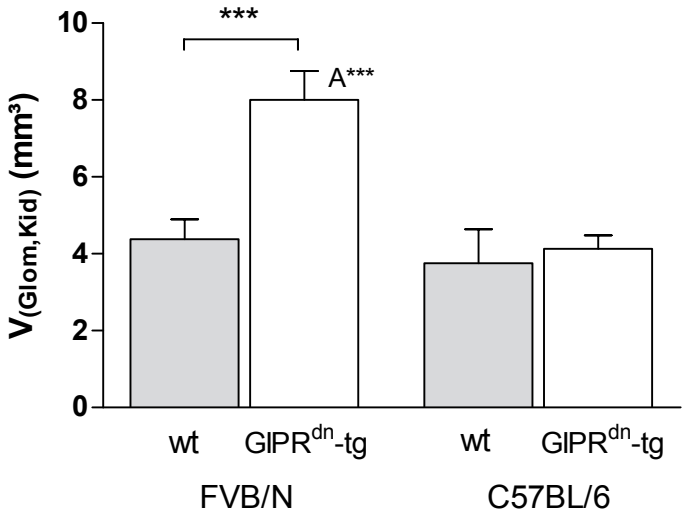

Figure 4.35 Total glomerular volume in both kidneys
Data are depicted as means ± SD, n=8. Significance calculated with Student's t-test. Welch's correction was used for GIPR^{dn}-tg C57BL/6 vs. C57BL/6-wt and GIPR^{dn}-tg FVB/N vs. GIPR^{dn}-tg C57BL/6J. Level of significance is displayed as $* = p \leq 0.05, ** = p \leq 0.01$ and $*** = p \leq 0.001$. "A" marks significant differences between GIPR^{dn}-tg FVB/N and GIPR^{dn}-tg C57BL/6J animals, "B" between FVB/N-wt and C57BL/6J-wt animals. **wt**: non-transgenic wild-type littermate controls, **GIPR^{dn}-tg**: GIPR^{dn}-transgenic mice

4.4.5 Total glomerular volume to body weight ratio

In GIPR^{dn}-tg FVB/N mice, the total glomerular volume per body weight is statistically significantly increased by the factor two compared to FVB/N-wt mice. There is no statistically significant difference in the total glomerular volume per body weight in GIPR^{dn}-tg C57BL/6J vs. C57BL/6J-wt mice or FVB/N-wt vs. C57BL/6J-wt mice. The total glomerular volume per body weight is statistically significantly increased by 93% in GIPR^{dn}-tg FVB/N mice, compared to GIPR^{dn}-tg C57BL/6J mice.

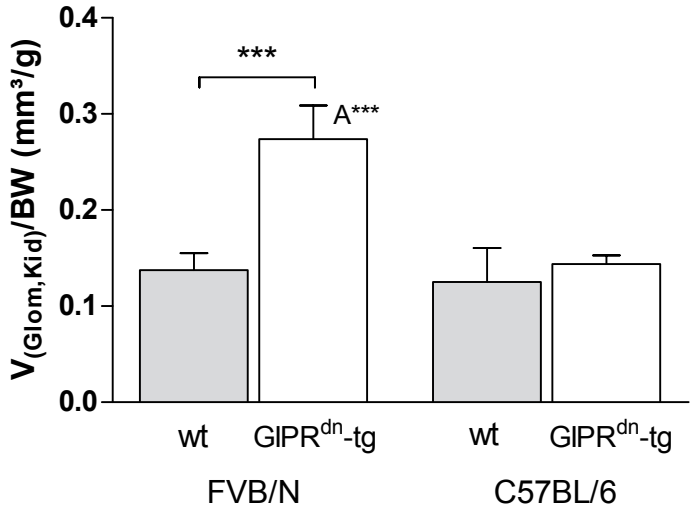

Figure 4.36 Total glomerular volume to body weight ratio
Data are depicted as means ± SD, n=8. Significance was calculated with Student's t-test for GIPR^{dn}-tg FVB/N vs. FVB/N-wt and FVB/N-wt vs. C57BL/6J-wt mice. Welch's correction was used for GIPR^{dn}-tg C57BL/6J vs. C57BL/6J mice and GIPR^{dn}-tg FVB/N vs. GIPR^{dn}-tg C57BL/6J mice. Level of significance is displayed as $* = p \leq 0.05, ** = p \leq 0.01$ and $*** = p \leq 0.001$. "A" marks significant differences between GIPR^{dn}-tg FVB/N and GIPR^{dn}-tg C57BL/6J animals, "B" between FVB/N-wt and C57BL/6J-wt animals. **wt**: non-transgenic wild-type littermate controls, **GIPR^{dn}-tg**: GIPR^{dn}-transgenic mice

4.4.6 Mean glomerular volume

The mean glomerular volume of GIPR^{dn}-tg FVB/N mice is statistically significantly increased by the factor 1.6 compared to FVB/N-wt mice. In GIPR^{dn}-tg C57BL/6J mice, the mean glomerular volume is statistically significantly increased by the factor 1.2 compared to C57BL/6J-wt mice. The mean glomerular volume of GIPR^{dn}-tg FVB/N mice is statistically significantly higher by the factor 2.3 compared to GIPR^{dn}-tg C57BL/6J mice. Compared to C57BL/6J-wt mice, the mean glomerular volume of FVB/N-wt mice is statistically significantly higher by the factor 1.8.

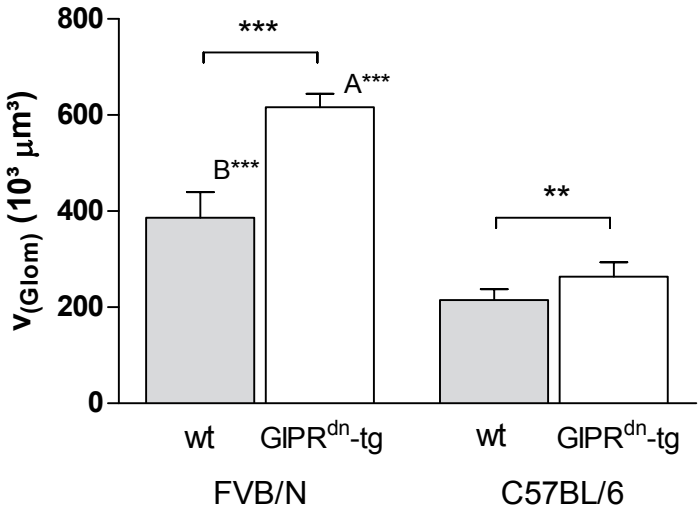

Figure 4.37 Mean glomerular volume
Data are depicted as means ± SD, n=8. Significance calculated with Student's t-test. Welch's correction was used for FVB/N-wt vs. C57BL/6J-wt. Level of significance is displayed as $* = p \leq 0.05, ** = p \leq 0.01$ and $*** = p \leq 0.001$. "A" marks significant differences between GIPR^{dn}-tg FVB/N and GIPR^{dn}-tg C57BL/6J animals, "B" between FVB/N-wt and C57BL/6J-wt animals. **wt**: non-transgenic wild-type littermate controls, **GIPR^{dn}-tg**: GIPR^{dn}-transgenic mice

4.4.7 Mean glomerular volume to body weight ratio

The mean glomerular volume per body weight in GIPR^{dn}-tg FVB/N mice is statistically significantly increased by the factor 1.8 compared to FVB/N-wt mice. GIPR^{dn}-tg C57BL/6J mice display an by 30% statistically significantly increased mean glomerular volume per body weight compared to C57BL/6J-wt mice. In GIPR^{dn}-tg FVB/N vs. GIPR^{dn}-tg C57BL/6J mice, the mean glomerular volume per body weight is statistically significantly higher by the factor 2.3. FVB/N-wt vs. C57BL/6J-wt mice display a by the factor 1.7 statistically significantly higher mean glomerular volume per body weight.

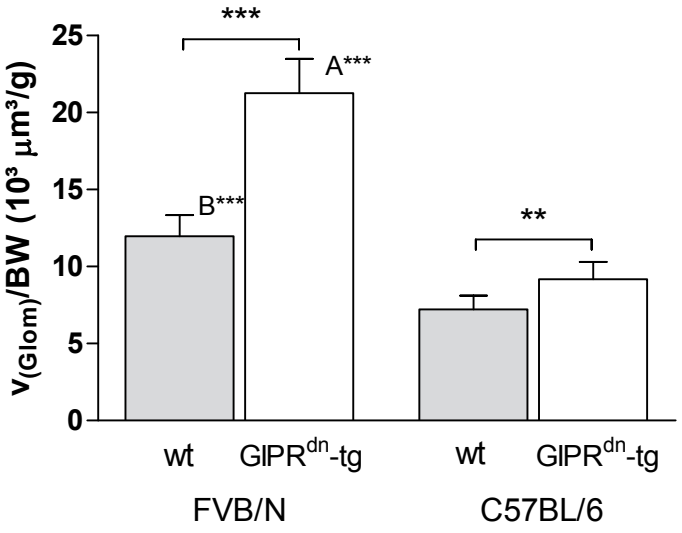

Figure 4.38 Mean glomerular volume to body weight ratio
Data are depicted as means $\pm$ SD, n=8. Significance calculated with Student's t-test. Welch's correction was used for FVB/N-wt vs. C57BL/6J-wt Level of significance is displayed as $* = p \leq 0.05, ** = p \leq 0.01$ and $*** = p \leq 0.001$. "A" marks significant differences between GIPR^{dn}-tg FVB/N and GIPR^{dn}-tg C57BL/6J animals, "B" between FVB/N-wt and C57BL/6J-wt animals. **wt**: non-transgenic wild-type littermate controls, **GIPR^{dn}-tg**: GIPR^{dn}-transgenic mice

4.4.8 Numerical volume density of podocytes in the glomerulus

GIPR^{dn}-tg FVB/N mice display a numerical volume density of podocytes in the glomerulus, that is approximately half as high as that of FVB/N-wt mice. In GIPR^{dn}-tg C57BL/6J vs. C57BL/6J-mice, no statistically significant difference is apparent. The glomerular numerical volume density of GIPR^{dn}-tg FVB/N mice is statistically significantly lower compared to GIPR^{dn}-tg C57BL/6J mice. FVB/N-wt mice display a statistically significantly lower numerical volume density of podocytes in the glomerulus compared to C57BL/6J-wt mice.

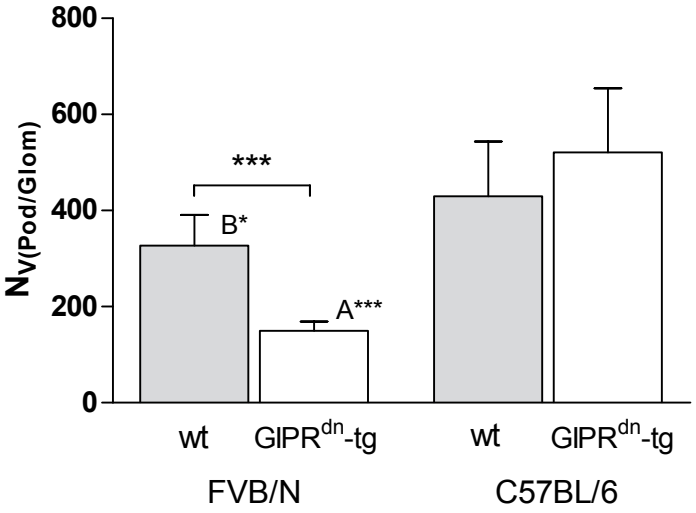

Figure 4.39 Numerical volume density of podocytes in the glomerulus
Data are depicted as means $\pm$ SD, n=8. Significance calculated with Student's t-test (GIPR^{dn}-tg C57BL/6J vs. C57BL/6J-wt mice, FVB/N-wt vs. C57BL/6J-wt mice). Welch's correction was used for GIPR^{dn}-tg FVB/N vs. FVB/N-wt mice and GIPR^{dn}-tg FVB/N vs. GIPR^{dn}-tg C57BL/6J mice. Level of significance is displayed as $* = p \leq 0.05, ** = p \leq 0.01$ and $*** = p \leq 0.001$. "A" marks significant differences between GIPR^{dn}-tg FVB/N and GIPR^{dn}-tg C57BL/6J animals, "B" between FVB/N-wt and C57BL/6J-wt animals. **wt**: non-transgenic wild-type littermate controls, **GIPR^{dn}-tg**: GIPR^{dn}-transgenic mice

4.4.9 Podocyte number per glomerulus

The number of podocytes per glomerulus is statistically significantly reduced by 27% in GIPR^{dn}-tg FVB/N mice compared to FVB/N-wt mice. There is no statistically significant difference in the number of podocytes per glomerulus in GIPR^{dn}-tg C57BL/6J vs. C57BL/6J-wt mice. A by 46% statistically significantly lower number of podocytes per glomerulus is presented by GIPR^{dn}-tg FVB/N mice compared to GIPR^{dn}-tg C57BL/6J mice. The number of podocytes per glomerulus is statistically significantly lower by 26% in FVB/N-wt mice compared to C57BL/6J-wt mice.

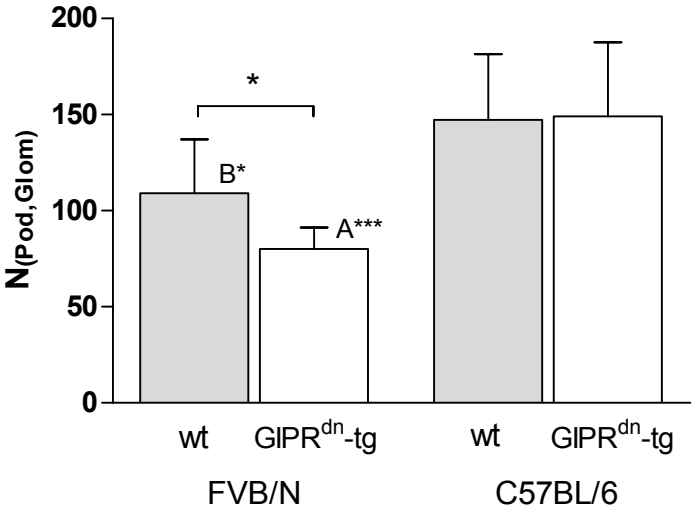

Figure 4.40 Podocyte number per glomerulus
Data are depicted as means ± SD, n=8. Significance calculated with Student's t-test. Welch's correction was used for GIPR^{dn}-tg FVB/N vs. FVB/N-wt and GIPR^{dn}-tg FVB/N vs. GIPR^{dn}-tg C57BL/6J. Level of significance is displayed as $* = p \leq 0.05, ** = p \leq 0.01$ and $*** = p \leq 0.001$. "A" marks significant differences between GIPR^{dn}-tg FVB/N and GIPR^{dn}-tg C57BL/6J animals, "B" between FVB/N-wt and C57BL/6J-wt animals. **wt**: non-transgenic wild-type littermate controls, **GIPR^{dn}-tg**: GIPR^{dn}-transgenic mice

4.4.10 Volume fraction of podocytes in the glomerulus

There is no statistically significant difference in the volume fraction of podocytes in the glomerulus of GIPR^{dn}-tg FVB/N vs. FVB/N-wt or GIPR^{dn}-tg C57BL/6J vs. C57BL/6J-wt mice. The volume fraction of GIPR^{dn}-tg FVB/N mice is statistically significantly lower by 11.13 percentage points compared to GIPR^{dn}-tg C57BL/6J mice. Compared to C57BL/6J-wt mice, the volume fraction of FVB/N-wt mice is statistically significantly lower by 6.39 percentage points.

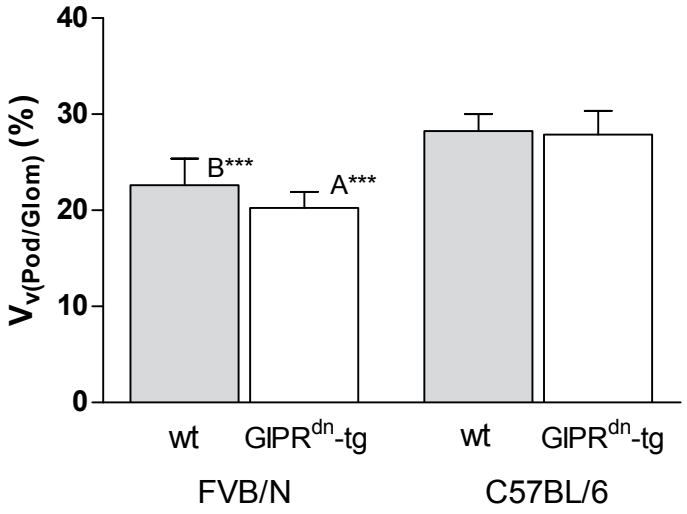

Figure 4.41 Volume fraction of podocytes in the glomerulus
Data are depicted as means ± SD, n=8. Significance calculated with Student's t-test. Level of significance is displayed as $* = p \leq 0.05, ** = p \leq 0.01$ and $*** = p \leq 0.001$. "A" marks significant differences between GIPR^{dn}-tg FVB/N and GIPR^{dn}-tg C57BL/6J animals, "B" between FVB/N-wt and C57BL/6J-wt animals. **wt**: non-transgenic wild-type littermate controls, **GIPR^{dn}-tg**: GIPR^{dn}-transgenic mice

4.4.11 Mean podocyte volume

The mean podocyte volume of GIPR^{dn}-tg FVB/N mice is statistically significantly increased by 93% compared to FVB/N-wt mice. In GIPR^{dn}-tg C57BL/6J mice, the mean podocyte volume is statistically significantly increased by 31% compared to C57BL/6J-wt mice. the mean podocyte volume of GIPR^{dn}-tg FVB/N mice is statistically significantly higher by the factor 2.1 Compared to GIPR^{dn}-tg C57BL/6J mice, the mean podocyte volume of GIPR^{dn}-tg FVB/N mice is statistically significantly higher by the factor 2.1. The mean podocyte volume of FVB/N-wt mice is statistically significantly higher by 44% compared to C57BL/6J-wt mice.

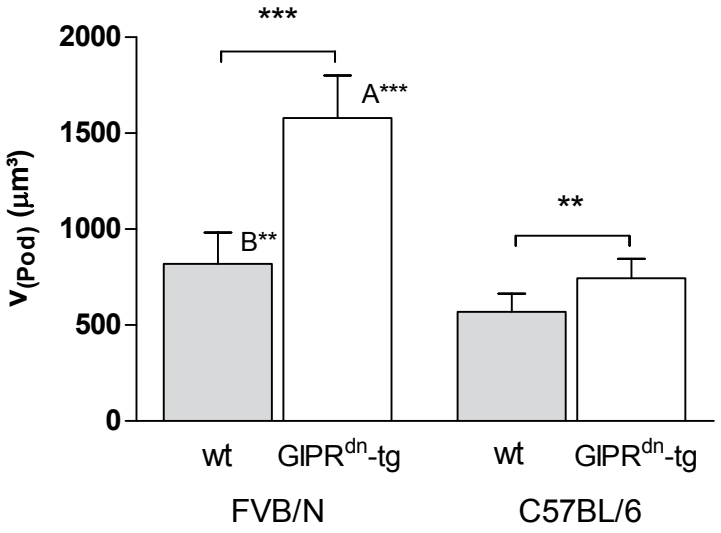

Figure 4.42 Mean podocyte volume
Data are depicted as means ± SD, n=8. Significance calculated with Student's t-test. Level of significance is displayed as $* = p \leq 0.05, ** = p \leq 0.01$ and $*** = p \leq 0.001$. "A" marks significant differences between GIPR^{dn}-tg FVB/N and GIPR^{dn}-tg C57BL/6J animals, "B" between FVB/N-wt and C57BL/6J-wt animals. **wt**: non-transgenic wild-type littermate controls, **GIPR^{dn}-tg**: GIPR^{dn}-transgenic mice

4.4.12 Volume fraction of mesangium in the glomerulus

In GIPR^{dn}-tg FVB/N mice, the volume fraction of mesangium in the glomerulus is statistically significantly increased by 3.7 percentage points compared to FVB/N-wt mice. The volume fraction of mesangium in the glomerulus of GIPR^{dn}-tg C57BL/6J mice is statistically significantly increased by 3.5 percentage points compared to C57BL/6J-wt mice. Compared to GIPR^{dn}-tg C57BL/6J mice, the volume fraction of mesangium in the glomerulus of GIPR^{dn}-tg FVB/N mice is statistically significantly higher by 4.4 percentage points. The volume fraction of mesangium in the glomerulus of FVB/N-wt mice is statistically significantly higher by 4.2 percentage points compared to C57BL/6J-wt mice.

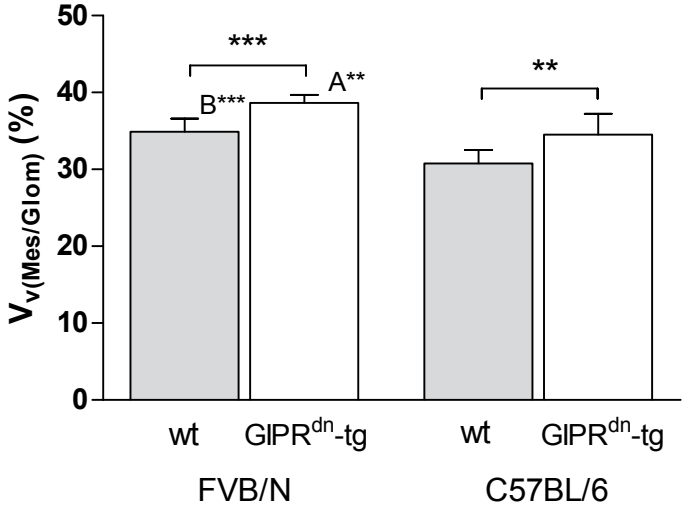

Figure 4.43 Volume fraction of mesangium in the glomerulus
Data are depicted as means ± SD, n=8. Significance calculated with Student's t-test. Level of significance is displayed as $* = p \leq 0.05, ** = p \leq 0.01$ and $*** = p \leq 0.001$. "A" marks significant differences between GIPR^{dn}-tg FVB/N and GIPR^{dn}-tg C57BL/6J animals, "B" between FVB/N-wt and C57BL/6J-wt animals. **wt**: non-transgenic wild-type littermate controls, **GIPR^{dn}-tg**: GIPR^{dn}-transgenic mice

4.4.13 Mean mesangial volume per glomerulus

The mean mesangial volume per glomerulus of GIPR^{dn}-tg FVB/N mice is statistically significantly increased by 73% compared to FVB/N-wt mice. In GIPR^{dn}-tg C57BL/6J mice, the mean mesangial volume per glomerulus is statistically significantly increased by 14% compared to C57BL/6J-wt mice. The mean mesangial volume per glomerulus of GIPR^{dn}-tg FVB/N mice is statistically significantly higher by the factor 3.7 compared to GIPR^{dn}-tg C57BL/6J mice. Compared to C57BL/6J-wt mice, the mean mesangial volume per glomerulus of FVB/N-wt mice is statistically significantly higher by the factor 2.2.

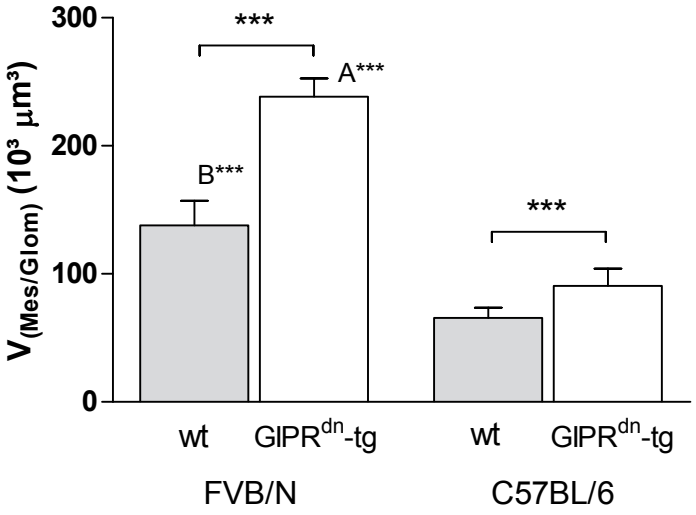

Figure 4.44 Mean glomerular mesangial volume
Data are depicted as means ± SD, n=8. Significance calculated with Student's t-test. Welch's correction was used for GIPR^{dn}-tg FVB/N vs. GIPR^{dn}-tg C57BL/6J and FVB/N-wt vs. C57BL/6J-wt. Level of significance is displayed as $* = p \leq 0.05, ** = p \leq 0.01$ and $*** = p \leq 0.001$. "A" marks significant differences between GIPR^{dn}-tg FVB/N and GIPR^{dn}-tg C57BL/6J animals, "B" between FVB/N-wt and C57BL/6J-wt animals. **wt**: non-transgenic wild-type littermate controls, **GIPR^{dn}-tg**: GIPR^{dn}-transgenic mice

4.4.14 Volume fraction of capillaries in the glomerulus

There is no statistically significant difference in the volume fraction of capillaries per glomerulus in GIPR^{dn}-tg FVB/N vs. FVB/N-wt mice. The volume fraction of capillaries in the glomerulus of GIPR^{dn}-tg C57BL/6J mice is statistically significantly decreased by 2.4 percentage points compared to C57BL/6J-wt mice. In GIPR^{dn}-tg FVB/N mice, the volume fraction of capillaries per glomerulus is statistically significantly increased by 3.6 percentage points compared to GIPR^{dn}-tg C57BL/6J mice. There is no statistically significant difference in the volume fraction of capillaries per glomerulus in FVB/N-wt vs. C57BL/6J-wt mice.

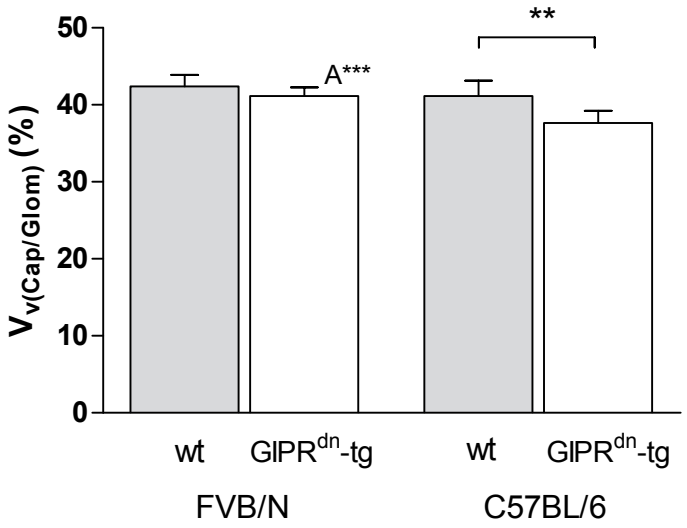

Figure 4.45 Volume fraction of capillaries per glomerulus
Data are depicted as means ± SD, n=8. Significance calculated with Student's t-test. Level of significance is displayed as $* = p \leq 0.05, ** = p \leq 0.01$ and $*** = p \leq 0.001$. "A" marks significant differences between GIPR^{dn}-tg FVB/N and GIPR^{dn}-tg C57BL/6J animals, "B" between FVB/N-wt and C57BL/6J-wt animals. **wt**: non-transgenic wild-type littermate controls, **GIPR^{dn}-tg**: GIPR^{dn}-transgenic mice

4.4.15 Mean capillary volume per glomerulus

The mean glomerular capillary volume per glomerulus of GIPR^{dn}-tg FVB/N mice is statistically significantly increased by 51% compared to FVB/N-wt mice. There is no statistically significant difference in the mean capillary volume of GIPR^{dn}-tg C57BL/6J vs. C57BL/6J-wt mice. A by the factor 2.8 statistically significantly higher mean glomerular capillary volume per glomerulus compared to GIPR^{dn}-tg C57BL/6J mice, is displayed by GIPR^{dn}-tg FVB/N mice. The mean glomerular capillary volume per glomerulus of FVB/N-wt mice is statistically significantly higher by the factor 1.8 compared to C57BL/6J-wt mice.

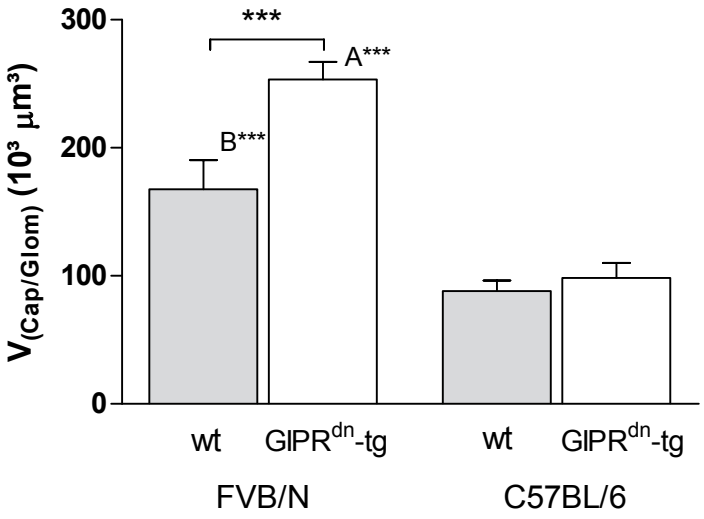

Figure 4.46 Mean glomerular capillary volume
Data are depicted as means ± SD, n=8. Significance calculated with Student's t-test. Welch's correction was used for GIPR^{dn}-tg FVB/N vs. FVB/N-wt and FVB/N-wt vs. C57BL/6J-wt. Level of significance is displayed as $* = p \leq 0.05, ** = p \leq 0.01$ and $*** = p \leq 0.001$. "A" marks significant differences between GIPR^{dn}-tg FVB/N and GIPR^{dn}-tg C57BL/6J animals, "B" between FVB/N-wt and C57BL/6J-wt animals. **wt**: non-transgenic wild-type littermate controls, **GIPR^{dn}-tg**: GIPR^{dn}-transgenic mice

4.4.16 Capillary length density in the glomerulus

The capillary length density per glomerulus of GIPR^{dn}-tg FVB/N mice is statistically significantly decreased by 28% compared to FVB/N-wt mice. Compared to GIPR^{dn}-tg C57BL/6J mice, the capillary length density per glomerulus of GIPR^{dn}-tg FVB/N mice is statistically significantly lower by 31%. There is no statistically significant difference in the capillary length density in the glomerulus of GIPR^{dn}-tg C57BL/6J vs. C57BL/6J-wt or FVB/N-wt vs. C57BL/6J-wt mice.

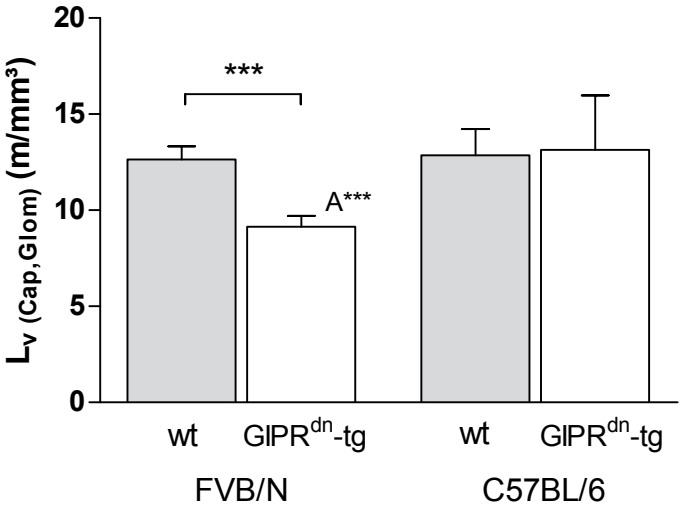

Figure 4.47 Capillary length density in the glomerulus
Data are depicted as means ± SD, n=8. Significance calculated with Student's t-test (GIPR^{dn}-tg FVB/N vs. FVB/N-wt and FVB/N-wt vs. C57BL/6J-wt) and Mann-Whitney u-test (GIPR^{dn}-tg C57BL/6J vs. C57BL/6J-wt and GIPR^{dn}-tg FVB/N vs. GIPR^{dn}-tg C57BL/6J). Level of significance is displayed as $* = p \leq 0.05, ** = p \leq 0.01$ and $*** = p \leq 0.001$. "A" marks significant differences between GIPR^{dn}-tg FVB/N and GIPR^{dn}-tg C57BL/6J animals, "B" between FVB/N-wt and C57BL/6J-wt animals. **wt**: non-transgenic wild-type littermate controls, **GIPR^{dn}-tg**: GIPR^{dn}-transgenic mice

4.4.17 Mean capillary length per glomerulus

In GIPR^{dn}-tg FVB/N mice, the mean capillary length per glomerulus is statistically significantly increased by 16% compared to FVB/N-wt mice. The mean capillary length per glomerulus of GIPR^{dn}-tg C57BL/6J mice is statistically significantly increased by 25% compared to C57BL/6J-wt mice. The mean capillary length per glomerulus of GIPR^{dn}-tg FVB/N mice is statistically significantly higher by 63% compared to GIPR^{dn}-tg C57BL/6J mice. The mean capillary length per glomerulus of FVB/N-wt mice is statistically significantly higher by 77% compared to C57BL/6J-wt mice.

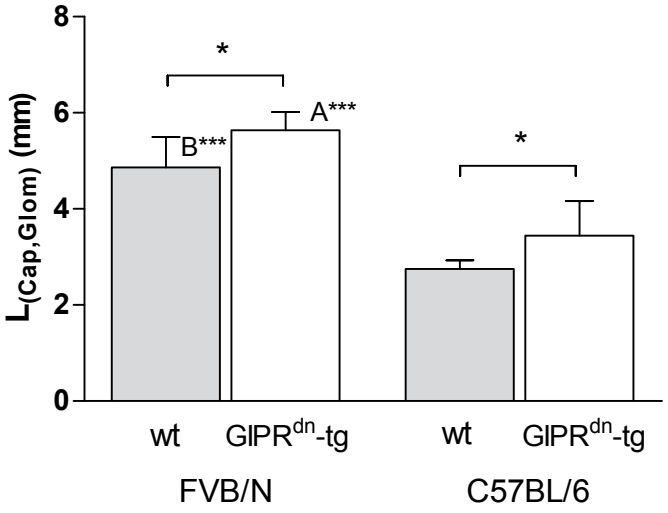

Figure 4.48 Mean capillary length per glomerulus
Data are depicted as means ± SD, n=8. Significance calculated with Student's t-test. Welch's correction was used for GIPR^{dn}-tg C57BL/6J vs. C57BL/6J-wt and FVB/N-wt vs. C57BL/6J-wt. Level of significance is displayed as $* = p \leq 0.05, ** = p \leq 0.01$ and $*** = p \leq 0.001$. "A" marks significant differences between GIPR^{dn}-tg FVB/N and GIPR^{dn}-tg C57BL/6J animals, "B" between FVB/N-wt and C57BL/6J-wt animals. **wt**: non-transgenic wild-type littermate controls, **GIPR^{dn}-tg**: GIPR^{dn}-transgenic mice

4.4.18 Filtration slit frequency

There is no statistically significant difference in the filtration slit frequency of of GIPR^{dn}-tg FVB/N vs. FVB/N-wt, GIPR^{dn}-tg C57BL/6J vs. C57BL/6J-wt or GIPR^{dn}-tg FVB/N vs. GIPR^{dn}-tg C57BL/6J mice. The filtration slit frequency in FVB/N-wt mice is slightly, but statistically significantly lower compared to C57BL/6J-wt mice.

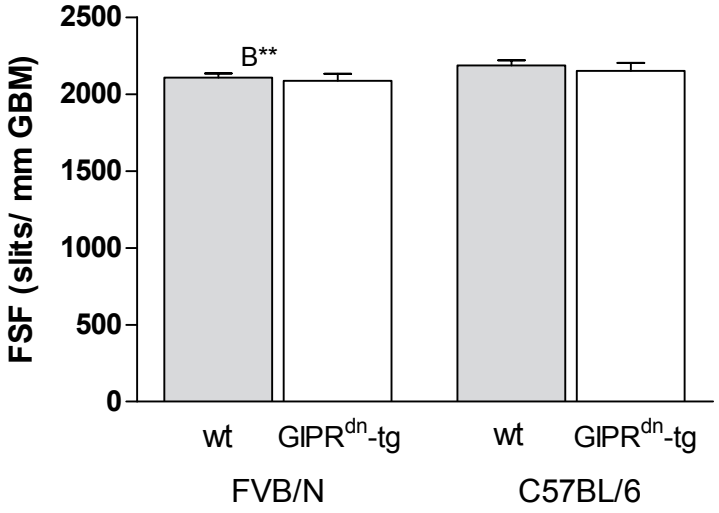

Figure 4.49 Filtration slit frequency
Data are depicted as means ± SD, n=5. Significance calculated with Student's t-test. Level of significance is displayed as $* = p \leq 0.05, ** = p \leq 0.01$ and $*** = p \leq 0.001$. "A" marks significant differences between GIPR^{dn}-tg FVB/N and GIPR^{dn}-tg C57BL/6J animals, "B" between FVB/N-wt and C57BL/6J-wt animals. **wt**: non-transgenic wild-type littermate controls, **GIPR^{dn}-tg**: GIPR^{dn}-transgenic mice

4.4.19 True harmonic mean thickness of the glomerular basement membrane (GBM)

The glomerular basement membrane thickness of GIPR^{dn}-tg FVB/N mice is statistically significantly increased by 7% compared to FVB/N-wt mice. There is no statistically significant difference in the glomerular basement membrane thickness of GIPR^{dn}-tg C57BL/6J vs. C57BL/6J-wt mice. The glomerular basement membrane thickness of GIPR^{dn}-tg FVB/N mice is statistically significantly greater by 17% compared to GIPR^{dn}-tg C57BL/6J mice.s In FVB/N-wt mice, the glomerular basement membrane thickness is statistically significantly greater by 11% compared to C57BL/6J-wt mice.

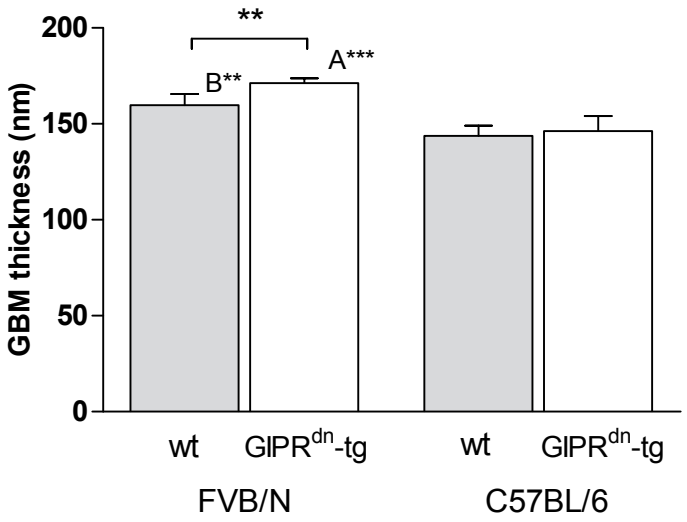

Figure 4.50 Glomerular basement membrane thickness
Data are depicted as means ± SD, n=5. Significance calculated with Student's t-test. Level of significance is displayed as $* = p \leq 0.05, ** = p \leq 0.01$ and $*** = p \leq 0.001$. "A" marks significant differences between GIPR^{dn}-tg FVB/N and GIPR^{dn}-tg C57BL/6J animals, "B" between FVB/N-wt and C57BL/6J-wt animals. **wt**: non-transgenic wild-type littermate controls, **GIPR^{dn}-tg**: GIPR^{dn}-transgenic mice

5 Discussion

5.1 General aspects

The present study was performed to examine the influence of the genetic background on the development and severity of diabetes mellitus and associated renal lesions in GIPR^{dn}-transgenic mice. Kidney architecture, blood pressure, blood glucose concentration and other factors that are suspected of playing a role in the development of renal lesions, were evaluated in the FVB/N and C57BL/6J strain and in GIPR^{dn}-tg mice of both backgrounds. The presence and severity of diabetes mellitus was evaluated in GIPR^{dn}-tg FVB/N and GIPR^{dn}-tg C57BL/6J mice. The results were interpreted in respect to strain-dependent differences between the FVB/N and C57BL/6J strain in general and their possible influence on the severity of diabetic lesions in GIPR^{dn}-tg mice. While genetic factors obviously play a role in determining phenotype, the identification of those factors was not an objective of the current study. The copy number and insertation place of the transgene were not examined, nor are differences between the different genetic backgrounds to be expected in this respect. To investigate differences in the severity of diabetes mellitus and susceptibility to diabetes-associated renal lesions, eight male GIPR^{dn}-tg mice on a FVB/N and C57BL/6J background and eight male wild-type FVB/N and C57BL/6J mice were monitored until the age of six months.
Age is still a central factor in mouse models of diabetic nephropathy. At 180 days of age, GIPR^{dn} transgenic mice on the CD1 background display many features of diabetic nephropathy (HERBACH et al., 2009), including podocyte hypertrophy, glomerular hypertrophy, glomerulosclerosis and thickening of the glomerular basement membrane. Only male mice were used in the present study, due to the well documented fact that male mice display more severe symptoms of diabetic nephropathy compared to their female litter mates (INADA et al., 2007; GURLEY

et al., 2006). One factor leading to this discrepancy might be the higher blood glucose levels and blood pressure displayed by male mice. The influence of the degree of hyperglycemia on the severity of diabetic nephropathy is well established in humans (UKPDS-GROUP, 1998; DCCT, 1995; WARRAM et al., 1995). Several small studies seem to suggest that this applies to mice as well (CAO et al., 2014; REDDI et al., 1990).
The FVB/N and C57BL/6J strains were chosen because of their popularity and wide-spread use as a genetic background for transgenic animal models of diseases, both in diabetes research and in medical research in general. Diabetic FVB/N mice have been noted for their high albumin excretion (XU et al., 2010). Most models of diabetic nephropathy do not reach the goal of a tenfold or higher increase in albumin levels, making the FVB/N background especially interesting for research. On the other hand, C57BL/6J mice are noted for their resistance to the development of diabetes-associated renal lesions (MA and FOGO, 2003; SHARMA et al., 2003; ZHENG et al., 1998).
Most comparable stereological studies use a sample size of 5-8 animals per group (SHEA et al., 2013; HARTNER et al., 2004; BUZELLO, 2000). To optimize the informative value of the performed analysis, the sample size was set at n=8 for most quantitative stereological evaluations. The analyzed data confirms that the sample size was sufficient to draw valid conclusions.

5.2 Diabetes mellitus in GIPR^{dn}-tg FVB/N and C57BL/6J mice

In the present study, GIPR^{dn}-tg FVB/N mice develop severe diabetes mellitus, while GIPR^{dn}-tg C57BL/6J mice develop a much milder diabetes. Both groups of transgenic mice display elevated casual glucose concentrations. In humans, high blood glucose levels correlate with an increased risk to develop DN, while strict management of hyperglycemia can postpone or prevent the development of DN. The severity of hyperglycemia can, but does not have to, contribute to the progression and severity of DN in mice (GURLEY et al., 2006). The blood glucose concentrations of db/db-transgenic C57BL/6J mice and of high fat diet diabetic C57BL/6J mice (NOONAN and BANKS, 2000; HUMMEL et al., 1972) remain below

the level defined as a diabetic condition (200-300mg/dl, (MARRERO et al., 2013; FOX, 2007)) and can be interpreted as a pre-diabetic state. Other models of diabetes mellitus, like STZ-induced diabetes mellitus type 1 or $Ins2^{Akita/+}$-mutants on a C57BL/6J background show markedly higher casual blood glucose concentrations of 300-500mg/dl, but still develop only mild diabetes-associated renal lesions. In summary, the blood glucose levels of C57BL/6J mice are dependent on the method of diabetes induction, and $GIPR^{dn}$-tg mice develop only mildly elevated blood glucose levels on the C57BL/6J background. $GIPR^{dn}$-tg FVB/N mice, on the other hand, display hyperglycemia consistent with diabetes mellitus. FVB/N mice seem to develop considerable hyperglycemia irrespective of the method of diabetes induction (CHANG et al., 2012; ZHENG et al., 2004). Solely db/db transgenic FVB/N mice display comparatively mild hyperglycemia with casual blood glucose concentrations of only 300-400mg/dl (Table 2.2, p.31). This suggests that the propensity towards developing severe hyperglycemia might be a characteristic trait of the FVB/N genetic background. In comparison, $GIPR^{dn}$-tg CD1 and BALB/c mice develop similar casual blood glucose concentrations of ca. 700mg/dl (POPPER, 2013). The difference in the level of hyperglycemia displayed by diabetic $GIPR^{dn}$-tg mice are important strain-specific features of the FVB/N and C57BL/6J background. The blood glucose concentrations of $GIPR^{dn}$-tg FVB/N and $GIPR^{dn}$-tg C57BL/6J mice may influence the development and severity of renal alterations in these mice.
In addition to hyperglycemia, hypertension is an important feature in the development of DN in human patients. Many mouse models of DN, including $GIPR^{dn}$-tg C57BL/6J mice fail to develop significant hypertension. Blood pressure measurements in conscious mice using tail cuff systems have been shown to be reasonably accurate (KREGE et al., 1995a,b), and as such were chosen as the least stressful option. FVB/N mice display an altogether increased systolic blood pressure compared to C57BL/6J mice, and $GIPR^{dn}$-tg FVB/N mice display increased systolic blood pressure compared to FVB/N-wt mice. $GIPR^{dn}$-tg CD1 and CD1-wt mice presented with systolic blood pressures of 100-120mmHg, $GIPR^{dn}$-tg BALB/c and BALB/c-wt with 130-150mmHg, with no significant increase in transgenic vs. wild-type mice (POPPER, 2013). This strain-dependent difference in systolic blood pressure might contribute to the progression of DN and the severity of renal lesions displayed by $GIPR^{dn}$-tg FVB/N mice.
Polyuria and polydipsia are cardinal symptoms of diabetes mellitus. Persistent hyperglycemia and increased filtration of glucose lead to a capacity overload of the

sodium-glucose linked transporter 2 (SGLT2) in the proximal tubule. The resulting glucosuria leads to osmotic diuresis, causing the polyuria and secondary polydipsia observed in GIPR^{dn}-tg FVB/N and C57BL/6J mice (GERICH, 2010). The water consumption and urine production is drastically increased in GIPR^{dn}-transgenic FVB/N and C57BL/6J mice compared to FVB/N-wt and C57BL/6J-wt mice. Water consumption and urine volume are considerably higher in GIPR^{dn}-tg FVB/N mice compared to GIPR^{dn}-tg C57BL/6J mice, reflecting the background-specific higher degree of hyperglycemia displayed by GIPR^{dn}-tg FVB/N animals. The severely hyperglycemic GIPR^{dn}-tg CD1 mice show an even higher water consumption and urine volume compared to GIPR^{dn}-tg FVB/N, with GIPR^{dn}-tg BABL/c mice falling in between GIPR^{dn}-tg FVB/N and GIPR^{dn}-tg C57BL/6J (POPPER, 2013).
Polyphagia accompanied by failure to gain weight or even weight loss is another common occurrence in diabetes in humans (GELLING, 2006). Though the average body weight of wild-type mice is slightly higher than that of diabetic mice, the difference is not statistically significant for either FVB/N or C57BL/6J mice. In spite of their unaltered body weight, GIPR^{dn}-tg mice consume a considerably higher amount of food. Additionally to hyperphagia and hyperglycemia, diabetics usually show changes in fat metabolism with increased blood triglyceride concentrations and, consequently, reduced high density lipoprotein cholesterol levels and elevated low density lipoprotein cholesterol levels (diabetic dyslipidemia). Diabetic dyslipidemia is associated with a higher risk for cardiovascular disease in human diabetes mellitus patients. Not all mouse models of diabetes mellitus develop diabetic dyslipidemia. However, the concentration of triglycerides in the blood of GIPR^{dn}-tg FVB/N and C57BL/6J mice is higher than that of their respective wild-type controls, with FVB/N mice displaying altogether higher levels than C57BL/6J mice. The increase of serum triglyceride concentrations in GIPR^{dn}-tg might be the result of the mutated GIP receptor expressed by this animal model of diabetes mellitus (PATEL et al., 2014; FARR and ADELI, 2012), compare 2.4.8.

5.3 Influence of the genetic background on the development of diabetic nephropathy in GIPR^{dn}-tg FVB/N and C57BL/6J mice

5.3.1 Kidney function of diabetic GIPR^{dn}-tg FVB/N and C57BL/6J mice

In healthy individuals, the kidney regulates osmolality, acid-base homeostasis and excretes products of metabolism. Serum and urine parameters, including albumin and creatinine, were measured in six months old mice in the present study. Total serum protein concentrations of GIPR^{dn}-tg FVB/N and C57BL/6J mice are slightly, but not significantly, decreased. Causative might be a lower albumin serum concentration, while the serum globulin concentration remains stable. Albumin is usually excreted in a healthy kidney in only negligible quantities, due to a balance of filtration and tubular reabsorption (RUSSO et al., 2007). Due to its small molecular weight of approximately 65kD, it is able to cross the filtration barrier formed by the glomerular basement membrane and the podocyte foot processes (COMPER, 2014; TOJO and KINUGASA, 2012). As an alternate filtration pathway, transport of albumin through the podocyte cell bodies has been proposed (KINUGASA et al., 2011; TOJO et al., 2008). The ability of albumin to cross the filtration barrier has been controversially discussed previously. Albumin excretion in mice has been shown to vary greatly in a both strain and gender dependent manner (GURLEY et al., 2010, 2006; BREYER et al., 2005a). Strains that have been noted for above average albumin excretion are FVB/N mice in general and DBA/2N and BALB/c in STZ-induced diabetes. C57BL/6J mice show the lowest urinary albumin excretion compared to other strains in models of DN, i.e. STZ or Ins2$^{Akita/+}$ (compare Table 2.2, p.31). Male diabetic mice show higher levels of albumin excretion in all investigated strains, and are more predisposed to develop DN in general, probably due to their physiologically higher blood pressure and blood glucose levels (GURLEY et al., 2010, 2006).

In case of alterations of the glomerular filtration barrier, the increased filtration of albumin may exceed the capacity for tubular reabsorption. Another study suggests, that the tubular reabsorption may be decreased in DN, leading to an increased

albumin excretion even in the absence of alterations of the filtration barrier (TOJO et al., 2001). At present, it is not known which level of albuminuria correlates with glomerular disease, as albumin excretion is so heavily dependent on age, sex and genetic background. Projecting from the situation in humans, mice are currently considered to display signs of glomerular disease, if albumin levels are tenfold higher compared to a control group with the same genetic background and gender (BROSIUS et al., 2009). Because of the polyuria displayed by GIPR^{dn}-tg C57BL/6J mice, the albumin concentration in the urine of GIPR^{dn}-tg C57BL/6J mice is significantly lower compared to C57BL/6J-wt mice. The renal loss of albumin in GIPR^{dn}-tg FVB/N is so great, that even though they develop severe polyuria, the urine albumin concentration is still almost twice as high as that of wild-type FVB/N. GIPR^{dn}-tg FVB/N display a twelve fold increase in daily albumin excretion compared to wild-type FVB/N mice. The FVB/N background appears to be prone to albuminuria in general, whereas models using C57BL/6J mice fail to develop increased albuminuria. GIPR^{dn}-tg CD1 and BALB/c mice fall in between GIPR^{dn}-tg FVB/N and C57BL/6J mice, with GIPR^{dn}-tg CD1 displaying an approximately 6-fold increase and GIPR^{dn}-tg BALB/c an approximately 2-fold increase in daily albumin excretion (POPPER, 2013). The strain-specific predisposition to develop proteinuria could compound renal lesions in GIPR^{dn}-tg FVB/N, due to the toxicity of misfiltrated protein to renal tissue (ABBATE et al., 2006; REMUZZI, 1999; MARSHALL and WILLIAMS, 1998).

Another integral part of phenotyping mouse models of diabetic nephropathy is the determination of serum and urine creatinine concentrations. Studies have shown that the measurement of creatinine serum concentrations in autoanalyzers through creatinase activity overestimates the creatinine concentration approximately twofold (DUNN et al., 2004; MEYER et al., 1985). However, if evaluated in conjunction with serum urea concentrations, the enzymatic determination of creatinine concentration is thought to be suitable as a screening method for renal function (BROSIUS et al., 2009). Increased serum creatinine levels in the absence of elevated serum urea nitrogen levels speak against significant renal impairment in GIPR^{dn}-tg mice on both the FVB/N and C57BL/6J genetic background. Creatinine measurements are also commonly used as a method to determine glomerular filtration rate (GFR) in mice, by measuring creatinine clearance. In the presence of elevated creatinine serum levels, the only reliable method to determine GFR in mice is by measuring FITC-inulin clearance (QI et al., 2004). Part of the problem

is the overestimation of creatinine serum concentrations by most measurement techniques. But even using the gold standard for measuring serum creatinine concentrations in mice, the high pressure liquid chromatography (HPLC), GFR calculation using creatinine yields unsatisfactory results. While creatinine is mostly filtrated in the glomerulus, it can also be secreted in the tubulus (SPITHOVEN et al., 2013). And as creatinine is being produced in muscle tissue, decreased muscle mass in subadult, old, female or sedentary mice and strain-dependent differences in muscle endowment influence serum creatinine levels, making formulas calculating GFR from serum creatinine unsuitable (HORIO, 2014). However, it is still useful as a simple way to detect considerable changes in GFR. The estimated glomerular filtration rate of GIPR^{dn}-tg FVB/N and C57BL/6J is lower than that of their respective wild-type controls. though only the difference between GIPR^{dn}-tg C57BL/6J and wild-type C57BL/6J mice is statistically significant. This points toward the possibility of a slight renal impairment. To either confirm or exclude the possibility of a renal impairment, serum cystatin C concentrations were measured in all animals. Cystatin C is a small, 120-amino-acid protein produced at a constant rate in all cell nuclei (FILLER et al., 2005; ABRAHAMSON et al., 1990; GRUBB and LOFBERG, 1982), that belongs to the family of cysteine proteinase inhibitors. Due to its low molecular weight of approximately 13.3 kilodaltons, it is able to pass through the filtration slits formed by the podocyte foot processes (GRUBB, 2010). Though cystatin C is then almost entirely reabsorbed by the tubulus epithelial cells, it does not re-enter the bloodstream, as it is instantly catabolized (JACOBSSON et al., 1995). No other elimination pathway is currently known (GRUBB, 2010; FILLER et al., 2005). Though recent studies have shown that cystatin C serum concentration is indeed dependent on such factors as muscle mass, gender and age, the effects on cystatin C serum levels are low compared to serum creatinine levels. This test is especially effective in the detection of mild renal impairment and has been shown to be superior to the assessment of renal function through creatinine serum concentrations or blood urea nitrogen concentrations in mice (SONG et al., 2009). GIPR^{dn}-tg FVB/N and C57BL/6 show no statistically significant differences in serum cystatin C concentrations and consequently are not renally impaired at the age of six months. Equally, six month old GIPR^{dn}-tg CD1 and BALB/c mice displayed no difference in serum cystatin C concentrations (POPPER, 2013) or any other sign of renal insufficiency.

In addition to albumin and creatinine, sodium and chloride concentrations were

measured in both serum and urine. Adverse effects of sodium on blood pressure and the role of increased dietary sodium uptake on hypertension in human patients have been discussed controversially. Reduced sodium uptake may have beneficial effects on blood pressure and kidney function (CAMPBELL et al., 2014) in at least some forms of hypertension. FVB/N-wt mice display both higher serum sodium concentrations and higher blood pressure compared to C57BL/6J-wt mice. However, the higher blood pressure seen in GIPR^{dn}-tg FVB/N mice compared to FVB/N-wt and GIPR^{dn}-tg C57BL/6J mice does not correlate with an increase in serum sodium concentration and there are no differences in dietary sodium uptake between the different groups of mice. There does not appear to be a causality between the higher sodium serum concentrations of FVB/N-wt vs. C57BL/6J-wt mice and the more severe presentation of DN in GIPR^{dn}-tg FVB/N compared to GIPR^{dn}-tg C57BL/6J mice. High urinary sodium excretion combined with albuminuria has been associated with increased mortality in human patients with chronic kidney disease (MCQUARRIE et al., 2014). However, measurable urine sodium and chloride concentrations are substantially lower in transgenic mice compared to their respective wild type controls, with a number of samples falling below the testing range for urinary sodium. The total urinary sodium excretion of GIPR^{dn}-tg FVB/N mice is not increased compared to FVB/N-wt, C57BL/6J-wt mice or GIPR^{dn}-tg C57BL/6J mice, and as such is not considered a determining factor in the progression of renal lesions in this mouse model of diabetes mellitus.

5.3.2 Semiquantitative analysis and quantitative stereological analyses of kidneys

Reduction of non-stereological bias through tissue preparation, embedding and linear tissue shrinkage correction factors

Different forms of bias can greatly influence the quality of quantitative stereology. Unlike design-based methods, model-based stereological methods are often associated with stereological bias. This bias can often be reduced by using correction factors, but design-based methods should be preferred. Non-stereological bias includes artifacts of tissue preparation like tissue shrinkage and recognition bias

through incomplete stain penetration, and can be reduced through optimal tissue preparation. The purpose of vascular perfusion is the best possible preservation of the natural state and architecture of tissues, similar to the situation in a living animal (TRACHSEL et al., 2011). Prevention of the collapse of blood vessels enables accurate measurements of the glomerulus. Removing the erythrocytes from the blood vessels also simplifies the counting of glomerular components. The prompt fixation of the tissue avoids autolytical artifacts.
Tissue shrinkage and tissue deformation are important factors to be considered in choosing an appropriate embedding method for stereological investigations (DORPH-PETERSEN et al., 2001). Paraffin embedding, while offering many advantages, produces the greatest degree of tissue shrinkage and deformation. Section thickness of paraffin sections varies greatly, even when cut in one session from the same block, which makes paraffin embedding unsuitable for the measurement of certain parameters (SCHNEIDER and OCHS, 2014). GMA/MMA embedding is far more time-consuming, but has the benefit of retaining the tissue architecture and producing regular, even sections with little variation in section height (SCHNEIDER and OCHS, 2014; BADDELEY et al., 2006). One of the best embedding method for stereological purposes is embedding in glycid ether, which causes only minimal tissue shrinkage and deformation compared to other embedding media. Nominal and actual section thickness of glycid ether embedded kidney slices differ only slightly. Negative aspects of this embedding method are the high expenditure of time, technical difficulty and high cost of supplies. The estimation of podocyte number and mean podocyte volume in the glomerulus, glomerular basement membrane thickness and filtration slit frequency were performed on glycid ether embedded tissue samples, to provide maximum effectivity. Additionally, well established correction factors for linear tissue shrinkage in a variety of embedding materials (WANKE, 1996), were used to minimize bias. The physical disector method, currently the gold standard in design-based stereological methods for particle counting, was used to determine particle numbers. The physical disector method relies on correct section thickness to produce reliable results. So far, it has been common practice to calculate particle numbers with the disector method using the nominal section thickness without verifying the actual section thickness. By measuring the actual section thickness of a number of sections of GMA/MMA-embedded murine kidney tissue, an average section thickness of slightly over 1μm was calculated.

Glomerulosclerosis index of FVB/N, C57BL/6J and GIPR^{dn}-tg mice

In the present study, the glomerulosclerosis index was determined according to the method of EL NAHAS et al. (1991), as a measure of the severity of diabetes-associated renal lesions. Glomerulosclerosis is one of the defining pathological changes of DN. The combined silver methenamine and PAS staining method for extracellular matrix ensures maximum specificity by facilitating the differentiation of extracellular matrix from cell cytoplasm (BROSIUS et al., 2009), while still allowing for an assessment of glomerular morphology. With a glomerulosclerosis index increased more than threefold in this study, GIPR^{dn}-tg FVB/N mice have shown significant glomerular alterations consistent with diabetic nephropathy in mice. Correspondently, the capillary length density in the glomerulus is statistically significantly decreased in GIPR^{dn}-tg FVB/N mice. The glomerulosclerosis index of GIPR^{dn}-tg C57BL/6J is not statistically significantly increased compared to wild-type mice on the C57BL/6J and FVB/N background. As GIPR^{dn}-tg C57BL/6J do not develop severe hyperglycemia or albuminuria, this failure to develop glomerulosclerotic lesions is not surprising. Whether this failure to develop glomerulosclerotic lesions is due to the insufficient hyperglycemia or is strain-specific to C57BL/6J mice, has been shown by a combined model of Lepr$^{db/db}$ and Sur1$^{-/-}$ transgenic C57BL/6J mice (C57BL/6J$^{Sur1\text{-}/\text{-},db/db}$). The sulfonylurea receptor 1 (Sur1) is a subunit of the adenosintriphosphat-sensitive potassium channel in beta cells. The loss of Sur1 in Sur1$^{-/-}$ mice causes a defective insulin secretion (SEGHERS et al., 2000). Unlike C57BL/6J$^{db/db}$ mice, these C57BL/6J$^{Sur1\text{-}/\text{-},db/db}$ mice displayed severe obesity and hyperglycemia similar to FVB/N$^{db/db}$ mice. The degree of glomerulosclerosis displayed by the C57BL/6J$^{Sur1\text{-}/\text{-},db/db}$ mice was not increased compared to C57BL/6$^{db/db}$ mice with only mild hyperglycemia (CHUA et al., 2010). The results of this study and a previous study on susceptibility loci to nephropathy in mice seem to suggest that the resistance to the development of glomerulosclerosis is a trait inherent to the C57BL/6J background, and attributable to a dominant locus on chromosome 5 (CHUA et al., 2010; PAPETA et al., 2009). The study also identified a major locus on chromosome 8, which appeared to influence the higher susceptibility to nephropathy in FVB/N mice (CHUA et al., 2010). Comparing the results of the present study with a similar study (POPPER, 2013) using different genetic backgrounds, it appears that the glomerulosclerosis index of GIPR^{dn}-tg CD1 mice is higher compared to GIPR^{dn}-tg FVB/N mice, possibly a consequence

of the higher blood glucose concentrations displayed by GIPR^{dn}-tg CD1 mice. The glomerulosclerosis index of GIPR^{dn}-tg BALB/c falls in between that of GIPR^{dn}-tg-FVB/N and GIPR^{dn}-tg C57BL/6J mice (POPPER, 2013).

Quantitative stereological analyses of kidneys of FVB/N, C57BL/6J and GIPR^{dn}-tg mice

To investigate differences in kidney morphology and their effect on the susceptibility to diabetes-associated renal lesions, multiple stereological parameters were determined in wild-type FVB/N and C57BL/6J mice and GIPR^{dn}-tg mice of both backgrounds. The total kidney volume of GIPR^{dn}-tg animals was significantly higher than that of their respective wild-type controls, a common finding associated with diabetes mellitus and DN in both humans and mice (BLANTZ and SINGH, 2014; HABIB, 2013). Most of the increase in kidney volume of diabetic patients may be attributable to tubular hyperplasia and hypertrophy, and interstitial expansion (SEYER-HANSEN et al., 1980). Possibly, heightened filtration and active reabsorption of glucose and fluids play a role in increasing kidney volume (BILOUS, 2001). There is a strain-dependent difference in kidney volume, with FVB/N-wt mice presenting with altogether bigger kidneys compared to C57BL/6J-wt mice, in spite of similar body weight. A higher percental increase of kidney volume in GIPR^{dn}-tg FVB/N mice compared to GIPR^{dn}-tg C57BL/6J mice implicates a more severe reaction to hyperglycemia and higher susceptibility to the development of renal disease.
Many recent studies have emphasized the influence of low congenital nephron number on the development and progression of kidney disease in various species (CEBRIAN et al., 2014; BOUBRED et al., 2013; SCHLOTE et al., 2013; BRENNER and MACKENZIE, 1997). Rats with unilateral renal agenesis and reduced nephron numbers in the remaining kidney show more severe glomerular hypertrophy than a uninephrectomized control group (WANG et al., 2014). Prematurely delivered CD1 mice showed approximately 26% lower nephron number, lower GFR, higher blood pressure and increased urinary albumin excretion compared to CD1 mice delivered full-term (STELLOH et al., 2012). However, there is no statistically significant difference in the nephron endowment of FVB/N-wt and C57BL/6J-wt mice. Causes discussed for decreased congenital nephron numbers include maternal and fetal malnutrition, premature birth and maternal diabetes. None of those factors apply

to the animals used in the present study. The nephron number determined in this study for FVB/N and C57BL/6J mice agrees with previously published data for C57BL/6J and C3H/HeJ mice, and appears to be unexceptional for laboratory mice (MURAWSKI et al., 2010). GIPR^{dn}-tg status appears to have no negative effect on kidney development and nephron number. The differences in kidney lesions between GIPR^{dn}-tg FVB/N and C57BL/6J mice appear to be unrelated to changes in nephron number and no significant loss of nephrons at the age of six months can be observed. The mechanisms through which low congenital nephron number influences the progression of renal disease are currently still under discussion, but increased blood pressure appears to play an integral role (BRENNER et al., 1988). The increase in blood pressure can potentially be attributed to changes in sodium re-absorption in the tubule instead of directly to the lower number of nephrons (BAUMANN et al., 2003). The idea, that low nephron number leads to a higher GFR per nephron and subsequent scarring of the glomerulus, has also been proposed (MILLER et al., 1991). Other studies noted that the kidney compensates for the decreased number of glomeruli through glomerular hypertrophy, leading to podocytopathy (BENZ et al., 2011; MANALICH et al., 2000). While FVB/N-wt mice display average nephron endowment, a higher mean glomerular volume and higher blood pressure are present.

Another parameter suspected of influencing susceptibility to DN is the mean glomerular volume. A high mean glomerular volume is considered a risk factor for glomerular injury in humans. Pima Indians, the majority of whom develop diabetes mellitus, and people of african or hispanic origin display a higher mean glomerular volume compared to caucasians or asians (LEMLEY, 2003; LAWSON et al., 1996; SCHMIDT et al., 1992; BILOUS et al., 1989). Compared to diabetes patients of caucasian descent, a higher percentage of these ethnic groups develops DN and the progression of the disease is more severe (DREYER et al., 2013; LEMLEY, 2008). The mean glomerular volume of FVB/N-wt mice is almost twice as high as that of C57BL/6-wt mice, which is a considerable strain-dependent difference. While there is no significant difference in the total glomerular volume of FVB/N-wt and C57BL/6J-wt mice, the volume fraction of glomeruli per kidney is considerably higher in C57BL/6J-wt mice. Volume fraction of glomeruli in the kidney, total glomerular volume and mean glomerular volume of GIPR^{dn}-tg FVB/N are increased at more than 25-50% compared to FVB/N-wt mice, whereas GIPR^{dn}-tg C57BL/6J mice only display a slight increase in mean glomerular volume

compared to C57BL/6J-wt mice. Summarized, FVB/N-wt mice possess larger kidneys with larger glomeruli and a lower volume fraction of glomeruli in the kidneys compared to C57BL/6J mice, without showing a difference in total nephron number. Glomerular hypertrophy, as displayed by GIPR^{dn}-tg FVB/N mice, is one of the hallmarks of DN (FOGO and ICHIKAWA, 1991). A study by POPPER (2013) examined kidney morphology in GIPR^{dn}-tg CD1 and BALB/c mice. Subsequently, the results of the present study are compared to those of POPPER (2013). CD1-wt and GIPR^{dn}-tg CD1 mice display a slightly lower mean glomerular volume compared to FVB/N-wt and GIPR^{dn}-tg FVB/N mice respectively, while BALB/c-wt and GIPR^{dn}-tg BALB/c mice display a slightly higher mean glomerular compared to C57BL/6-wt and GIPR^{dn}-tg C57BL/6 mice (POPPER, 2013). GIPR^{dn}-tg CD1 display a comparable percental increase in mean glomerular volume compared to CD1-wt mice as GIPR^{dn}-tg FVB/N to FVB/N-wt mice. A similar percental increase in mean glomerular volume is present in GIPR^{dn}-tg mice on the BALB/c and C57BL/6J backgrounds compared to their wild-type control groups. The presumed higher risk for renal alterations associated with a high mean glomerular volume seems to apply to the situation in GIPR^{dn}-tg FVB/N mice, as they develop more severe albuminuria and glomerulosclerotic lesions than C57BL/6J mice. The low mean glomerular volume of C57BL/6J mice seems to confer a resistance to the development of renal lesions irrespective of the state of hyperglycemia.
The mean capillary volume in the glomerulus of GIPR^{dn}-tg C57BL/6J mice does not differ significantly from that of wild-type C57BL/6J controls. The volume fraction of capillaries in the glomerulus is slightly decreased in GIPR^{dn}-tg C57BL/6J mice. This is probably due to the mild mesangial expansion and podocyte hypertrophy displayed by GIPR^{dn}-tg C57BL/6J mice, instead of a collapse of glomerular capillaries, which was not observed in the present studies. In contrast, the volume fraction of capillaries in the glomerulus in GIPR^{dn}-tg FVB/N mice is not decreased compared to FVB/N-wt mice, and their mean capillary volume in the glomerulus is increased by the factor 1.5 compared to FVB/N-wt mice. To differentiate between a de novo growth of capillaries and capillary dilation and distortion due to mesangial failure, capillary length density and mean capillary length per glomerulus were assessed in GIPR^{dn}-tg FVB/N, FVB/N-wt, GIPR^{dn}-tg C57BL/6J and C57BL/6J-wt mice. The mean capillary length per glomerulus is increased in GIPR^{dn}-tg mice of both the FVB/N and the C57BL/6J background compared to their respective wild-type control mice.. However, the capillary length density is

decreased by 28% in GIPR^{dn}-tg FVB/N mice compared to FVB/N-wt mice, while no significant differences between FVB/N-wt, C57BL/6-wt and GIPR^{dn}-tg C57BL/6J mice can be observed. Mechanical stress due to high intraglomerular pressure can damage the mesangium's connection to the GBM and promote mesangial expansion. Consequently, the normal glomerular architecture can no longer be maintained and capillaries dilate and may display ballooning (LEMLEY et al., 1992; SAKAI et al., 1992). Distorted and dilated capillaries can be observed in the majority of glomeruli in GIPR^{dn}-tg FVB/N mice, suggesting that mesangial failure due to increased intraglomerular pressure may be present in GIPR^{dn}-tg FVB/N mice. Due to the kidney's ability to regulate blood flow through the organ (Bayliss myogenic response) and tubuloglomerular feedback, the increased intraglomerular pressure apparently present in GIPR^{dn}-tg FVB/N is not necessarily a consequence of the increased systolic blood pressure displayed by GIPR^{dn}-tg FVB/N mice. The existence of differences in hemodynamics specific to the FVB/N background can not be precluded at this time. GIPR^{dn}-tg CD1 and GIPR^{dn}-tg BALB/c display similarly decreased capillary length densities compared to GIPR^{dn}-tg FVB/N mice and distorted capillaries are present as well. The capillary length density of CD1-wt and BALB/c-wt mice is comparable to FVB/N-wt and C57BL/6J-wt mice (POPPER, 2013).

Laminin, fibronectin and collagen IV are the three most significant extracellular glomerular matrix proteins associated with mesanigal expansion, which marks the beginning of glomerulosclerosis (PUGLIESE et al., 1997). Detection of collagen IV through immunohistochemistry allows the assessment of extracellular matrix components in the glomerulus and clearly marks basement membranes in the interstitium (BROSIUS et al., 2009). Immunohistochemical detection of laminin, fibronectin and collagen IV shows an increased accumulation of matrix proteins in GIPR^{dn}-tg FVB/N and GIPR^{dn}-tg C57BL/6J mice compared to their wild-type controls. Transforming growth factor β1 has been shown to play a pivotal role in the development of mesangial expansion and interstitial fibrosis. It increases the synthesis of extracellular matrix proteins and prevents matrix degradation (ZIYADEH, 2004; SHARMA and ZIYADEH, 1994; ZIYADEH et al., 1994). TGF-β1 accumulation detected trough IHC is increased in GIPR^{dn}-tg FVB/N, but not in GIPR^{dn}-tg C57BL/6J mice. Stereological analysis of the mean mesangial volume per glomerulus shows considerable mesangial expansion of over 70% volume increase in GIPR^{dn}-tg FVB/N mice vs. FVB/N-wt mice, compared to a 14%

increase in GIPR^{dn}-tg C57BL/6J vs. C57BL/6J-wt mice. That difference in the increase of the mean mesangial volume per glomerulus is reflected in the higher glomerulosclerosis index shown by GIPR^{dn}-tg FVB/N mice compared to GIPR^{dn}-tg C57BL/6J. The mean mesangial volume per glomerulus of wild-type FVB/N is considerably higher than that of wild-type C57BL/6J mice, another important difference between the two strains that may contribute to the higher susceptibility of the FVB/N background to the development of diabetes-associated renal lesions. The higher volume fraction of mesangium per glomerulus of GIPR^{dn}-tg FVB/N mice compared to GIPR^{dn}-tg C57BL/6J mice proves that the observed difference in mean mesangial volume per glomerulus is not simply due to the higher mean glomerular volume displayed by FVB/N mice, but is indeed a strain-related difference.

Podocytes play an integral role in kidney function and the development and progression of renal diseases. Their foot processes form part of the filtration barrier and are indispensable for homeostasis. Mature podocytes are unable to replicate and detach from the glomerular capillary wall once their lifespan ends. Parietal podocytes present on the Bowman's capsule migrate to the glomerulus to replace the lost podocytes (SCHULTE et al., 2014), but if the body's capacity to recruit new podocytes to the glomerulus is exceeded, the number of mature podocytes forming filtration slits begins to drop. Podocyte hypertrophy and podocyte loss are features of diabetic nephropathy and are fundamental processes in the development of chronic kidney insufficiency. Several different mechanisms leading to podocyte loss in the diabetic kidney have been discussed, among them apoptosis, insufficient production of podocyte-protective substances and mechanical detachment through high pressure and glomerular hypertrophy (BROSIUS and COWARD, 2014; KRIZ and LEMLEY, 2014). In the progression of diabetic nephropathy, the glomerular hypertrophy and ongoing loss of podocytes leads to podocyte hypertrophy, as the remaining podocytes grow in size to cover the emerging gaps in the filtration barrier. Traditionally, fewer and larger podocytes are regarded as a contributing factor in the development of diabetic nephropathy in humans (LEMLEY, 2003). Hyperglycemia is thought to have direct effects on podocyte growth as well (HOSHI et al., 2002). Their foot processes broaden, stop to interlock, separate from the GMB and proteinuria develops (WHITE and BILOUS, 2004). The podocyte numbers of FVB/N-wt mice are already considerably lower compared to C57BL/6J-wt mice, and GIPR^{dn}-tg FVB/N show significantly lower podocyte numbers compared to

FVB/N-wt mice, which can be interpreted as podocyte loss. Alternatively, if the increase in the mean podocyte volume of GIPR^{dn}-tg FVB/N mice is independent of podocyte loss, fewer podocytes might be required to cover the glomerular basement membrane as the volume of the podocytes increases over time. No significantly decrease in the number of podocytes per glomerulus is observable in GIPR^{dn}-tg C57BL/6J mice compared to C57BL/6J-wt mice.
The volume fraction of podocytes per glomerulus is strain-dependently lower in FVB/N-wt mice compared to C57BL/6J-wt mice. The podocyte volume shows strain-specific differences as well, with FVB/N-wt mice displaying a higher mean podocyte volume compared to C57BL/6J-wt mice. An increase in podocyte volume can be observed in transgenic mice of both strains, but the degree of hypertrophy is considerably greater in GIPR^{dn}-tg FVB/N compared to GIPR^{dn}-tg C57BL/6J mice. Subsequently, the results of the present study were compared with the results of a previous study by POPPER (2013), in which the kidney morphology of GIPR^{dn}-tg CD1 mice, GIPR^{dn}-tg BALB/c mice and their respective wild-type control mice were studied. CD1-wt, BALB/c-wt, GIPR^{dn}-tg CD1 and GIPR^{dn}-tg BALB/c display podocyte numbers comparable to FVB/N-wt mice. The mean podocyte volume of CD1-wt and BALB/c-wt mice is comparable to the mean podocyte volume of C57BL/6J-wt mice. GIPR^{dn}-tg BALB/c mice display podocyte hypertrophy comparable to GIPR^{dn}-tg C57BL/6J mice. GIPR^{dn}-tg CD1 mice develop more severe podocyte hypertrophy compared to GIPR^{dn}-tg C57BL/6J and GIPR^{dn}-tg BALB/c, but their podocytes only reach approximately a third of the mean podocyte volume of GIPR^{dn}-tg FVB/N mice (POPPER, 2013). In view of the severe albuminuria and increased glomerulosclerosis index displayed by GIPR^{dn}-tg FVB/N, the results seem to concur with the hypothesis that few, large podocytes can be considered as a risk factor in the development of nephropathies. The higher podocyte number and lower podocyte volume of the C57BL/6J background on the other hand, may have a protective effect on the development of proteinuria and glomerulosclerosis (STEFFES et al., 2001). Recently, a study on podocyte volumes and numbers in GLUT4-deficient mice noted that they showed less signs of diabetic nephropathy in spite of displaying larger and fewer podocytes (GUZMAN et al., 2014) than their wild-type controls, with podocyte number having been determined by counting WT1 positive nuclei. These findings implicate, that while low podocyte number and high podocyte volume can be associated with an increased risk for developing DN or a more severe progression of DN, several other predisposing factors are

probably required for the development of severe DN. The strain-dependent severe hyperglycemia, hypertension and high mean glomerular volume of FVB/N mice are such other predisposing factors and could explain the severity of lesions developed by diabetic FVB/N mice. C57BL/6J mice only display strain-specific kidney characteristics associated with a suspectedly low risk of contracting DN, and do not develop anything but mild renal changes in most models of diabetes mellitus (SHARMA et al., 2003; ZHENG et al., 1998; HUMMEL et al., 1972), including the GIPR^{dn} mouse model.
The filtration slit frequency of FVB/N-wt mice is slightly, but statistically significantly lower compared to C57BL/6J-wt mice, but no other statistically significant differences are apparent. The glomerular basement membrane shows an increase in thickness in GIPR^{dn}-tg FVB/N mice compared to FVB/N-wt mice, but not in GIPR^{dn}-tg C57BL/6J mice compared to C57BL/6J-wt mice. Correspondingly, GIPR^{dn}-tg CD1, but not GIPR^{dn}-tg BALB/c, display an increased GBM thickness (POPPER, 2013). As thickening of the GBM has been shown to go hand in hand with a change in GBM architecture that leads to increased permeability (ISOGAI et al., 1999), this correlates well with the differences in proteinuria displayed by GIPR^{dn}-tg mice of the FVB/N, C57BL/6J, CD1 and BALB/c genetic backgrounds.

5.4 Conclusions

The hypothesis that the genetic background influences the severity of the diabetic metabolic state and the susceptibility to diabetic nephropathy (BREYER and QI, 2010; BROSIUS et al., 2009), and that strain-dependent differences in kidney composition play a role in the differences in susceptibility to diabetic nephropathy, is supported by the findings of this study. The way genetic factors determine the quantitative traits investigated in this study is still unclear and their identification is not the aim of this study. GIPR^{dn}-transgenic mice on a FVB/N background display severe hyperglycemia, hypertension, polyuria and severe albuminuria. GIPR^{dn}-transgenic mice on a C57BL/6J background, on the other hand, display only mildly elevated blood glucose levels, no hypertension or albuminuria, and mild polyuria. The degree of hyperglycemia, hypertension and albuminuria displayed

by GIPR^{dn}-tg FVB/N and C57BL/6J mice may be influenced by differences specific to the respective background strain. The higher degree of hyperglycemia and hypertension displayed by GIPR^{dn}-tg FVB/N mice may influence the development of renal lesions, but other mouse models of diabetes have demonstrated, that a higher blood glucose concentraion and higher blood pressure do not have to lead to more severe lesions in the absence of other risk factors. The kidneys of FVB/N-wt mice are characterized by large glomeruli, a low number of podocytes and larger podocytes compared to C57BL/6J-wt mice. The combination of these features may contribute to the development of albuminuria and renal lesions that share some aspects with human DN. The kidneys of C57BL/6J-wt mice contain small glomeruli with a higher number of podocytes, which are comparatively small, possibly explaining their apparent resistance to injury. FVB/N-wt and C57BL/6J-wt mice display a comparable nephron endowment, and GIPR^{dn}-tg FVB/N and C57BL/6J mice do not show a lower nephron number compared to FVB/N-wt or C57BL/6J-wt mice. While GIPR^{dn}-FVB/N mice can be considered a suitable model of human DN and the use of the FVB/N strain as a genetic background in models of diabetes and diabetic nephropathy can be recommended, the C57BL/6J strain appears to be not ideally suited for research on diabetes-associated kidney lesions in this model of disease. As a model to study resistance to kidney lesions, however, it may be highly interesting.

6 Summary

Diabetic nephropathy is one of the most important sequelas of diabetes mellitus. The pathogenically relevent processes underlying this disease are only insufficiently understood, and existing mouse models fail to recreate the human disease in all its aspects. Therefore, much effort has been put into the development of novel mouse models of DN. Recently, the impact of the genetic background on the development of renal lesions has come into the focus of research. Transgenic mice expressing a dominant negative glucose-dependent insulinotropic polypeptide receptor (GIPR^{dn}-tg mice), controlled by the rat proinsulin 2 promotor, were chosen as a model of diabetes. To investigate strain dependent morphological differences and their possible influence on susceptibility to develop DN, GIPR^{dn}-tg mice were investigated on a genetic background prone to albuminuria (FVB/N) and on a background noted for its relative resistance to the development of renal injury (C57BL/6J).

Eight male GIPR^{dn}-tg FVB/N, GIPR^{dn}-tg C57BL/6J mice and their respective wild-type controls at the age of six months were analysed. Clinical parameters were investigated, and morphological kidney parameters were analysed quantitative stereologically, semiquantitatively and qualitatively.

Clinically, GIPR^{dn}-tg FVB/N mice developed severe hyperglycemia, polydypsia, polyuria and showed elevated systolic blood pressure levels compared to wild-type FVB/N mice. The GIPR^{dn}-tg FVB/N mice displayed an increase in daily albumin excretion of approximately 12 times compared to wild-type FVB/N. Compared to C57BL/6J-wt mice, GIPR^{dn}-tg C57BL/6J mice developed only mildly increased casual blood glucose concentrations and polyuria. Albuminuria or elevated blood pressure in GIPR^{dn}-tg C57BL/6J mice compared to wild-type C57BL/6J were not observed. The results of the present study indicate that pronounced strain-dependent differences in the diabetic metabolic state exist between GIPR^{dn}-tg FVB/N and GIPR^{dn}-tg C57BL/6J mice.

FVB/N-wt mice displayed a higher kidney volume, comparable nephron endowment, higher mean and total glomerular volume, higher mean podocyte volume and lower podocyte number compared to C57BL/6J-wt mice, showing that statistically significant differences in kidney morphology are present between the FVB/N and C57BL/6J strain. GIPR^{dn}-tg mice on the FVB/N background showed pronounced glomerulosclerosis, renal hypertrophy and glomerular hypertrophy with mesangial expansion, dilated and distorted glomerular capillaries, podocyte hypertrophy, reduced podocyte numbers and GBM thickening compared to FVB/N-wt mice. GIPR^{dn}-tg mice on the C57BL/6J background displayed an only slightly increased kidney and mean glomerular volume and mild podocyte hypertrophy compared to C57BL/6J-wt mice. Reduced podocyte numbers, dilation of glomerular capillaries or GBM thickening compared to C57BL/6J-wt mice were not observed. GIPR^{dn}-tg FVB/N mice displayed a higher glomerulosclerosis index, higher mean and total glomerular volume, higher mean podocyte volume, lower podocyte number and higher glomerular basement thickness compared to GIPR^{dn}-tg C57BL/6J mice. The differences already present in quantitative morphological kidney parameters between wild-type mice of the both strains are exacerbated by the presence of diabetes. The strain-dependent differences in clinical parameters like hyperglycemia, blood pressure and albuminuria may influence susceptibility to renal lesions, but strain-dependent variations in mean glomerular volume, podocyte volume and podocyte number also appear to play a role in both genetic backgrounds. The mild presentation of renal lesions in GIPR^{dn}-tg C57BL/6J may be partially attributable to the lower casual blood glucose concentrations, but other models of diabetes have reported similar findings in diabetic C57BL/6J mice displaying higher blood glucose concentrations. This suggests that kidney morphology is also at least partially responsible for the low susceptibility to the development of renal lesions in the C57BL/6J strain.

In summary, this study demonstrates the importance of choosing the right genetic background for murine models of DN, based on its susceptibility to develop severe renal lesions. In the light of the predisposing factors displayed by FVB/N mice and the correspondingly more severe renal lesions displayed by diabetic FVB/N mice, GIPR^{dn}-tg FVB/N mice can be endorsed as a useful mouse model of DN. GIPR^{dn}-tg C57BL/6J mice are less suitable as a model of DN due to the C57BL/6J genetic background's apparent resistance to the development of DN, but may offer valuable insight into the mechanisms of resistance to diabetes and renal disease.

7 Zusammenfassung

Die diabetische Nephropathie stellt eine der bedeutendsten Folgeerkrankungen von Diabetes dar. Die der Erkrankung zugrunde liegenden pathogenen Prozesse sind bisher nur unzureichend bekannt und derzeitige Mausmodelle sind nicht in der Lage, die Erkrankung des Menschen vollständig darzustellen. Daher wird viel Aufwand in die Entwicklung neuer Mausmodelle für die diabetische Nephropathie investiert. In letzter Zeit rückte vor allem der Einfluss des genetischen Hintergrundes in den Fokus der Forschung. Transgene Mäuse, die einen dominant-negativen glukoseabhängigen insulinotropen Polypeptidrezeptor unter der Kontrolle des Ratten Proinsulin 2 Promotors exprimieren (GIPR^{dn}-tg Mäuse) wurden als Diabetesmodell ausgewählt. Um Licht auf stammabhängige Unterschiede in der quantitativen Morphologie der Niere und deren möglichen Einfluss auf die Empfänglichkeit für die Entwicklung von diabetische Nephropathie zu werfen, wurden GIPR^{dn}-tg Mäuse auf einem zu Albuminurie neigenden (FVB/N) und einem für Nierenläsionen eher unempfindlichen (C57BL/6J) genetischen Hintergrund untersucht.
Die Analysen erfolgten an je acht sechs Monate alten GIPR^{dn}-tg FVB/N-Mäusen, GIPR^{dn}-tg C57BL/6J-Mäusen und den zugehörigen Wildtyp-Kontrolltieren und umfassten klinische und klinisch-chemische sowie qualitative, semiquantitative und quantitativ-morphologische Untersuchungen der Nieren.
Klinisch zeigten GIPR^{dn}-tg FVB/N-Mäuse hochgradige Hyperglykämie, Polydypsie, Polyurie, erhöhten Blutdruck, sowie eine gegenüber FVB/N-wt Mäusen um den Faktor zwölf erhöhte täglich ausgeschiedene Albuminmenge im Urin. GIPR^{dn}-tg C57BL/6J-Mäuse zeigten nur geringfügig erhöhte Blutglukosespiegel und geringgradige Polyurie im Vergleich zu C57BL/6J-wt Mäusen. Die Ergebnisse dieser Studie zeigen, dass zwischen GIPR^{dn}-tg FVB/N- und C57BL/6J-Mäusen erhebliche stammabhängige Unterschiede in der diabetischen Stoffwechsellage bestehen.

FVB/N-Mäuse wiesen im Vergleich zu C57BL/6J-Mäusen eine ähnliche Glomerulumanzahl, ein höheres Nieren-, Glomerulum- und Podozytenvolumen und eine niedrigere Podozytenzahl auf. Dies zeigt, das signifikante stammabhängige Unterschiede in der Nierenmorphologie zwischen FVB/N- und C57BL/6J-Mäusen bestehen. GIPR^{dn}-tg FVB/N-Mäuse zeigten im Vergleich zu FVB/N-wt Mäusen Glomerulosklerose, renale, glomeruläre und podozytäre Hypertrophie, dilatierte glomeruläre Kapillaren, eine erniedrigte Podozytenzahl und einer Verdickung der glomerulären Basalmembran (GBM). Dagegen wiesen GIPR^{dn}-tg C57BL/6J vs. C57BL/6-wt Mäuse nur wenig erhöhte Nieren-, Glomerulum- und Podozytenvolumina auf. Im Vergleich zu GIPR^{dn}-tg C57BL/6J wiesen GIPR^{dn}-tg FVB/N Mäuse einen höheren Glomerulosklerosеindex, ein höheres mittleres Glomerulum- und Podozytenvolumen, eine niedrigere Podozytenzahl und eine höhere GBM-Dicke auf. Die zwischen den Wildtyp-Mäusen beider Stämme bestehenden renalen morphologischen Unterschiede werden bei Vorhandensein von Diabetes noch ausgeprägter. Die stammabhängigen Unterschiede in Parametern wie Hyperglykämie, Blutdruck und Albuminurie können möglicherweise die Empfänglichkeit gegenüber renalen Veränderungen beeinflussen, aber auch stammabhängige Differenzen im mittleren Glomerulum- und Podozytenvolumen und der Podozytenzahl scheinen eine Rolle in beiden genetischen Hintergründen zu spielen. Die geringfügige Ausprägung der renalen Alterationen in GIPR^{dn}-tg C57BL/6J Mäusen mag teilweise in den niedrigeren Blutglukosekonzentrationen begründet sein. Andere Diabetesmodelle liefern jedoch trotz höherer Blutglukosekonzentrationen vergleichbare Ergebnisse für C57BL/6J-Mäuse. Dies legt die Vermutung nahe, dass die Nierenmorphologie ebenfalls einen Einfluss auf die niedrigere Empfänglichkeit des C57BL/6J-Stammes für die Entwicklung von Nierenläsionen hat.
Zusammenfassend kann festgestellt werden, dass die Auswahl eines für Nierenläsionen prädisponierten genetischen Hintergrundes für Mausmodelle diabetischer Nephropathie eine wichtige Rolle spielt. Angesichts der Faktoren, die FVB/N-Mäuse für diabetische Nephropathie zu prädisponieren scheinen und der entsprechend schwereren Nierenläsionen, können GIPR^{dn}-tg FVB/N-Mäuse als Modell für DN empfohlen werden. Dagegen erscheinen GIPR^{dn}-tg C57BL/6J-Mäuse auf Grund der relativen Unempfindlichkeit des genetischen Hintergrundes gegenüber Nierenläsionen als Modell für DN weniger geeignet, sie sind allerdings als Modell für die Untersuchung von Resistenzfaktoren gegenüber Diabetes oder Nephropathien von Interesse.

Appendix

Summary of results On the following pages, the most important results of both the clinical analyses, the glomerulosclerosis and the quantitative stereological analyses have been compiled. Statistically significant differences have been marked.

Table A.1 Summary of results of clinical analyses

Parameter	Wild-types		GIPR^{dn}-transgenics		Level of significance			
	FVB/N	C57BL/6	FVB/N	C57BL/6	1	2	3	4
Blood pressure measurement								
Systolic blood pressure (mmHg)	118±12	92±26	145±22	105±30	**	-	**	*
Diastolic blood pressure (mmHg)	94±13	68±25	103±23	80±30	-	-	-	*
Blood glucose concentration								
Fasting blood glucose (mg/dl)	109±15	91±9	366±82	122±35	***	*	***	*
Casual blood glucose (mg/dl)	136±19	169±17	793±193	468±84	***	***	***	**
Serum parameters								
Serum albumin concentration (g/dl)	1.35±0.19	1.47±0.05	1.03±0.13	1.20±0.08	*	***	*	-
Serum creatinin concentration (mg/dl)	0.39±0.05	0.43±0.02	0.79±0.09	0.62±0.07	***	***	*	-
Serum urea concentration (mg/dl)	68±12	64±10	72±5	69±14	-	-	-	-
Serum cystatin c concentration (ng/ml)	709±156	606±65	600±218	537±254	-	-	-	-
Serum total protein concentration (g/dl)	6.7±1.0	6.0±0.1	5.6±1.7	5.5±0.5	-	-	-	-
Serum triglycerides concentration (mg/dl)	279±60	63±10	332±125	117±35	-	**	*	***
Serum sodium concentration (mmol/l)	159±5	151±2	152±17	145±2	-	**	-	*
Serum chloride concentration (mmol/l)	120±3	118±2	109±13	112±2	-	**	-	-

1: GIPR^{dn}-tg FVB/N vs. FVB/N-wt
2: GIPR^{dn}-tg C57BL/6J vs. C57BL/6J
3: GIPR^{dn}-tg FVB/N vs. GIPR^{dn}-tg C57BL/6J
4: FVB/N-wt vs. C57BL/6J-wt
Levels of significance: - not significant, * $p \leq 0.05$, ** $p \leq 0.01$, *** $p \leq 0.001$

Table A.2 Summary of results of clinical analyses 2

Parameter	Wild-types		GIPR^{dn}-transgenics		Level of significance			
	FVB/N	C57BL/6	FVB/N	C57BL/6	1	2	3	4
Urine parameters								
Urine albumin concentration (10^3 ng/ml)	91±65	77±44	171±126	13±7	-	***	***	-
Albumin excretion (10^3 ng/d)	172±93	87±32	2048±1049	62±28	***	-	***	*
Urine creatinin concentration (mg/dl)	22±17	42±12	2±0,4	12±6	*	***	-	*
Urine albumin-creatinin ratio (μg/mg)	402±242	191±110	3354±2487	140±41	***	-	***	*
Urine urea concentration (mg/dl)	998±138	>4237,2	1841±548	2175±357	-	-	-	-
Urine sodium concentration (mmol/l)	81±46	64±25	21±0	33±12	-	-	-	-
Urine chloride concentration (mmol/l)	149±34	163±12	36±10	43±7	***	***	-	-
Estimated glomerular filtration rate (l/h)	5.4±2.9	5.2±2.4	4.0±1.5	3.1±0.6	-	*	-	-
Metabolic parameters								
Body weight (g)	32±2	30±2	29±4	29±2	-	-	-	-
Food consumption (g/g/d)	0.09±0.02	0.07±0.02	0.14±0.04	0.11±0.01	**	***	-	-
Water consumption (ml/g/d)	0.13±0.05	0.13±0.02	0.58±0.18	0.26±0.08	***	**	***	-
Urine volume (ml/g/d)	2.7±1.8	1.3±0.4	14.3±4.9	4.6±2.4	***	**	***	-

1: GIPR^{dn}-tg FVB/N vs. FVB/N-wt
2: GIPR^{dn}-tg C57BL/6J vs. C57BL/6J
3: GIPR^{dn}-tg FVB/N vs. GIPR^{dn}-tg C57BL/6J
4: FVB/N-wt vs. C57BL/6J-wt
Levels of significance: - not significant, * $p \leq 0.05$, ** $p \leq 0.01$, *** $p \leq 0.001$

Table A.3 Summary of results of morphological analyses

Parameter	Wild-types		GIPR^{dn}-transgenics		Level of significance			
	FVB/N	C57BL/6	FVB/N	C57BL/6	1	2	3	4
Glomerulosclerosis index	0.13±0.06	0.10±0.01	0.44±0.10	0.12±0.04	***	-	***	-
Total kidney volume (mm^3)	220±14	154±16	284±19	172±17	***	*	***	***
Total nephron number	20431±405	19944±444	21506±1046	20214±1519	-	-	-	-
Vol. fraction of glomeruli per kidneys (%)	2.0±0.3	2.5±0.3	2.8±0.2	2.5±0.2	***	-	**	**
Total glomerular volume per kidneys (mm^3)	4.4±0.5	3.8±0.9	8.0±0.8	4.1±0.4	***	-	***	-
Mean glomerular volume (10^3 μm^3)	386±54	215±23	616±28	264±30	***	**	***	***
Num. volume density of podocytes per glom.	±	±	±	±	***	-	***	*
Podocyte number per glom.	109±28	147±34	80±11	149±39	*	-	***	*
Vol. fraction of podocytes per glom. (%)	23±3	28±2	20±2	28±2	-	-	***	***
Mean podocyte volume (μm^3)	819±163	569±95	1580±222	744±102	***	**	***	**
Vol. fraction of mesangium per glom. (%)	35±2	31±2	39±1	35±3	***	**	**	***
Mean glomerular mesangial volume (10^3 μm^3)	138±19	66±8	238±14	91±13	***	***	***	***
Vol. fraction of capillaries per glom. (%)	42±2	41±2	41±1	38±2	-	**	***	-
Mean glomerular capillary volume (10^3 μm^3)	168±23	88±9	253±14	98±12	***	-	***	***
Capillary length density per glom. (m/mm^3)	12.6±0.7	12.9±1.4	9.1±0.6	13.2±2.8	***	-	***	-
Mean capillary length per glom. (mm)	4.9±0.6	2.8±0.2	5.6±0.4	3.5±0.7	*	*	***	***
Filtration slit frequency (n/mm)	2108±27	2185±33	2087±46	2151±52	-	-	-	**
Glomerular basement membrane thickness (nm)	160±6	144±5	171±3	146±8	**	-	***	**

1: GIPR^{dn}-tg FVB/N vs. FVB/N-wt
2: GIPR^{dn}-tg C57BL/6J vs. C57BL/6J
3: GIPR^{dn}-tg FVB/N vs. GIPR^{dn}-tg C57BL/6J
4: FVB/N-wt vs. C57BL/6J-wt
Levels of significance: - not significant, * $p \leq 0.05$, ** $p \leq 0.01$, *** $p \leq 0.001$

Bibliography

ABBATE M., ZOJA C. and REMUZZI G. (2006) *How does proteinuria cause progressive renal damage?*. J Am Soc Nephrol **17**(11): 2974–2984.

ABRAHAMSON M., OLAFSSON I., PALSDOTTIR A., ULVSBACK M., LUNDWALL A., JENSSON O. and GRUBB A. (1990) *Structure and expression of the human cystatin C gene*. Biochem J **268**(2): 287–294.

AMERICANDIABETESASSOCIATION (2003) *Peripheral arterial disease in people with diabetes*. Diabetes Care **26**(12): 3333–3341.

AMERICANDIABETESASSOCIATION (2013) *Standards of medical care in diabetes–2013*. Diabetes Care **36 Suppl 1**: 11–66.

AMERICANDIABETESASSOCIATION (2014) *Diagnosis and Classification of Diabetes Mellitus*. Diabetes Care **37**(Supplement 1): S81–S90.

AN Y., XU F., LE W., GE Y., ZHOU M., CHEN H., ZENG C., ZHANG H. and LIU Z. (2015) *Renal histologic changes and the outcome in patients with diabetic nephropathy*. Nephrol Dial Transplant **30**(2): 257–266.

ANDRIKOPOULOS S., MASSA C.M., ASTON-MOURNEY K., FUNKAT A., FAM B.C., HULL R.L., KAHN S.E. and PROIETTO J. (2005) *Differential effect of inbred mouse strain (C57BL/6, DBA/2, 129T2) on insulin secretory function in response to a high fat diet*. J Endocrinol **187**(1): 45–53.

AVOGARO A., VIGILI DE KREUTZENBERG S., NEGUT C., TIENGO A. and SCOGNAMIGLIO R. (2004) *Diabetic cardiomyopathy: a metabolic perspective*. Am J Cardiol **93**(8A): 13A–16A.

BADDELEY A., DORPH-PETERSEN K.A. and VEDEL JENSEN E.B. (2006) *A note on the stereological implications of irregular spacing of sections*. J Microsc **222**(Pt 3): 177–181.

BAILEY D.W. (1977) *Genetic drift: the problem and its possible solution by frozen-embryo storage*. Ciba Found Symp (52): 291–303.

BAKER N., GREEN A., KRISHNAN S. and RAYMAN G. (2007) *Microvascular and C-fiber function in diabetic charcot neuroarthropathy and diabetic peripheral neuropathy*. Diabetes Care **30**(12): 3077–3079.

BAUMANN M., HERMANS J.J.R., DEBETS J., SMITS J.F.M. and STRUIJKER-BOUDIER H.A.J. (2003) *Early transient TGF beta 1 inhibition alters intrarenal growth and increases blood pressure in spontaneously hypertensive rats (SHR)*. 8th Annual Meeting European Council Blood Pressure and Cardiovasc Res (ECCR) **Seeheim**(Germany): 19.

BECK J.A., LLOYD S., HAFEZPARAST M., LENNON-PIERCE M., EPPIG J.T., FESTING M.F. and FISHER E.M. (2000) *Genealogies of mouse inbred strains*. Nat Genet **24**(1): 23–25.

BENZ K., CAMPEAN V., CORDASIC N., KARPE B., NEUHUBER W., MALL G., HARTNER A., HILGERS K.F. and AMANN K. (2011) *Early glomerular alterations in genetically determined low nephron number*. Am J Physiol Renal Physiol **300**(2): F521–530.

BERKMAN J. and RIFKIN H. (1973) *Unilateral nodular diabetic glomerulosclerosis (Kimmelstiel-Wilson): report of a case*. Metab Clin Exp **22**(5): 715–722.

BERONIADE V.C., LEFEBVRE R. and FALARDEAU P. (1987) *Unilateral nodular diabetic glomerulosclerosis: recurrence of an experiment of nature*. Am J Nephrol **7**(1): 55–59.

BETZ B. and CONWAY B.R. (2014) *Recent advances in animal models of diabetic nephropathy*. Nephron Exp Nephrol **126**(4): 191–195.

BHASIN R. and GHOBRIAL I. (2013) *Diabetic myonecrosis: a diagnostic challenge in patients with long-standing diabetes*. J Community Hosp Intern Med Perspect **3**(1).

BIELSCHOWSKY F. and BIELSCHOWSKY M. (1956) *The New Zealand strain of obese mice; their response to stilboestrol and to insulin*. Aust J Exp Biol Med Sci **34**(3): 181–198.

BILOUS R. (2001) Renal Structural Damage in IDDM and NIDDM - Functional Relationships, In: Diabetic Nephropathy ed. Hasslacher C. John Wiley & Sons, Ltd, Chichester, UK.

BILOUS R.W., MAUER S.M., SUTHERLAND D.E. and STEFFES M.W. (1989) *Mean glomerular volume and rate of development of diabetic nephropathy*. Diabetes **38**(9): 1142–1147.

BLAES N., PECHER C., MEHRENBERGER M., CELLIER E., PRADDAUDE F., CHEVALIER J., TACK I., COUTURE R. and GIROLAMI J.P. (2012) *Bradykinin inhibits high glucose- and growth factor-induced collagen synthesis in mesangial cells through the B2-kinin receptor*. Am J Physiol Renal Physiol **303**(2): 293–303.

BLANTZ R.C. and SINGH P. (2014) *Glomerular and tubular function in the diabetic kidney*. Adv Chronic Kidney Dis **21**(3): 297–303.

BOUBRED F., SAINT-FAUST M., BUFFAT C., LIGI I., GRANDVUILLEMIN I. and SIMEONI U. (2013) *Developmental origins of chronic renal disease: an integrative hypothesis*. Int J Nephrol **2013**: 346067.

BRENNER B.M. (1983) *Hemodynamically mediated glomerular injury and the progressive nature of kidney disease*. Kidney Int **23**(4): 647–655.

BRENNER B.M., GARCIA D.L. and ANDERSON S. (1988) *Glomeruli and blood pressure. Less of one, more the other?*. Am J Hypertens **1**(4 Pt 1): 335–347.

BRENNER B.M. and MACKENZIE H.S. (1997) *Nephron mass as a risk factor for progression of renal disease*. Kidney Int Suppl **63**: S124–127.

BREYER M.D., BOTTINGER E., BROSIUS F.C., COFFMAN T.M., FOGO A., HARRIS R.C., HEILIG C.W. and SHARMA K. (2005a) *Diabetic nephropathy: of mice and men*. Adv Chronic Kidney Dis **12**(2): 128–145.

BREYER M.D., BOTTINGER E., BROSIUS F.C., COFFMAN T.M., HARRIS R.C., HEILIG C.W. and SHARMA K. (2005b) *Mouse models of diabetic nephropathy*. J Am Soc Nephrol **16**(1): 27–45.

BREYER M.D. and QI Z. (2010) *Better nephrology for mice–and man*. Kidney Int **77**(6): 487–489.

BROSIUS F.C. (2010) *Susceptible mice: identifying a diabetic nephropathy disease locus using a murine model*. Kidney Int **78**(5): 431–432.

BROSIUS F.C., ALPERS C.E., BOTTINGER E.P., BREYER M.D., COFFMAN T.M., GURLEY S.B., HARRIS R.C., KAKOKI M., KRETZLER M., LEITER E.H., LEVI M., MCINDOE R.A., SHARMA K., SMITHIES O., SUSZTAK K., TAKAHASHI N. and TAKAHASHI T. (2009) *Mouse models of diabetic nephropathy*. J Am Soc Nephrol **20**(12): 2503–2512.

BROSIUS F.C. and COWARD R.J. (2014) *Podocytes, signaling pathways, and vascular factors in diabetic kidney disease*. Adv Chronic Kidney Dis **21**(3): 304–310.

BUCHAN A.M., POLAK J.M., CAPELLA C., SOLCIA E. and PEARSE A.G. (1978) *Electronimmunocytochemical evidence for the K cell localization of gastric inhibitory polypeptide (GIP) in man*. Histochemistry **56**(1): 37–44.

BUSCH M., CHOURBAJI S., DAMMANN P., GEROLD S., HAEMISCH A., JIRKOF P., OEHLERT P., OSTERKAMP A., OTT S., PETERS S., SPEKL K. and TSAI P.P. (2014) Tiergerechte Haltung von Labormäusen. Technical report, Ausschuss für Tiergerechte Labortierhaltung, GV-SOLAS.

BUZELLO M. (2000) *Comparison of two stereological methods for quantitative renal morphology: a modified fractionator and modified Weibel-Gomez method*. Pathol Res Pract **196**(2): 111–117.

CAMPBELL K.L., JOHNSON D.W., BAUER J.D., HAWLEY C.M., ISBEL N.M., STOWASSER M., WHITEHEAD J.P., DIMESKI G. and MCMAHON E. (2014) *A randomized trial of sodium-restriction on kidney function, fluid volume and adipokines in CKD patients*. BMC Nephrol **15**: 57.

CAO Y., HAO Y., LI H., LIU Q., GAO F., LIU W. and DUAN H. (2014) *Role of endoplasmic reticulum stress in apoptosis of differentiated mouse podocytes induced by high glucose*. Int J Mol Med **33**(4): 809–816.

CARLSON E.C., AUDETTE J.L., KLEVAY L.M., NGUYEN H. and EPSTEIN P.N. (1997) *Ultrastructural and functional analyses of nephropathy in calmodulin-induced diabetic transgenic mice*. Anat Rec **247**(1): 9–19.

CDC (2011) *National Diabetes Fact Sheet: national estimates and general information on diabetes and prediabetes in the United States, 2011*. Centers for Disease Control and Prevention, US Department of Health and Human Services .

CEBRIAN C., ASAI N., D'AGATI V. and COSTANTINI F. (2014) *The number of fetal nephron progenitor cells limits ureteric branching and adult nephron endowment*. Cell Rep **7**(1): 127–137.

CHANG J.H. and GURLEY S.B. (2012) *Assessment of diabetic nephropathy in the Akita mouse*. Methods Mol Biol **933**: 17–29.

CHANG J.H., PAIK S.Y., MAO L., EISNER W., FLANNERY P.J., WANG L., TANG Y., MATTOCKS N., HADJADJ S., GOUJON J.M., RUIZ P., GURLEY S.B. and SPURNEY R.F. (2012) *Diabetic kidney disease in FVB/NJ Akita mice: temporal pattern of kidney injury and urinary nephrin excretion*. PLoS ONE **7**(4): e33942.

CHEN L.M., LI X.W., HUANG L.W., LI Y., DUAN L. and ZHANG X.J. (2002) *[The early pathological changes of KKAy mice with type 2 diabetes]*. Zhongguo Yi Xue Ke Xue Yuan Xue Bao **24**(1): 71–75.

CHOW F., OZOLS E., NIKOLIC-PATERSON D.J., ATKINS R.C. and TESCH G.H. (2004a) *Macrophages in mouse type 2 diabetic nephropathy: correlation with diabetic state and progressive renal injury*. Kidney Int **65**(1): 116–128.

CHOW F.Y., NIKOLIC-PATERSON D.J., ATKINS R.C. and TESCH G.H. (2004b) *Macrophages in streptozotocin-induced diabetic nephropathy: potential role in renal fibrosis*. Nephrol Dial Transplant **19**(12): 2987–2996.

CHRISTENSEN M., CALANNA S., HOLST J.J., VILSBØLL T. and KNOP F.K. (2013) *Glucose-dependent Insulinotropic Polypeptide: Blood Glucose Stabilizing Effects in Patients with Type 2 diabetes*. J Clin Endocrinol Metab jc20133644.

CHUA S., LI Y., LIU S.M., LIU R., CHAN K.T., MARTINO J., ZHENG Z., SUSZTAK K., D'AGATI V.D. and GHARAVI A.G. (2010) *A susceptibility gene for kidney disease in an obese mouse model of type II diabetes maps to chromosome 8*. Kidney Int **78**(5): 453–462.

CHUA S., LIU S.M., LI Q., YANG L., THASSANAPAFF V.T. and FISHER P. (2002) *Differential beta cell responses to hyperglycaemia and insulin resistance in two novel congenic strains of diabetes (FVB- Lepr (db)) and obese (DBA- Lep (ob)) mice*. Diabetologia **45**(7): 976–990.

COLLINS A.J., FOLEY R.N., CHAVERS B., GILBERTSON D., HERZOG C., JOHANSEN K., KASISKE B., KUTNER N., LIU J., ST PETER W., GUO H., GUSTAFSON S., HEUBNER B., LAMB K., LI S., LI S., PENG Y., QIU Y., ROBERTS T., SKEANS M., SNYDER J., SOLID C., THOMPSON B., WANG C., WEINHANDL E., ZAUN D., ARKO C., CHEN S.C., DANIELS F., EBBEN J., FRAZIER E., HANZLIK C., JOHNSON R., SHEETS D., WANG X., FORREST B., CONSTANTINI E., EVERSON S., EGGERS P. and AGODOA L. (2012) *United States Renal Data System 2011 Annual Data Report: Atlas of chronic kidney disease end-stage renal disease in the United States*. Am J Kidney Dis **59**(1 Suppl 1): 1–420.

COMPER W.D. (2014) *Albuminuria is controlled primarily by proximal tubules*. Nat Rev Nephrol **10**(3): 180.

CORWELL B., KNIGHT B., OLIVIERI L. and WILLIS G.C. (2014) *Current diagnosis and treatment of hyperglycemic emergencies*. Emerg Med Clin North Am **32**(2): 437–452.

D. H. PERCY S.W.B. (2007) Pathology of laboratory rodents and rabbits. Blackwell Publishing, Oxford, UK.

DAHLHOFF M., PFISTER S., BLUTKE A., ROZMAN J., KLINGENSPOR M., DEUTSCH M.J., RATHKOLB B., FINK B., GIMPFL M., HRABĚ DE ANGELIS M., ROSCHER A.A., WOLF E. and ENSENAUER R. (2014) *Peri-conceptional obesogenic exposure*

induces sex-specific programming of disease susceptibilities in adult mouse offspring. Biochim Biophys Acta **1842**(2): 304–317.

DANAEI G., FINUCANE M.M., LU Y., SINGH G.M., COWAN M.J., PACIOREK C.J., LIN J.K., FARZADFAR F., KHANG Y.H., STEVENS G.A., RAO M., ALI M.K., RILEY L.M., ROBINSON C.A., EZZATI M., DANAEI G., FINUCANE M.M., LU Y., SINGH G.M., COWAN M.J., PACIOREK C.J., LIN J.K., FARZADFAR F., KHANG Y.H., STEVENS G.A., RAO M., ALI M.K., RILEY L.M., ROBINSON C.A., EZZATI M., ABDEEN Z., AEKPLAKORN W., AFIFI M.M., AGABITI-ROSEI E., SALINAS C.A., ALNSOUR M., AMBADY R., BARBAGALLO C.M., BARCELO A., BARROS H., BAUTISTA L.E., BENETOS A., BJERREGAARD P., BO S., BOVET P., BURSZTYN M., CABRERA DE LEON A., CASTELLANO M., CASTETBON K., CHAOUKI N., CHEN C.J., CHUA L., CIFKOVA R., CORSI A.M., DELGADO E., DOI Y., ESTEGHAMATI A., FALL C.H., FAN J.G., FERRECCIO C., FEZEU L., FULLER E.L., GIAMPAOLI S., GOMEZ L.F., CARVAJAL R.G., HERMAN W.H., HERRERA V.M., HO S., HUSSAIN A., IKEDA N., JAFAR T.H., JONAS J.B., KADIKI O.A., KARALIS I., KATZ J., KHALILZADEH O., KIECHL S., KURJATA P., LEE J., LEE J., LIM S., LIM T.O., LIN C.C., LIN X., LIN H.H., LIU X., LORBEER R., MA S., MAGGI S., MAGLIANO D.J., MCFARLANE-ANDERSON N., MIETTOLA J., MIRANDA J.J., MOHAMED M.K., MOHAN V., MOKDAD A., MORALES D.D., NABIPOUR I., NAKAGAMI T., NANGIA V., NEUHAUSER H., NOALE M., ONAT A., OROSTEGUI M., PANAGIOTAKOS D.B., PASSOS V.M., PEREZ C., PICHARDO R., PIN PHUA H., PLANS P., QIAO Q., RAMOS L.R., RAMPAL S., RAMPAL L., REDON J., REVILLA L., ROSERO-BIXBY L., SANISOGLU S.Y., SCAZUFCA M., SCHAAN B.D., SEKURI C., SHERA A.S., SHI Z., SILVA E., SIMONS L.A., SODERBERG S., SOLFRIZZI V., SOYSAL A., STEIN A.D., STESSMAN J., VANDERPUMP M.P., VIET L., VOLLENWEIDER P., WANG N., WANG Y.X., WASPADJI S., WILLEIT J., WOODWARD M., XU L., YANG X., YOON J.S., YU Z., ZHANG J. and ZHANG L. (2011) *National, regional, and global trends in fasting plasma glucose and diabetes prevalence since 1980: systematic analysis of health examination surveys and epidemiological studies with 370 country-years and 2·7 million participants*. Lancet **378**(9785): 31–40.

DCCT (1995) *Intensive therapy and progression to clinical albuminuria in patients with insulin dependent diabetes mellitus and microalbuminuria. Microalbuminuria Collaborative Study Group, United Kingdom*. BMJ **311**(7011): 973–977.

DEEN W.M., LAZZARA M.J. and MYERS B.D. (2001) *Structural determinants of glomerular permeability*. Am J Physiol Renal Physiol **281**(4): F579–596.

DESCHEPPER C.F., OLSON J.L., OTIS M. and GALLO-PAYET N. (2004) *Characterization of blood pressure and morphological traits in cardiovascular-related organs in 13 different inbred mouse strains*. J Appl Physiol **97**(1): 369–376.

DESSAPT C., BARADEZ M.O., HAYWARD A., DEI CAS A., THOMAS S.M., VIBERTI G. and GNUDI L. (2009) *Mechanical forces and TGFbeta1 reduce podocyte adhesion through alpha3beta1 integrin downregulation*. Nephrol Dial Transplant **24**(9): 2645–2655.

DING K.H., SHI X.M., ZHONG Q., KANG B., XIE D., BOLLAG W.B., BOLLAG R.J., HILL W., WASHINGTON W., MI Q.S., INSOGNA K., CHUTKAN N., HAMRICK M. and ISALES C.M. (2008) *Impact of glucose-dependent insulinotropic peptide on age-induced bone loss*. J Bone Miner Res **23**(4): 536–543.

DORPH-PETERSEN K.A., NYENGAARD J.R. and GUNDERSEN H.J. (2001) *Tissue shrinkage and unbiased stereological estimation of particle number and size*. J Microsc **204**(Pt 3): 232–246.

DREYER G., HULL S., MATHUR R., CHESSER A. and YAQOOB M.M. (2013) *Progression of chronic kidney disease in a multi-ethnic community cohort of patients with diabetes mellitus*. Diabet Med **30**(8): 956–963.

DRUMOND M.C. and DEEN W.M. (1994) *Structural determinants of glomerular hydraulic permeability*. Am J Physiol **266**(1 Pt 2): 1–12.

DUNN S.R., QI Z., BOTTINGER E.P., BREYER M.D. and SHARMA K. (2004) *Utility of endogenous creatinine clearance as a measure of renal function in mice*. Kidney Int **65**(5): 1959–1967.

DUNNING B.E. and GERICH J.E. (2007) *The role of alpha-cell dysregulation in fasting and postprandial hyperglycemia in type 2 diabetes and therapeutic implications*. Endocr Rev **28**(3): 253–283.

EL-AOUNI C., HERBACH N., BLATTNER S.M., HENGER A., RASTALDI M.P., JARAD G., MINER J.H., MOELLER M.J., ST-ARNAUD R., DEDHAR S., HOLZMAN L.B., WANKE R. and KRETZLER M. (2006) *Podocyte-specific deletion of integrin-linked kinase results in severe glomerular basement membrane alterations and progressive glomerulosclerosis*. J Am Soc Nephrol **17**(5): 1334–1344.

FARR S. and ADELI K. (2012) *Incretin-based therapies for treatment of postprandial dyslipidemia in insulin-resistant states*. Curr Opin Lipidol **23**(1): 56–61.

FILLER G., BOKENKAMP A., HOFMANN W., LE BRICON T., MARTINEZ-BRU C. and GRUBB A. (2005) *Cystatin C as a marker of GFR–history, indications, and future research*. Clin Biochem **38**(1): 1–8.

FILMETRICS-INC. (2012) Thin-film measurements. San Diedo, USA.

FOGO A. and ICHIKAWA I. (1991) *Evidence for a pathogenic linkage between glomerular hypertrophy and sclerosis*. Am J Kidney Dis **17**(6): 666–669.

FOX J. (2007) The Mouse in Biomedical Research: Normative Biology, Husbandry and Models: 3. Academic Press, Elsevier, USA.

FURUHAMA K. and ONODERA T. (1983) *A simple technique for repeated blood collection from the tail vein of the rat*. J Toxicol Sci **8**(2): 116–163.

GALLWITZ B., WITT M., MORYS-WORTMANN C., FOLSCH U.R. and SCHMIDT W.E. (1996) *GLP-1/GIP chimeric peptides define the structural requirements for specific ligand-receptor interaction of GLP-1*. Regul Pept **63**(1): 17–22.

GANGADHARIAH M.H., LUTHER J.M., GARCIA V., PAUEKSAKON P., ZHANG M.Z., HAYWARD S.W., LOVE H.D., FALCK J.R., MANTHATI V.L., IMIG J.D., SCHWARTZMAN M.L., ZENT R., CAPDEVILA J.H. and POZZI A. (2014) *Hypertension Is a Major Contributor to 20-Hydroxyeicosatetraenoic Acid-Mediated Kidney Injury in Diabetic Nephropathy*. J Am Soc Nephrol .

GELLING R.W. (2006) *Diabetic hyperphagia–ghrelin in the driver's seat*. Endocrinology **147**(6): 2631–2633.

GELLING R.W., WHEELER M.B., XUE J., GYOMOREY S., NIAN C., PEDERSON R.A. and MCINTOSH C.H. (1997) *Localization of the domains involved in ligand binding and activation of the glucose-dependent insulinotropic polypeptide receptor*. Endocrinology **138**(6): 2640–2643.

GERALDES P., HIRAOKA-YAMAMOTO J., MATSUMOTO M., CLERMONT A., LEITGES M., MARETTE A., AIELLO L.P., KERN T.S. and KING G.L. (2009) *Activation of PKC-delta and SHP-1 by hyperglycemia causes vascular cell apoptosis and diabetic retinopathy*. Nat Med **15**(11): 1298–1306.

GERICH J.E. (2010) *Role of the kidney in normal glucose homeostasis and in the hyperglycaemia of diabetes mellitus: therapeutic implications*. Diabet Med **27**(2): 136–142.

GRUBB A. (2010) *Non-invasive estimation of glomerular filtration rate (GFR). The Lund model: Simultaneous use of cystatin C- and creatinine-based GFR-prediction equations, clinical data and an internal quality check*. Scand J Clin Lab Invest **70**(2): 65–70.

GRUBB A. and LOFBERG H. (1982) *Human gamma-trace, a basic microprotein: amino acid sequence and presence in the adenohypophysis*. Proc Natl Acad Sci USA **79**(9): 3024–3027.

GUNDERSEN H.J. (1978) *Estimators of the number of objects per area unbiased by edge effects*. Microsc Acta **81**(2): 107–117.

GUO M., RICARDO S.D., DEANE J.A., SHI M., CULLEN-MCEWEN L. and BERTRAM J.F. (2005) *A stereological study of the renal glomerular vasculature in the db/db mouse model of diabetic nephropathy*. J Anat **207**(6): 813–821.

GURLEY S.B., CLARE S.E., SNOW K.P., HU A., MEYER T.W. and COFFMAN T.M. (2006) *Impact of genetic background on nephropathy in diabetic mice*. Am J Physiol Renal Physiol **290**(1): F214–222.

GURLEY S.B., MACH C.L., STEGBAUER J., YANG J., SNOW K.P., HU A., MEYER T.W. and COFFMAN T.M. (2010) *Influence of genetic background on albuminuria and kidney injury in Ins2(+/C96Y) (Akita) mice*. Am J Physiol Renal Physiol **298**(3): F788–795.

GUZMAN J., JAUREGUI A.N., MERSCHER-GOMEZ S., MAIGUEL D., MURESAN C., MITROFANOVA A., DIEZ-SAMPEDRO A., SZUST J., YOO T.H., VILLARREAL R., PEDIGO C., MOLANO R.D., JOHNSON K., KAHN B., HARTLEBEN B., HUBER T.B., SAHA J., BURKE G.W., ABEL E.D., BROSIUS F.C. and FORNONI A. (2014) *Podocyte-specific GLUT4-deficient mice have fewer and larger podocytes and are protected from diabetic nephropathy*. Diabetes **63**(2): 701–714.

GV-SOLAS (2011) *Beschleunigte Rückkreuzung - "Speed"-kongene Stämme*. Ausschuss für Genetik und Labortierzucht .

HABIB S.L. (2013) *Alterations in tubular epithelial cells in diabetic nephropathy*. J Nephrol **26**(5): 865–869.

HARDIKAR P.S., JOSHI S.M., BHAT D.S., RAUT D.A., KATRE P.A., LUBREE H.G., JERE A., PANDIT A.N., FALL C.H. and YAJNIK C.S. (2013) *Response to comment on: Hardikar et al. Spuriously high prevalence of prediabetes diagnosed by HbA(1c) in young indians partly explained by hematological factors and iron deficiency anemia. Diabetes Care 2012;35:797-802*. Diabetes Care **36**(2): e24.

HARTNER A., EIFERT T., HAAS C.S., TUYSUZ C., HILGERS K.F., REINHARDT D.P. and AMANN K. (2004) *Characterization of the renal phenotype in a mouse model of Marfan syndrome*. Virchows Arch **445**(4): 382–388.

HARVEY S.J., ZHENG K., SADO Y., NAITO I., NINOMIYA Y., JACOBS R.M., HUDSON B.G. and THORNER P.S. (1998) *Role of distinct type IV collagen networks in glomerular development and function*. Kidney Int **54**(6): 1857–1866.

HELLERSTROM C. and HELLMAN B. (1963) *The Islets of Langerhans in yellow obese mice*. Metab Clin Exp **12**: 527–536.

HERBACH N. (2002) Clinical and pathological characterization of a novel transgenic animal novel of diabetes mellitus expressing a dominant negative glucose-dependent insulionotropic polypeptide receptor ($GIPR^{dn}$). Dissertation, Ludwig-Maximilians-Universität, Munich.

HERBACH N., BERGMAYR M., GOKE B., WOLF E. and WANKE R. (2011) *Postnatal development of numbers and mean sizes of pancreatic islets and beta-cells in healthy mice*

and GIPR(dn) transgenic diabetic mice. PLoS ONE **6**(7): e22814.

HERBACH N., GOEKE B., SCHNEIDER M., HERMANNS W., WOLF E. and WANKE R. (2005) *Overexpression of a dominant negative GIP receptor in transgenic mice results in disturbed postnatal pancreatic islet and beta-cell development*. Regul Pept **125**(1-3): 103–117.

HERBACH N., SCHAIRER I., BLUTKE A., KAUTZ S., SIEBERT A., GOKE B., WOLF E. and WANKE R. (2009) *Diabetic kidney lesions of GIPRdn transgenic mice: podocyte hypertrophy and thickening of the GBM precede glomerular hypertrophy and glomerulosclerosis*. Am J Physiol Renal Physiol **296**(4): F819–829.

HERMANNS W., LIEBIG K. and SCHULZ L.C. (1981) *Postembedding immunohistochemical demonstration of antigen in experimental polyarthritis using plastic embedded whole joints*. Histochemistry **73**(3): 439–446.

HJALMARSSON C., JOHANSSON B.R. and HARALDSSON B. (2004) *Electron microscopic evaluation of the endothelial surface layer of glomerular capillaries*. Microvasc Res **67**(1): 9–17.

HORIO M. (2014) *[New topics regarding equations for GFR estimation based on serum creatinine and cystatin C]*. Rinsho Byori **62**(2): 153–162.

HOSHI S., SHU Y., YOSHIDA F., INAGAKI T., SONODA J., WATANABE T., NOMOTO K. and NAGATA M. (2002) *Podocyte injury promotes progressive nephropathy in zucker diabetic fatty rats*. Lab Invest **82**(1): 25–35.

HUMMEL K.P., COLEMAN D.L. and LANE P.W. (1972) *The influence of genetic background on expression of mutations at the diabetes locus in the mouse. I. C57BL-KsJ and C57BL-6J strains*. Biochem Genet **7**(1): 1–13.

INADA A., ARAI H., NAGAI K., MIYAZAKI J., YAMADA Y., SEINO Y. and FUKATSU A. (2007) *Gender difference in ICER Igamma transgenic diabetic mouse*. Biosci Biotechnol Biochem **71**(8): 1920–1926.

INGALLS A.M., DICKIE M.M. and SNELL G.D. (1950) *Obese, a new mutation in the house mouse*. J Hered **41**(12): 317–318.

ISOGAI S., MOGAMI K., SHIINA N. and YOSHINO G. (1999) *Initial ultrastructural changes in pore size and anionic sites of the glomerular basement membrane in streptozotocin-induced diabetic rats and their prevention by insulin treatment*. Nephron **83**(1): 53–58.

ITO T., TANIMOTO M., YAMADA K., KANEKO S., MATSUMOTO M., OBAYASHI K., HAGIWARA S., MURAKOSHI M., AOKI T., WAKABAYASHI M., GOHDA T., FUNABIKI K., MAEDA K., HORIKOSHI S. and TOMINO Y. (2006) *Glomerular changes in the KK-Ay/Ta mouse: a possible model for human type 2 diabetic nephropathy*. Nephrology (Carlton) **11**(1): 29–35.

JACOBSSON B., LIGNELID H. and BERGERHEIM U.S. (1995) *Transthyretin and cystatin C are catabolized in proximal tubular epithelial cells and the proteins are not useful as markers for renal cell carcinomas*. Histopathology **26**(6): 559–564.

JANI A., POLHEMUS C., CORRIGAN G., KWON O., MYERS B.D. and PAVLAKIS M. (2002) *Determinants of hypofiltration during acute renal allograft rejection*. J Am Soc Nephrol **13**(3): 773–778.

JARRETT R.J., VIBERTI G.C., ARGYROPOULOS A., HILL R.D., MAHMUD U. and MURRELLS T.J. (1984) *Microalbuminuria predicts mortality in non-insulin-dependent diabetics*. Diabet Med **1**(1): 17–19.

KAKOKI M., SULLIVAN K.A., BACKUS C., HAYES J.M., OH S.S., HUA K., GASIM A.M., TOMITA H., GRANT R., NOSSOV S.B., KIM H.S., JENNETTE J.C., FELDMAN E.L. and SMITHIES O. (2010) *Lack of both bradykinin B1 and B2 receptors enhances nephropathy, neuropathy, and bone mineral loss in Akita diabetic mice*. Proc Natl Acad Sci USA **107**(22): 10190–10195.

KANETSUNA Y., TAKAHASHI K., NAGATA M., GANNON M.A., BREYER M.D., HARRIS R.C. and TAKAHASHI T. (2007) *Deficiency of endothelial nitric-oxide synthase confers susceptibility to diabetic nephropathy in nephropathy-resistant inbred mice*. Am J Pathol **170**(5): 1473–1484.

KAPLAN A.M. and VIGNA S.R. (1994) *Gastric inhibitory polypeptide (GIP) binding sites in rat brain*. Peptides **15**(2): 297–302.

KAYNAK G., BIRSEL O., GUVEN M.F. and O?UT T. (2013) *An overview of the Charcot foot pathophysiology*. Diabet Foot Ankle **4**.

KERN T.S. (2007) *Contributions of inflammatory processes to the development of the early stages of diabetic retinopathy*. Exp Diabetes Res **2007**: 95103.

KHOSHNOODI J., SIGMUNDSSON K., OFVERSTEDT L.G., SKOGLUND U., OBRINK B., WARTIOVAARA J. and TRYGGVASON K. (2003) *Nephrin promotes cell-cell adhesion through homophilic interactions*. Am J Pathol **163**(6): 2337–2346.

KIMMELSTIEL P. and WILSON C. (1936) *Intercapillary Lesions in the Glomeruli of the Kidney*. Am J Pathol **12**(1): 83–98.

KINUGASA S., TOJO A., SAKAI T., TSUMURA H., TAKAHASHI M., HIRATA Y. and FUJITA T. (2011) *Selective albuminuria via podocyte albumin transport in puromycin nephrotic rats is attenuated by an inhibitor of NADPH oxidase*. Kidney Int **80**(12): 1328–1338.

KITAMOTO Y., TOKUNAGA H. and TOMITA K. (1997) *Vascular endothelial growth factor is an essential molecule for mouse kidney development: glomerulogenesis and nephrogenesis*. J Clin Invest **99**(10): 2351–2357.

KOJIMA K. and KERJASCHKI D. (2002) *Is podocyte shape controlled by the dystroglycan complex?*. Nephrol Dial Transplant **17 Suppl 9**: 23–24.

KONDO H. and USHIKI T. (1985) *Stratified laminae fenestratae (alveolus fenestratus endothelialis) in the glomerular capillaries of the mouse kidney*. Arch Histol Jpn **48**(1): 117–122.

KREGE J.H., HODGIN J.B., HAGAMAN J.R. and SMITHIES O. (1995a) *A noninvasive computerized tail-cuff system for measuring blood pressure in mice*. Hypertension **25**(5): 1111–1115.

KREGE J.H., JOHN S.W., LANGENBACH L.L., HODGIN J.B., HAGAMAN J.R., BACHMAN E.S., JENNETTE J.C., O'BRIEN D.A. and SMITHIES O. (1995b) *Male-female differences in fertility and blood pressure in ACE-deficient mice*. Nature **375**(6527): 146–148.

KRETZLER M. (2002) *Regulation of adhesive interaction between podocytes and glomerular basement membrane*. Microsc Res Tech **57**(4): 247–253.

KRIZ W. and LEMLEY K.V. (2014) *A Potential Role for Mechanical Forces in the Detachment of Podocytes and the Progression of CKD*. J Am Soc Nephrol .

LAWSON M.L., SOCHETT E.B., CHAIT P.G., BALFE J.W. and DANEMAN D. (1996) *Effect of puberty on markers of glomerular hypertrophy and hypertension in IDDM*. Diabetes **45**(1): 51–55.

LEITER E.H. (1982) *Multiple low-dose streptozotocin-induced hyperglycemia and insulitis in C57BL mice: influence of inbred background, sex, and thymus*. Proc Natl Acad Sci USA **79**(2): 630–634.

LEITER E.H. and REIFSNYDER P.C. (2004) *Differential levels of diabetogenic stress in two new mouse models of obesity and type 2 diabetes*. Diabetes **53 Suppl 1**: 4–11.

LEMLEY K.V. (2003) *A basis for accelerated progression of diabetic nephropathy in Pima Indians*. Kidney Int Suppl (83): 38–42.

LEMLEY K.V. (2008) *Diabetes and chronic kidney disease: lessons from the Pima Indians*. Pediatr Nephrol **23**(11): 1933–1940.

LEMLEY K.V., ELGER M., KOEPPEN-HAGEMANN I., KRETZLER M., NAGATA M., SAKAI T., UIKER S. and KRIZ W. (1992) *The glomerular mesangium: capillary support function and its failure under experimental conditions*. Clin Investig **70**(9): 843–856.

LI G., VEENSTRA A.A., TALAHALLI R.R., WANG X., GUBITOSI-KLUG R.A., SHEIBANI N. and KERN T.S. (2012) *Marrow-derived cells regulate the development of early diabetic retinopathy and tactile allodynia in mice*. Diabetes **61**(12): 3294–3303.

LIU A., DARDIK A. and BALLERMANN B.J. (1999) *Neutralizing TGF-beta1 antibody infusion in neonatal rat delays in vivo glomerular capillary formation 1*. Kidney Int **56**(4): 1334–1348.

LIU M., HAATAJA L., WRIGHT J., WICKRAMASINGHE N.P., HUA Q.X., PHILLIPS N.F., BARBETTI F., WEISS M.A. and ARVAN P. (2010) *Mutant INS-gene induced diabetes of youth: proinsulin cysteine residues impose dominant-negative inhibition on wild-type proinsulin transport*. PLoS ONE **5**(10): e13333.

LIZICAROVA D., KRAHULEC B., HIRNEROVA E., GASPAR L. and CELECOVA Z. (2014) *Risk factors in diabetic nephropathy progression at present*. Bratisl Lek Listy **115**(8): 517–521.

LU M., WHEELER M.B., LENG X.H. and BOYD A.E. (1993) *The role of the free cytosolic calcium level in beta-cell signal transduction by gastric inhibitory polypeptide and glucagon-like peptide I(7-37)*. Endocrinology **132**(1): 94–100.

LUSIS A.J. (2000) *Atherosclerosis*. Nature **407**(6801): 233–241.

MA L.J. and FOGO A.B. (2003) *Model of robust induction of glomerulosclerosis in mice: importance of genetic background*. Kidney Int **64**(1): 350–5.

MACEDO C.S., LERCO M.M., CAPELLETTI S.M., SILVA R.J., PINHEIRO D.D.E.O. and SPADELLA C.T. (2007) *Reduction of podocytes number in late diabetic alloxan nephropathy: prevention by glycemic control*. Acta Cir Bras **22**(5): 337–341.

MANALICH R., REYES L., HERRERA M., MELENDI C. and FUNDORA I. (2000) *Relationship between weight at birth and the number and size of renal glomeruli in humans: a histomorphometric study*. Kidney Int **58**(2): 770–773.

MARRERO I., HAMM D.E. and DAVIES J.D. (2013) *High-throughput sequencing of islet-infiltrating memory CD4+ T cells reveals a similar pattern of TCR VÎ usage in prediabetic and diabetic NOD mice*. PLoS ONE **8**(10): e76546.

MARSHALL T. and WILLIAMS K.M. (1998) *Clinical analysis of human urinary proteins using high resolution electrophoretic methods*. Electrophoresis **19**(10): 1752–1770.

MASCARENHAS J.V. and JUDE E.B. (2013) *Pathogenesis and medical management of diabetic Charcot neuroarthropathy*. Med Clin North Am **97**(5): 857–872.

MAUER S.M., STEFFES M.W., ELLIS E.N., SUTHERLAND D.E., BROWN D.M. and GOETZ F.C. (1984) *Structural-functional relationships in diabetic nephropathy*. J Clin Invest **74**(4): 1143–1155.

MCQUARRIE E.P., TRAYNOR J.P., TAYLOR A.H., FREEL E.M., FOX J.G., JARDINE A.G. and MARK P.B. (2014) *Association between urinary sodium, creatinine, albumin, and long-term survival in chronic kidney disease*. Hypertension **64**(1): 111–117.

MENG H., ZHANG D. and YANG H. (2013) *Effects of amyloid precursor protein 17 peptide on the protection of diabetic encephalopathy and improvement of glycol metabolism in the diabetic rat*. J Diabetes Res **2013**: 689841.

MERLINE R., LAZAROSKI S., BABELOVA A., TSALASTRA-GREUL W., PFEILSCHIFTER J., SCHLUTER K.D., GUNTHER A., IOZZO R.V., SCHAEFER R.M. and SCHAEFER L. (2009) *Decorin deficiency in diabetic mice: aggravation of nephropathy due to overexpression of profibrotic factors, enhanced apoptosis and mononuclear cell infiltration*. J Physiol Pharmacol **60 Suppl 4**: 5–13.

MEYER M.H., MEYER R.A., GRAY R.W. and IRWIN R.L. (1985) *Picric acid methods greatly overestimate serum creatinine in mice: more accurate results with high-performance liquid chromatography*. Anal Biochem **144**(1): 285–290.

MICHAUD E.J., BULTMAN S.J., KLEBIG M.L., VAN VUGT M.J., STUBBS L.J., RUSSELL L.B. and WOYCHIK R.P. (1994) *A molecular model for the genetic and phenotypic characteristics of the mouse lethal yellow (Ay) mutation*. Proc Natl Acad Sci USA **91**(7): 2562–2566.

MILLER P.L., RENNKE H.G. and MEYER T.W. (1991) *Glomerular hypertrophy accelerates hypertensive glomerular injury in rats*. Am J Physiol **261**(3 Pt 2): F459–465.

MILLS E., KUHN C.M., FEINGLOS M.N. and SURWIT R. (1993) *Hypertension in CB57BL/6J mouse model of non-insulin-dependent diabetes mellitus*. Am J Physiol **264**(1 Pt 2): R73–78.

MITU G.M., WANG S. and HIRSCHBERG R. (2007) *BMP7 is a podocyte survival factor and rescues podocytes from diabetic injury*. Am J Physiol Renal Physiol **293**(5): F1641–1648.

MOGENSEN C.E. (1998) *Combined high blood pressure and glucose in type 2 diabetes: double jeopardy. British trial shows clear effects of treatment, especially blood pressure reduction*. BMJ **317**(7160): 693–694.

MOGENSEN C.E., CHRISTENSEN C.K. and VITTINGHUS E. (1983) *The stages in diabetic renal disease. With emphasis on the stage of incipient diabetic nephropathy*. Diabetes **32 Suppl 2**: 64–78.

MONTGOMERY M.K., HALLAHAN N.L., BROWN S.H., LIU M., MITCHELL T.W., COONEY G.J. and TURNER N. (2013) *Mouse strain-dependent variation in obesity and glucose homeostasis in response to high-fat feeding*. Diabetologia **56**(5): 1129–1139.

MORTON D.B., ABBOT D., BARCLAY R., CLOSE B.S., EWBANK R., GASK D., HEATH M., MATTIC S., POOLE T., SEAMER J., SOUTHEE J., THOMPSON A., TRUSSELL B., WEST C. and JENNINGS M. (1993) *Removal of blood from laboratory mammals and birds. First report of the BVA/FRAME/RSPCA/UFAW Joint Working Group on Refinement*. Lab Anim **27**(1): 1–22.

MOSS S.E., KLEIN R. and KLEIN B.E. (1991) *Cause-specific mortality in a population-based study of diabetes*. Am J Public Health **81**(9): 1158–1162.

MOURA NETO A., ZANTUT-WITTMANN D.E., FERNANDES T.D., NERY M. and PARISI M.C. (2013) *Risk factors for ulceration and amputation in diabetic foot: study in a cohort of 496 patients*. Endocrine **44**(1): 119–124.

MOUSEGENOMEINFORMATICS () *Guidelines for Nomenclature of Mouse and Rat Strains*. International Committee on Standardized Genetic Nomenclature for Mice.

MULLER W.A. (1998) *Diabetes mellitus–long time survival*. J Insur Med **30**(1): 17–27.

MURAWSKI I.J., MAINA R.W. and GUPTA I.R. (2010) *The relationship between nephron number, kidney size and body weight in two inbred mouse strains*. Organogenesis **6**(3): 189–194.

EL NAHAS A.M., BASSETT A.H., COPE G.H. and LE CARPENTIER J.E. (1991) *Role of growth hormone in the development of experimental renal scarring*. Kidney Int **40**(1): 29–34.

NOGI Y., NAGASHIMA M., TERASAKI M., NOHTOMI K., WATANABE T. and HIRANO T. (2012) *Glucose-dependent insulinotropic polypeptide prevents the progression of macrophage-driven atherosclerosis in diabetic apolipoprotein E-null mice*. PLoS ONE **7**(4): e35683.

NOONAN W.T. and BANKS R.O. (2000) *Renal function and glucose transport in male and female mice with diet-induced type II diabetes mellitus*. Proc Soc Exp Biol Med **225**(3): 221–230.

NYBERG J., ANDERSON M.F., MEISTER B., ALBORN A.M., STROM A.K., BREDERLAU A., ILLERSKOG A.C., NILSSON O., KIEFFER T.J., HIETALA M.A., RICKSTEN A. and ERIKSSON P.S. (2005) *Glucose-dependent insulinotropic polypeptide is expressed in adult hippocampus and induces progenitor cell proliferation*. J Neurosci **25**(7): 1816–1825.

NYENGAARD J.R. (1999) *Stereologic methods and their application in kidney research*. J Am Soc Nephrol **10**(5): 1100–1123.

OHLSON M., SORENSSON J. and HARALDSSON B. (2001) *A gel-membrane model of glomerular charge and size selectivity in series*. Am J Physiol Renal Physiol **280**(3): 396–405.

PAPETA N., CHAN K.T., PRAKASH S., MARTINO J., KIRYLUK K., BALLARD D., BRUGGEMAN L.A., FRANKEL R., ZHENG Z., KLOTMAN P.E., ZHAO H., D'AGATI V.D., LIFTON R.P. and GHARAVI A.G. (2009) *Susceptibility loci for murine HIV-associated nephropathy encode trans-regulators of podocyte gene expression*. J Clin Invest **119**(5): 1178–1188.

PATEL V.J., JOHARAPURKAR A.A., SHAH G.B. and JAIN M.R. (2014) *Effect of GLP-1 Based Therapies on Diabetic Dyslipidemia*. Curr Diabetes Rev .

PEREIRA L., MATTHES J., SCHUSTER I., VALDIVIA H.H., HERZIG S., RICHARD S. and GOMEZ A.M. (2006) *Mechanisms of [Ca2+]i transient decrease in cardiomyopathy of db/db type 2 diabetic mice*. Diabetes **55**(3): 608–615.

POPPER B.A. (2013) Impact of the genetic background on the development of diabetes-associated renal lesions in GIPR^{dn} transgenic diabetic mice. Dissertation,

Ludwig-Maximilians-Universität, Munich.

PRIES A.R., SECOMB T.W. and GAEHTGENS P. (2000) *The endothelial surface layer*. Pflugers Arch **440**(5): 653–666.

PUGLIESE G., PRICCI F., ROMEO G., PUGLIESE F., MENE P., GIANNINI S., CRESCI B., GALLI G., ROTELLA C.M., VLASSARA H. and DI MARIO U. (1997) *Upregulation of mesangial growth factor and extracellular matrix synthesis by advanced glycation end products via a receptor-mediated mechanism*. Diabetes **46**(11): 1881–1887.

QI Z., FUJITA H., JIN J., DAVIS L.S., WANG Y., FOGO A.B. and BREYER M.D. (2005) *Characterization of susceptibility of inbred mouse strains to diabetic nephropathy*. Diabetes **54**(9): 2628–2637.

QI Z., WHITT I., MEHTA A., JIN J., ZHAO M., HARRIS R.C., FOGO A.B. and BREYER M.D. (2004) *Serial determination of glomerular filtration rate in conscious mice using FITC-inulin clearance*. Am J Physiol Renal Physiol **286**(3): F590–596.

RAJASHEKHAR G., RAMADAN A., ABBURI C., CALLAGHAN B., TRAKTUEV D.O., EVANS-MOLINA C., MATURI R., HARRIS A., KERN T.S. and MARCH K.L. (2014) *Regenerative therapeutic potential of adipose stromal cells in early stage diabetic retinopathy*. PLoS ONE **9**(1): e84671.

RAMAGE I.J., HOWATSON A.G., MCCOLL J.H., MAXWELL H., MURPHY A.V. and BEATTIE T.J. (2002) *Glomerular basement membrane thickness in children: a stereologic assessment*. Kidney Int **62**(3): 895–900.

REDDI A.S., VELASCO C.A., REDDY P.R., KHAN M.Y. and CAMERINI-DAVALOS R.A. (1990) *Diabetic microangiopathy in KK mice. VI. Effect of glycemic control on renal glycoprotein metabolism and established glomerulosclerosis*. Exp Mol Pathol **53**(2): 140–151.

REMUZZI A., MAZERSKA M., GEPHARDT G.N., NOVICK A.C., BRENNER B.M. and REMUZZI G. (1995) *Three-dimensional analysis of glomerular morphology in patients with subtotal nephrectomy*. Kidney Int **48**(1): 155–162.

REMUZZI G. (1999) *Nephropathic nature of proteinuria*. Curr Opin Nephrol Hypertens **8**(6): 655–663.

RENNER S., FEHLINGS C., HERBACH N., HOFMANN A., VON WALDTHAUSEN D.C., KESSLER B., ULRICHS K., CHODNEVSKAJA I., MOSKALENKO V., AMSELGRUBER W., GOKE B., PFEIFER A., WANKE R. and WOLF E. (2010) *Glucose intolerance and reduced proliferation of pancreatic beta-cells in transgenic pigs with impaired glucose-dependent insulinotropic polypeptide function*. Diabetes **59**(5): 1228–1238.

REYNOLDS E.S. (1963) *The use of lead citrate at high pH as an electron-opaque stain in electron microscopy*. J Cell Biol **17**: 208–212.

ROGLIC G., COLHOUN H.M., STEVENS L.K., LEMKES H.H., MANES C. and FULLER J.H. (1998) *Parental history of hypertension and parental history of diabetes and microvascular complications in insulin-dependent diabetes mellitus: the EURODIAB IDDM Complications Study*. Diabet Med **15**(5): 418–426.

ROSELLI S., HEIDET L., SICH M., HENGER A., KRETZLER M., GUBLER M.C. and ANTIGNAC C. (2004) *Early glomerular filtration defect and severe renal disease in podocin-deficient mice*. Mol Cell Biol **24**(2): 550–560.

ROSSINI A.A., APPEL M.C., WILLIAMS R.M. and LIKE A.A. (1977) *Genetic influence of the streptozotocin-induced insulitis and hyperglycemia*. Diabetes **26**(10): 916–920.

RUBLER S., DLUGASH J., YUCEOGLU Y.Z., KUMRAL T., BRANWOOD A.W. and GRISHMAN A. (1972) *New type of cardiomyopathy associated with diabetic glomerulosclerosis*. Am J Cardiol **30**(6): 595–602.

RUSSO L.M., SANDOVAL R.M., MCKEE M., OSICKA T.M., COLLINS A.B., BROWN D., MOLITORIS B.A. and COMPER W.D. (2007) *The normal kidney filters nephrotic levels of albumin retrieved by proximal tubule cells: retrieval is disrupted in nephrotic states*. Kidney Int **71**(6): 504–513.

SAKAI N., CHUN J., DUFFIELD J.S., WADA T., LUSTER A.D. and TAGER A.M. (2013) *LPA1-induced cytoskeleton reorganization drives fibrosis through CTGF-dependent fibroblast proliferation*. FASEB J **27**(5): 1830–1846.

SAKAI T., LEMLEY K.V., HACKENTHAL E., NAGATA M., NOBILING R. and KRIZ W. (1992) *Changes in glomerular structure following acute mesangial failure in the isolated perfused kidney*. Kidney Int **41**(3): 533–541.

SCHIFFER M., BITZER M., ROBERTS I.S., KOPP J.B., TEN DIJKE P., MUNDEL P. and BOTTINGER E.P. (2001) *Apoptosis in podocytes induced by TGF-beta and Smad7*. J Clin Invest **108**(6): 807–816.

SCHLAGER G. and WEIBUST R.S. (1967) *Genetic control of blood pressure in mice*. Genetics **55**(3): 497–506.

SCHLOTE J., SCHRODER A., DAHLMANN A., KARPE B., CORDASIC N., DANIEL C., HILGERS K.F., TITZE J., AMANN K. and BENZ K. (2013) *Cardiovascular and renal effects of high salt diet in GDNF+/- mice with low nephron number*. Kidney Blood Press Res **37**(4-5): 379–391.

SCHMIDT K., PESCE C., LIU Q., NELSON R.G., BENNETT P.H., KARNITSCHNIG H., STRIKER L.J. and STRIKER G.E. (1992) *Large glomerular size in Pima Indians: lack of change with diabetic nephropathy*. J Am Soc Nephrol **3**(2): 229–235.

SCHNEIDER J.P. and OCHS M. (2014) *Alterations of mouse lung tissue dimensions during processing for morphometry: a comparison of methods*. Am J Physiol Lung Cell Mol Physiol **306**(4): L341–350.

SCHONHERR E., SUNDERKOTTER C., IOZZO R.V. and SCHAEFER L. (2005) *Decorin, a novel player in the insulin-like growth factor system*. J Biol Chem **280**(16): 15767–15772.

SCHULTE K., BERGER K., BOOR P., JIRAK P., GELMAN I.H., ARKILL K.P., NEAL C.R., KRIZ W., FLOEGE J., SMEETS B. and MOELLER M.J. (2014) *Origin of parietal podocytes in atubular glomeruli mapped by lineage tracing*. J Am Soc Nephrol **25**(1): 129–141.

SCHWENK R.W., VOGEL H. and SCHURMANN A. (2013) *Genetic and epigenetic control of metabolic health*. Mol Metab **2**(4): 337–347.

SEGHERS V., NAKAZAKI M., DEMAYO F., AGUILAR-BRYAN L. and BRYAN J. (2000) *Sur1 knockout mice. A model for K(ATP) channel-independent regulation of insulin secretion*. J Biol Chem **275**(13): 9270–9277.

SEYER-HANSEN K., HANSEN J. and GUNDERSEN H.J. (1980) *Renal hypertrophy in experimental diabetes. A morphometric study*. Diabetologia **18**(6): 501–505.

SHARMA K., MCCUE P. and DUNN S.R. (2003) *Diabetic kidney disease in the db/db mouse*. Am J Physiol Renal Physiol **284**(6): F1138–F1144.

SHARMA K. and ZIYADEH F.N. (1994) *Renal hypertrophy is associated with upregulation of TGF-beta 1 gene expression in diabetic BB rat and NOD mouse*. Am J Physiol **267**(6 Pt 2): F1094–1001.

SHEA K., STEWART S. and ROUSE R. (2013) *Assessment Standards: Comparing Histopathology, Digital Image Analysis, and Stereology for Early Detection of Experimental Cisplatin-induced Kidney Injury in Rats*. Toxicol Pathol .

SIMS E.K., HATANAKA M., MORRIS D.L., TERSEY S.A., KONO T., CHAUDRY Z.Z., DAY K.H., MOSS D.R., STULL N.D., MIRMIRA R.G. and EVANS-MOLINA C. (2013) *Divergent compensatory responses to high-fat diet between C57BL6/J and C57BLKS/J inbred mouse strains*. Am J Physiol Endocrinol Metab **305**(12): E1495–1511.

SINHA S., EKKA M., SHARMA U., P R., PANDEY R.M. and JAGANNATHAN N.R. (2014) *Assessment of changes in brain metabolites in Indian patients with type-2 diabetes mellitus using proton magnetic resonance spectroscopy*. BMC Res Notes **7**(1): 41.

SONG S., MEYER M., TURK T.R., WILDE B., FELDKAMP T., ASSERT R., WU K., KRIBBEN A. and WITZKE O. (2009) *Serum cystatin C in mouse models: a reliable and precise marker for renal function and superior to serum creatinine*. Nephrol Dial Transplant **24**(4): 1157–1161.

SPITHOVEN E.M., MEIJER E., BOERTIEN W.E., SINKELER S.J., TENT H., DE JONG P.E., NAVIS G. and GANSEVOORT R.T. (2013) *Tubular secretion of creatinine in autosomal dominant polycystic kidney disease: consequences for cross-sectional and*

longitudinal performance of kidney function estimating equations. Am J Kidney Dis **62**(3): 531–540.

STEFFES M.W., SCHMIDT D., MCCRERY R. and BASGEN J.M. (2001) *Glomerular cell number in normal subjects and in type 1 diabetic patients*. Kidney Int **59**(6): 2104–2113.

STELLOH C., ALLEN K.P., MATTSON D.L., LERCH-GAGGL A., REDDY S. and EL-MEANAWY A. (2012) *Prematurity in mice leads to reduction in nephron number, hypertension, and proteinuria*. Transl Res **159**(2): 80–89.

STERIO D.C. (1984) *The unbiased estimation of number and sizes of arbitrary particles using the disector*. J Microsc **134**(Pt 2): 127–136.

STORER J.B. (1966) *Longevity and gross pathology at death in 22 inbred mouse strains*. J Gerontol **21**(3): 404–409.

VON TELL D., ARMULIK A. and BETSHOLTZ C. (2006) *Pericytes and vascular stability*. Exp Cell Res **312**(5): 623–629.

TERVAERT T.W., MOOYAART A.L., AMANN K., COHEN A.H., COOK H.T., DRACHENBERG C.B., FERRARIO F., FOGO A.B., HAAS M., DE HEER E., JOH K., NOEL L.H., RADHAKRISHNAN J., SESHAN S.V., BAJEMA I.M. and BRUIJN J.A. (2010) *Pathologic classification of diabetic nephropathy*. J Am Soc Nephrol **21**(4): 556–563.

TESCH G.H. (2007) *Role of macrophages in complications of type 2 diabetes*. Clin Exp Pharmacol Physiol **34**(10): 1016–1019.

TOJO A. and KINUGASA S. (2012) *Mechanisms of glomerular albumin filtration and tubular reabsorption*. Int J Nephrol **2012**: 481520.

TOJO A., ONOZATO M.L., HA H., KURIHARA H., SAKAI T., GOTO A., FUJITA T. and ENDOU H. (2001) *Reduced albumin reabsorption in the proximal tubule of early-stage diabetic rats*. Histochem Cell Biol **116**(3): 269–276.

TOJO A., ONOZATO M.L., KITIYAKARA C., KINUGASA S., FUKUDA S., SAKAI T. and FUJITA T. (2008) *Glomerular albumin filtration through podocyte cell body in puromycin aminonucleoside nephrotic rat*. Med Mol Morphol **41**(2): 92–98.

TOMINO Y. (2012) *Lessons From the KK-Ay Mouse, a Spontaneous Animal Model for the Treatment of Human Type 2 Diabetic Nephropathy*. Nephrourol Mon **4**(3): 524–529.

TOMINO Y., TANIMOTO M., SHIKE T., SHIINA K., FAN Q., LIAO J., GOHDA T., MAKITA Y. and FUNABIKI K. (2005) *Pathogenesis and treatment of type 2 diabetic nephropathy: lessons from the spontaneous KK/Ta mouse model*. Curr Diabetes Rev **1**(3): 281–286.

TRACHSEL S., PURKABIRI K., LOUP O., JENNI H., EBERLE B., OCHS M. and KADNER A. (2011) *High-quality lung fixation by controlled closed loop perfusion for stereological analysis in a large animal model*. J Surg Res **166**(2): 97–102.

UEDA H., IKEGAMI H., YAMATO E., FU J., FUKUDA M., SHEN G., KAWAGUCHI Y., TAKEKAWA K., FUJIOKA Y. and FUJISAWA T. (1995) *The NSY mouse: a new animal model of spontaneous NIDDM with moderate obesity*. Diabetologia **38**(5): 503–508.

UKPDS-GROUP (1998) *Effect of intensive blood-glucose control with metformin on complications in overweight patients with type 2 diabetes (UKPDS 34). UK Prospective Diabetes Study (UKPDS) Group*. Lancet **352**(9131): 854–865.

USDIN T.B., MEZEY E., BUTTON D.C., BROWNSTEIN M.J. and BONNER T.I. (1993) *Gastric inhibitory polypeptide receptor, a member of the secretin-vasoactive intestinal peptide receptor family, is widely distributed in peripheral organs and the brain*. Endocrinology **133**(6): 2861–2870.

VAZQUEZ-BENITEZ G., DESAI J.R., XU S., GOODRICH G.K., SCHROEDER E.B., NICHOLS G.A., SEGAL J., BUTLER M.G., KARTER A.J., STEINER J.F., NEWTON K.M., MORALES L.S., PATHAK R.D., THOMAS A., REYNOLDS K., KIRCHNER H.L., WAITZFELDER B., ELSTON LAFATA J., ADIBHATLA R., XU Z. and O'CONNOR P.J. (2015) *Preventable Major Cardiovascular Events Associated With Uncontrolled Glucose, Blood Pressure, and Lipids and Active Smoking in Adults With Diabetes With and Without Cardiovascular Disease: A Contemporary Analysis*. Diabetes Care .

VILSBØLL T., KRARUP T., MADSBAD S. and HOLST J.J. (2002) *Defective amplification of the late phase insulin response to glucose by GIP in obese Type II diabetic patients*. Diabetologia **45**(8): 1111–1119.

VITAL C., VALLAT J.M., LE BLANC M., MARTIN F. and COQUET M. (1973) *[Peripheral neuropathies caused by diabetes mellitus. Ultrastructural study of 12 biopsied cases].* J Neurol Sci **18**(4): 381–398.

VOLZ A. (1997) Klonierung und funktionelle Charakterisierung des humanen GIP-Rezeptors, Dissertation. Ph.D. thesis, Universität Marburg.

WANG X., JOHNSON A.C., WILLIAMS J.M., WHITE T., CHADE A.R., ZHANG J., LIU R., ROMAN R.J., LEE J.W., KYLE P.B., SOLBERG-WOODS L. and GARRETT M.R. (2014) *Nephron Deficiency and Predisposition to Renal Injury in a Novel One-Kidney Genetic Model*. J Am Soc Nephrol .

WANKE R. (1996) Zur Morpho- und Pathogenese der progressiven Glomerulosklerose. Habilitation, Ludwig-Maximilians-Universität, Munich.

WARRAM J.H., MANSON J.E. and KROLEWSKI A.S. (1995) *Glycosylated hemoglobin and the risk of retinopathy in insulin-dependent diabetes mellitus*. N Engl J Med **332**(19): 1305–1306.

WARTIOVAARA J., OFVERSTEDT L.G., KHOSHNOODI J., ZHANG J., MAKELA E., SANDIN S., RUOTSALAINEN V., CHENG R.H., JALANKO H., SKOGLUND U. and TRYGGVASON K. (2004) *Nephrin strands contribute to a porous slit diaphragm scaffold as revealed by electron tomography*. J Clin Invest **114**(10): 1475–1483.

WASADA T., MCCORKLE K., HARRIS V., KAWAI K., HOWARD B. and UNGER R.H. (1981) *Effect of gastric inhibitory polypeptide on plasma levels of chylomicron triglycerides in dogs*. J Clin Invest **68**(4): 1106–1107.

WATANABE Y., ITOH Y., YOSHIDA F., KOH N., TAMAI H., FUKATSU A., MATSUO S., HOTTA N. and SAKAMOTO N. (1991) *Unique glomerular lesion with spontaneous lipid deposition in glomerular capillary lumina in the NON strain of mice*. Nephron **58**(2): 210–218.

Waterston R.H., Lindblad-Toh K., Birney E., Rogers J., Abril J.F., Agarwal P., Agarwala R., Ainscough R., Alexandersson M., An P., Antonarakis S.E., Attwood J., Baertsch R., Bailey J., Barlow K., Beck S., Berry E., Birren B., Bloom T., Bork P., Botcherby M., Bray N., Brent M.R., Brown D.G., Brown S.D., Bult C., Burton J., Butler J., Campbell R.D., Carninci P., Cawley S., Chiaromonte F., Chinwalla A.T., Church D.M., Clamp M., Clee C., Collins F.S., Cook L.L., Copley R.R., Coulson A., Couronne O., Cuff J., Curwen V., Cutts T., Daly M., David R., Davies J., Delehaunty K.D., Deri J., Dermitzakis E.T., Dewey C., Dickens N.J., Diekhans M., Dodge S., Dubchak I., Dunn D.M., Eddy S.R., Elnitski L., Emes R.D., Eswara P., Eyras E., Felsenfeld A., Fewell G.A., Flicek P., Foley K., Frankel W.N., Fulton L.A., Fulton R.S., Furey T.S., Gage D., Gibbs R.A., Glusman G., Gnerre S., Goldman N., Goodstadt L., Grafham D., Graves T.A., Green E.D., Gregory S., Guigo R., Guyer M., Hardison R.C., Haussler D., Hayashizaki Y., Hillier L.W., Hinrichs A., Hlavina W., Holzer T., Hsu F., Hua A., Hubbard T., Hunt A., Jackson I., Jaffe D.B., Johnson L.S., Jones M., Jones T.A., Joy A., Kamal M., Karlsson E.K., Karolchik D., Kasprzyk A., Kawai J., Keibler E., Kells C., Kent W.J., Kirby A., Kolbe D.L., Korf I., Kucherlapati R.S., Kulbokas E.J., Kulp D., Landers T., Leger J.P., Leonard S., Letunic I., Levine R., Li J., Li M., Lloyd C., Lucas S., Ma B., Maglott D.R., Mardis E.R., Matthews L., Mauceli E., Mayer J.H., McCarthy M., McCombie W.R., McLaren S., McLay K., McPherson J.D., Meldrim J., Meredith B., Mesirov J.P., Miller W., Miner T.L., Mongin E., Montgomery K.T., Morgan M., Mott R., Mullikin J.C., Muzny D.M., Nash W.E., Nelson J.O., Nhan M.N., Nicol R., Ning Z., Nusbaum C., O'Connor M.J., Okazaki Y., Oliver K., Overton-Larty E., Pachter L., Parra G., Pepin K.H., Peterson J., Pevzner P., Plumb R., Pohl C.S., Poliakov A., Ponce T.C., Ponting C.P., Potter S., Quail M., Reymond A., Roe B.A., Roskin K.M., Rubin E.M., Rust A.G., Santos R., Sapojnikov V., Schultz B., Schultz J., Schwartz M.S., Schwartz S., Scott C., Seaman S., Searle S., Sharpe T., Sheridan A., Shownkeen R., Sims S., Singer J.B., Slater G., Smit A., Smith D.R., Spencer B., Stabenau A., Stange-Thomann N., Sugnet C., Suyama M., Tesler G., Thompson J., Torrents D., Trevaskis E., Tromp J., Ucla C., Ureta-Vidal A., Vinson J.P., Von Niederhausern A.C., Wade C.M.,

WALL M., WEBER R.J., WEISS R.B., WENDL M.C., WEST A.P., WETTERSTRAND K., WHEELER R., WHELAN S., WIERZBOWSKI J., WILLEY D., WILLIAMS S., WILSON R.K., WINTER E., WORLEY K.C., WYMAN D., YANG S., YANG S.P., ZDOBNOV E.M., ZODY M.C. and LANDER E.S. (2002) *Initial sequencing and comparative analysis of the mouse genome*. Nature **420**(6915): 520–562.

WEIBEL E.R. and GOMEZ D.M. (1962) *A principle for counting tissue structures on random sections*. J Appl Physiol **17**: 343–348.

WHITE K.E. and BILOUS R.W. (2004) *Structural alterations to the podocyte are related to proteinuria in type 2 diabetic patients*. Nephrol Dial Transplant **19**(6): 1437–1440.

WHO (1999) *Definition, diagnosis and classification of diabetes mellitus and its complications. Part 1: Diagnosis and classification of diabetes mellitus.*. Geneva.

WHO (2011) *Global status report on noncommunicable diseases 2010*. Geneva.

WILLIAMS E., TIMPERLEY W.R., WARD J.D. and DUCKWORTH T. (1980) *Electron microscopical studies of vessels in diabetic peripheral neuropathy*. J Clin Pathol **33**(5): 462–470.

WILLIAMS K.J., QIU G., USUI H.K., DUNN S.R., MCCUE P., BOTTINGER E., IOZZO R.V. and SHARMA K. (2007) *Decorin deficiency enhances progressive nephropathy in diabetic mice*. Am J Pathol **171**(5): 1441–1450.

XU G., KANETO H., LAYBUTT D.R., DUVIVIER-KALI V.F., TRIVEDI N., SUZUMA K., KING G.L., WEIR G.C. and BONNER-WEIR S. (2007) *Downregulation of GLP-1 and GIP receptor expression by hyperglycemia: possible contribution to impaired incretin effects in diabetes*. Diabetes **56**(6): 1551–1558.

XU J., HUANG Y., LI F., ZHENG S. and EPSTEIN P.N. (2010) *FVB mouse genotype confers susceptibility to OVE26 diabetic albuminuria*. Am J Physiol Renal Physiol **299**(3): F487–494.

YIP R.G., BOYLAN M.O., KIEFFER T.J. and WOLFE M.M. (1998) *Functional GIP receptors are present on adipocytes*. Endocrinology **139**(9): 4004–4007.

YIP R.G. and WOLFE M.M. (2000) *GIP biology and fat metabolism*. Life Sci **66**(2): 91–103.

ZHENG F., STRIKER G.E., ESPOSITO C., LUPIA E. and STRIKER L.J. (1998) *Strain differences rather than hyperglycemia determine the severity of glomerulosclerosis in mice*. Kidney Int **54**(6): 1999–2007.

ZHENG S., NOONAN W.T., METREVELI N.S., COVENTRY S., KRALIK P.M., CARLSON E.C. and EPSTEIN P.N. (2004) *Development of late-stage diabetic nephropathy in OVE26 diabetic mice*. Diabetes **53**(12): 3248–3257.

ZIYADEH F.N. (2004) *Mediators of diabetic renal disease: the case for tgf-Beta as the major mediator*. J Am Soc Nephrol **15 Suppl 1**: S55–57.

ZIYADEH F.N., SHARMA K., ERICKSEN M. and WOLF G. (1994) *Stimulation of collagen gene expression and protein synthesis in murine mesangial cells by high glucose is mediated by autocrine activation of transforming growth factor-beta*. J Clin Invest **93**(2): 536–542.

ZIYADEH F.N. and WOLF G. (2008) *Pathogenesis of the podocytopathy and proteinuria in diabetic glomerulopathy*. Curr Diabetes Rev **4**(1): 39–45.

Acknowledgement

First, I would like to thank Prof. Dr. Rüdiger Wanke for making this dissertation possible. His support and his vast knowledge of stereological and morphometrical methods were invaluable for the realization of this project. Discussions with him were always incredibly enlightening and motivating. I am also very grateful to the Head of the Institute of Veterinary Pathology, Prof. Dr. Walter Hermanns for his support of this project. Also, PD Dr. Nadja Herbach and Dr. Andreas Blutke for their supervision, instruction, help and constructive criticism in everything to do with pathological investigations and basic research. Lisa Pichl, for countless hours of instruction and help in animal handling and laboratory work and for creating a pleasant working atmosphere even at 7 in the morning. Heike Sperling, for the handling of the plastic embedding, Angela Siebert, Heidrun Schöl and Claudia Mair for their work and assistance at the electron microscope. Sabine Zwirz and Adrian Ciolovan for their loving care of the laboratory animals. I would also like to thank Bastian Popper, Alexandra Rieger and Judith Röder for their companionship, generous support and productive teamwork. My thanks also go to the rest of the many employees at the Institute of Veterinary Pathology, as they all contributed in their own way to this dissertation. And last, but not least, to the clinical chemistry team at the Klinikum Schwabing, München, who analysed serum and urine samples.